NASA Contractor Report 4441

Aerobrake Concepts for NTP Systems Study

Manuel I. Cruz

CONTRACT NAS1-19291
JUNE 1992

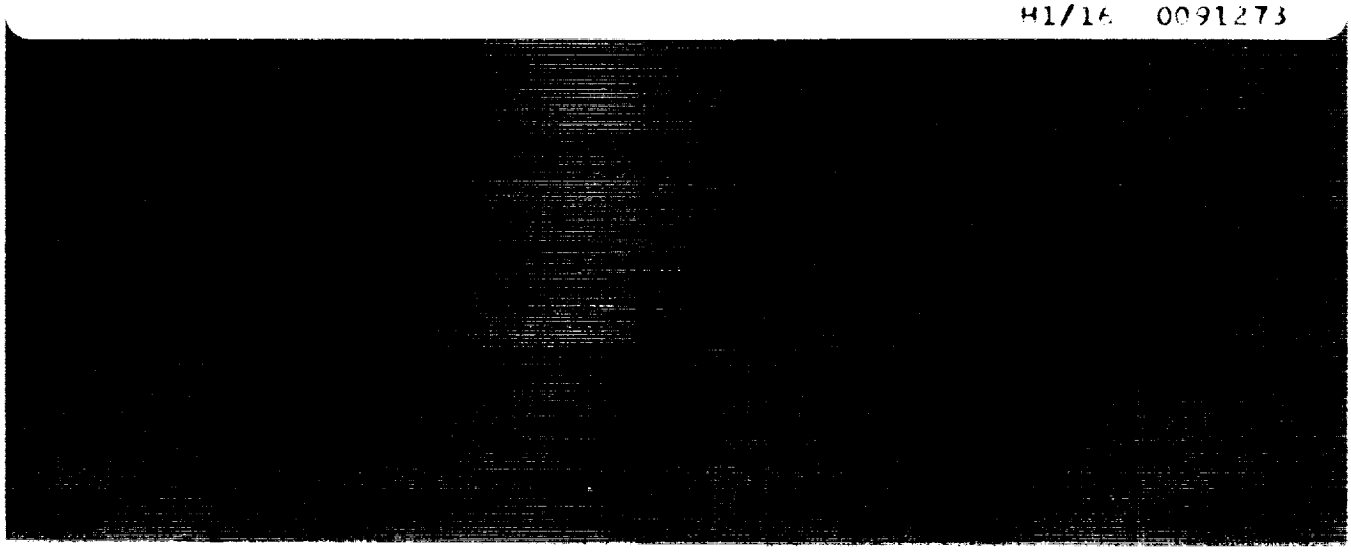

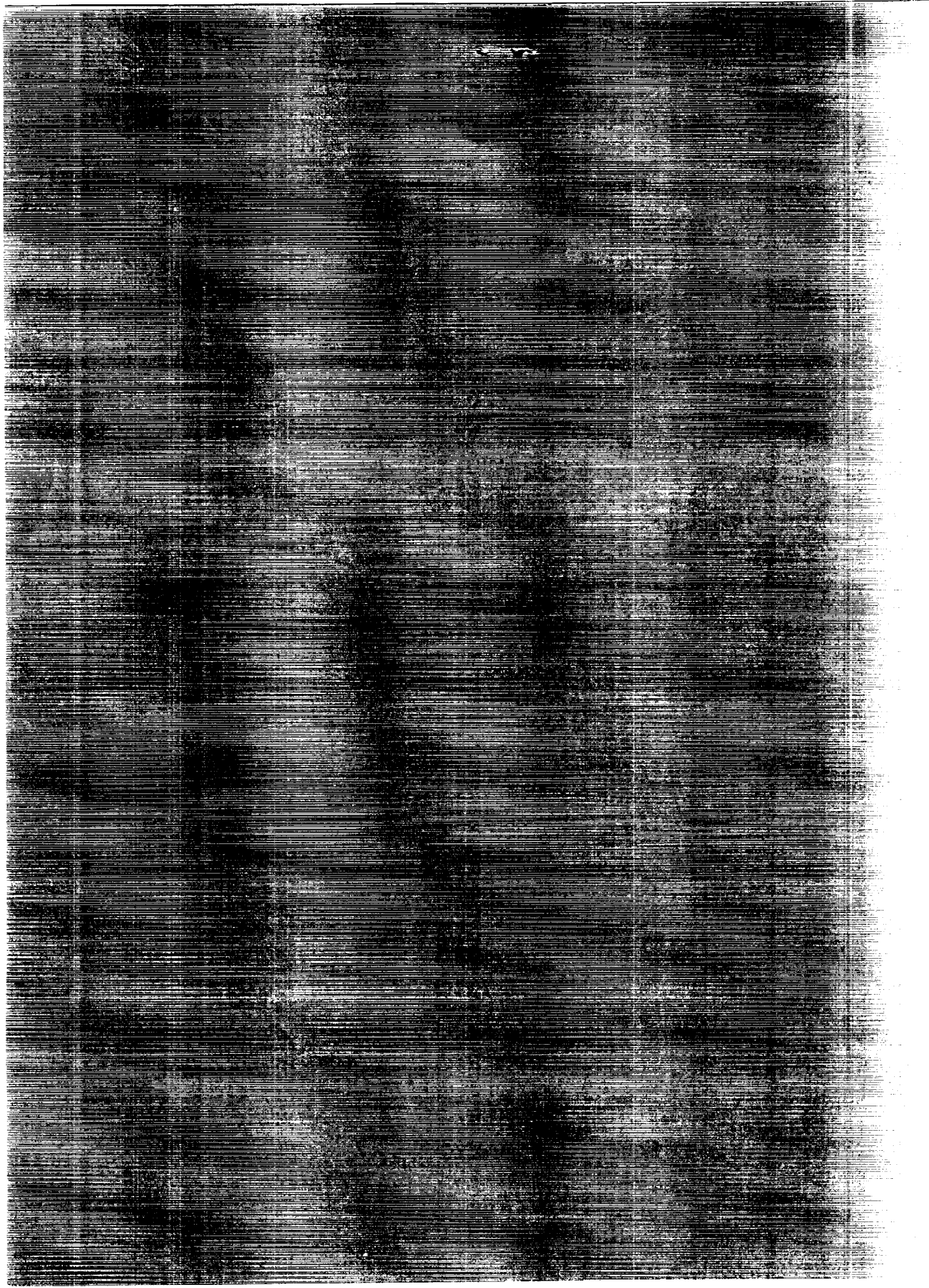

NASA Contractor Report 4441

Aerobrake Concepts for NTP Systems Study

Manuel I. Cruz
TRW
Federal Systems Division
Space & Technology Group
Redondo Beach, California

Prepared for
Langley Research Center
under Contract NAS1-19291

National Aeronautics and
Space Administration

Office of Management

Scientific and Technical
Information Program

1992

TABLE OF CONTENTS

AEROBRAKE CONCEPTS FOR NTP SYSTEMS STUDY
SUMMARY

The objective of this task was to develop Aerobrake concepts for manned Mars missions which utilize Nuclear Thermal Propulsion (NTP) for interplanetary transportation.

This study specifically addressed system requirements and designs which utilize aerodynamic deceleration for manned descent from Mars orbit. Concepts developed under Mars Rover Sample Return (MRSR) studies were assessed for applicability.

The most promising aerodynamic concepts for Mars entry to landing were ultra-low ballistic coefficient concepts which relied on space deployable and flexible blanket aerobrakes. The entry Thermal Protection System (TPS) requirements were such that current materials being researched and developed could endure the environments. Alternate concepts that rely on interplanetary transfer waste products (i.e. water, human waste, cellulose, etc.) could enhance the blanket TPS performance by providing sublimation and transpiration heat transfer mechanisms.

In addition, the use of automotive air bag technology for the terminal descent and touchdown phases provided significant reduction in the terminal chemical propulsion system requirements. This assumed a staged scenario with multiple gas (ambient gas and gas generator mixture) bags deployed at different times in the mission. This also provided a backup system for cushioned landing in the event of a chemical propulsion system failure used for the soft landing.

The more attractive approach for guiding the payload to a precise and safe landing required a ballistic non-lifting approach. This is a steep entry with terminal chemical propulsion maneuvering to the landing site. The terminal descent and touchdown Delta-V was minimized by the ultra-low ballistic coefficient entry.

The use of a lifting entry significantly reduces the aerodynamic loads (from 5 to 1 g). This requires L/D of about 0.5 or better. This, though, usually increases the terminal decelerator deployment speeds by a factor of 2 to 10, due to the accompanying increase of ballistic coefficient with L/D. In a de-orbit abort scenario, L/D does provide significant cross range capability to either change the orbit line of nodes or orbit inclination to different landing sites. At Mars with limited landing site availability or quick response need, the requirement for cross range capability is not clear. The landing error footprint comparison between a ballistic and an aeromaneuvering entry is of equal magnitude.

1. INTRODUCTION

1.1 MISSION DEFINITION

The manned exploration of the Mars surface will require entry and terminal descent to soft landing systems. These systems will deliver humans, habitats, logistical supplies, equipment, ascent vehicles and other freight to sites from where exploration will be staged. The landed payloads are expected to range from 1,000 kg to 23,000 kg in the early stages for these missions. Most of these payloads are delivered to the surface from Mars orbit. The scenario of choice for Mars orbit delivery for this study utilizes a Retro-propulsion maneuver with a Nuclear Thermal Propulsion System (see Figure 1.1.1). This study also considers delivery of some of these payloads on direct hyperbolic entry. These unmanned direct delivery payloads could potentially have arrived long before the manned modules in preparation of the surface expeditionary phase.

The parking orbit mass required to return to Earth is critical to execution of the mission. This is for both the mass required at Earth departure and an operationally simpler mission execution at Mars orbit. This study addresses this trade as it relates to the entry system and mission staging implications. This is coupled to the ascent vehicles requirements.

De-orbit entry and landing focuses primarily on the use of a passive ballistic entry with a ultra-low ballistic shape (see Figure 1.1.2). The terminal descent could rely on an option which utilizes an airbag to increase the area and reduce the terminal descent velocity much in the same manner as a parachute or ballute. The terminal landing depends on a chemical propulsion system with an impact cushion to soft land with the residual velocity and as a backup to the propulsion system in case of a failure.

1.2 STUDY OBJECTIVES AND SCOPE

The objective of this tasked study is to develop Aerobrake concepts for manned Mars missions which utilize Nuclear Thermal Propulsion (NTP). This study will address system requirements and designs which utilize aerodynamic deceleration for manned descent from Mars orbit. Concepts developed under Mars Rover Sample Return (MRSR) studies will be assessed for applicability.

1.3 STUDY RESULTS, CONCLUSIONS, AND RECOMMENDATIONS

The most promising aerodynamic concepts for Mars entry to landing were ultra-low ballistic coefficient concepts which relied on space deployable and flexible blanket aerobrakes. The entry Thermal Protection System (TPS) requirements were such that current materials being researched and developed could endure the environments. Alternate concepts that rely on interplanetary transfer waste products (i.e. water, human waste, cellulose, etc.) could enhance the blanket TPS performance by providing sublimation and transpiration heat transfer mechanisms.

In addition, the use of automotive air bag technology for the terminal descent and touchdown phases provided significant reduction in the terminal chemical

propulsion system requirements. This assumed a staged scenario with multiple gas (ambient gas and gas generator mixture) bags deployed at different times in the mission. This also provided a backup system for cushioned landing in the event of a chemical propulsion system failure used for the soft landing.

A preferred approach for guiding the payload to a precise and safe landing required a ballistic non-lifting approach. This is a steep entry with terminal chemical propulsion maneuvering to the landing site. The terminal chemical propulsion Delta-V was minimized by the ultra-low ballistic coefficient entry concept.

It is recommended that continued development of deployable and flexible aerobrakes, and cushioned landing concepts be a goal for space exploration. There are significant benefits to be gained from mission performance and spacecraft integration perspective. This is particularly true for exploration of atmosphere bearing planetary bodies as may well be the focus for both manned and unmanned exploration. Research dealing with computational fluid dynamics over very blunt and flexible structures, high temperature blankets (1100 to 2640 deg. K) and dynamics of large flexible aerodynamic structures should receive most of the emphasizes. The driving requirements, though, are for entry speeds corresponding to direct hyperbolic entry, greater than 5.8 km/sec. This extends the need for a 2640 deg. K blanket as opposed to a 1100 deg K blanket for orbital entry. Entry out of Mars orbit does not present significant challenges to the technology. It is primarily a design development challenge.

1.4 ACKNOWLEDGEMENTS

The study task monitor at NASA/LaRC was Charles Eldred. Consultations were conducted with Howard Goldstein at NASA/ARC.

TRW was able to draw upon a large technical pool in the performance of this study. The following individuals were principally consulted, although on a limited basis and from their work on related IR&D.

Donna Post - Aerodynamics & Aerothermodynamics
Tumkur Shivananda - Aerodynamics
Edward Zabrensky - Aerothermodynamics
Robert Senn - Materials
Fred Brewen - Materials
John Crawford - Structures & Dynamics
Ralph Colbert - Structures & Dynamics
Kevin Soranno - Configuration Design
Marc Ilgen - Terminal Descent & Touchdown

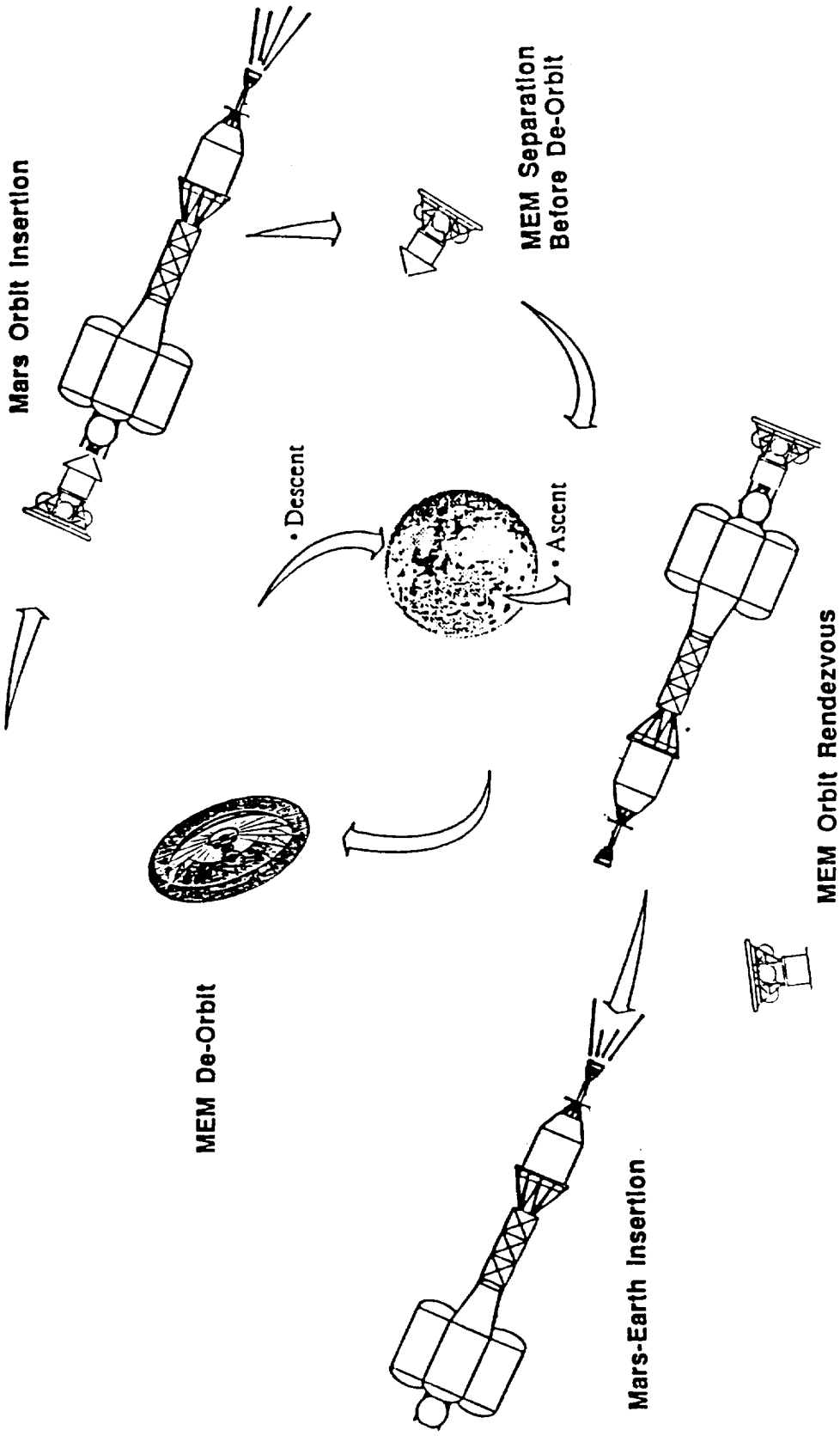

Figure 1.1.1 Mars Delivery Mission Scenario

Figure 1.1.2a Aerobrake Entry to Landing Mission Scenario Propulsive Touchdown

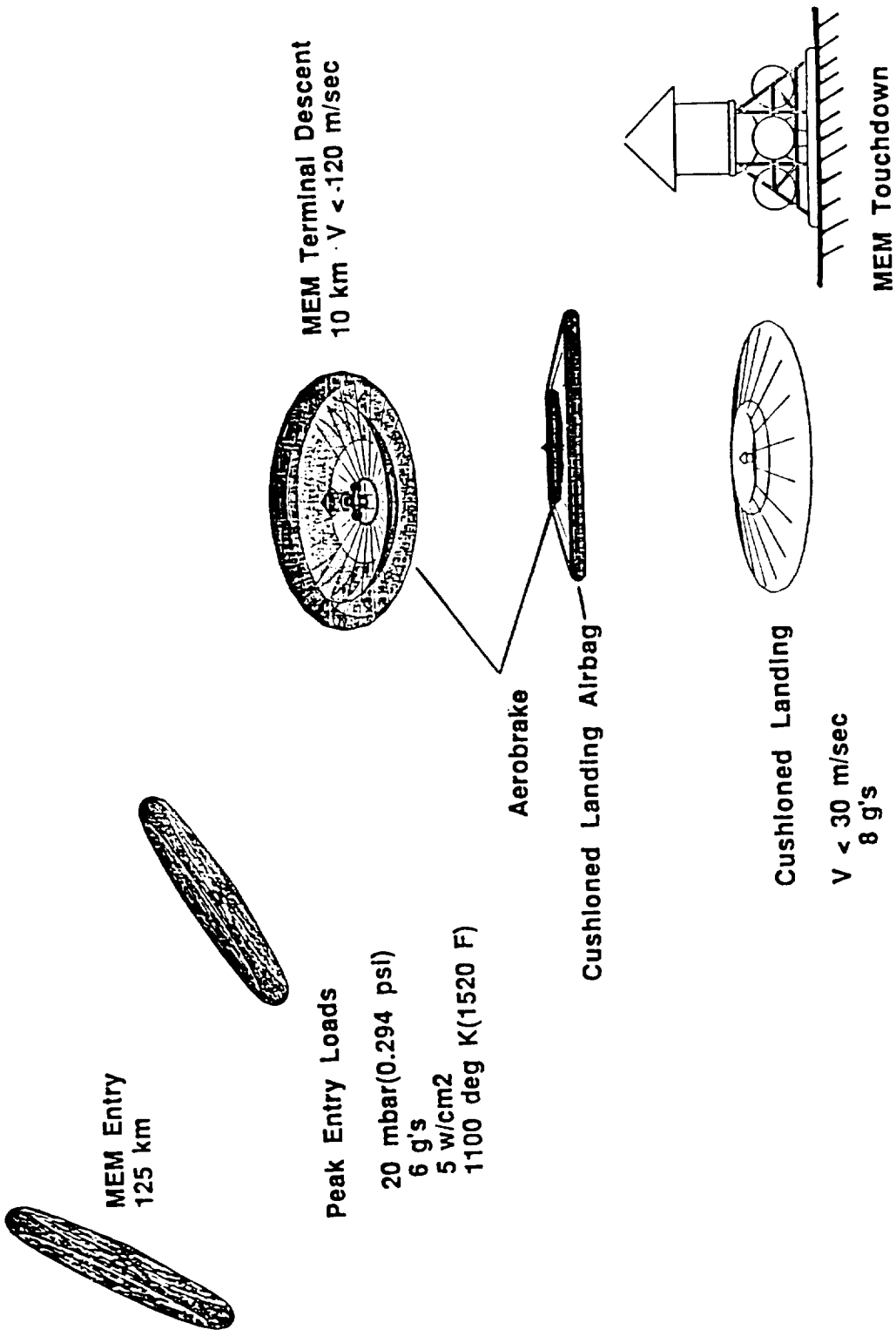

Figure 1.1.2b Aerobrake Entry to Landing Mission Scenario Cushioned Touchdown

2. REQUIREMENTS

2.1 PROJECT STUDY REQUIREMENTS

The only requirement provided by the NASA project office was that the manned entry systems not be subjected to sustained steady state aerodynamic entry loads greater than 5 to 6 g's.

2.2 DERIVED REQUIREMENTS

The following requirements were derived from the study which deal primarily with the entry to landing system:

1.) The ballistic aerobrake ballistic coefficient shall have a value of 5 to 25 kg/m^2.

2.) The entry trajectory shall be as steep as possible consistent with any entry aerodynamic load constraints.

3.) The Aerobrake blanket shall be designed to sustain single thermal loads of up to 1100 deg K for orbital entry and 2640 deg K for direct hyperbolic entry.

4.) The maximum aerobrake deflection shall be constrained to less than 13 cm over a 6 m span. An aerobrake blanket stiffness which results in a Young's modulus greater than 2070 Mega Pascal will also be required along with this maximum deflection.

5.) Nominally the aerobrake shall act as the terminal descent system.

6.) Using the aerobrake, the soft landing propulsion system shall require 600 m/sec Delta-V.

7.) The shock attenuation system at landing shall tolerate a 1 m/sec residual minimum Delta-V.

8.) The shock attenuation system shall tolerate a 30 to 100 m/sec impact in case of a propulsion system failure.

3. MISSION PERFORMANCE ANALYSIS

3.1 MARS PARKING ORBIT AND MISSION PERFORMANCE

Selection of the parking orbit to which the NTP will deliver the mission elements is critical to the design of the mission. It will affect the mass required at Mars delivery to effect the mission. This is driven by the amount of mass that must be returned from the Mars surface to the Earth return spacecraft for rendezvous and transfer of the crew and any other supplies. The entry system will be minimally affected by the parking orbit selection, since the entry speeds vary from 3.5 to 4.6 km/sec for the lowest to the highest orbit altitudes possible. A 500 km circular (2.1 hr) orbit and a 500 km X 1 Sol (24.2 hr) orbit are usually the limits for a Mars parking orbit for these class of missions requiring movement between the surface and orbit, and eventual return to Earth. This orbit range is limited by orbital decay and stability considerations.

References 3.6.1 and 3.6.2 suggest mass requirements for manned Mars mission spacecraft elements. These are reflected in Table 3.1.1 below in Tonnes (1000 kg or metric tons). This will form the basis for trades which determine potential aerobrake and lander requirements. An exploration program strategy can then be developed which capitalizes on the benefits of both NTP and aerobrakes.

Table 3.1.1 Mission and Mass.

Element	Mass, Tonnes
Crew(4) and Return Samples	1.5
Crew Earth Return Capsules	7.0 - 7.9
Mars Surface Habitat	21.0 - 23.0
Interplanetary Habitat	23.0

Mars Excursion Module (MEM) mass or aerobrake payload mass sensitivity analyses were conducted as a function of the parking orbit and the crew capsule mass that would return to the Earth return spacecraft. The mass required for the Mars Delivery/Earth Return spacecraft was also synthesized (The mass required on Mars approach to perform the mission). The mission scenario considers that the mission spacecraft elements are inserted into Mars orbit by an NTP system with an Isp of about 950 sec. The MEM is de-orbited using a storable propulsion system with an Isp of about 340 sec. The MEM aerobrakes to a terminal descent and soft lands using the storable propulsion system. After surface exploration activities are concluded, the MEM crew return in a capsule to the Earth return spacecraft using a storable propellant ascent vehicle. This crew capsule is left in Mars orbit with the crew returning to Earth in the interplanetary habitat (Earth return crew capsule). The Mars-Earth interplanetary transfer is performed using a NTP. At both Mars encounter and departure, it is assumed that the C3 (Vinf ^{2}) is consistent with 100 day one way flight times. This is about 100 km^2/sec^2 at Mars encounter and 20 km^2/sec^2 at Mars departure (Reference 3.6.3-see Figures 3.1.1 and 3.1.2).

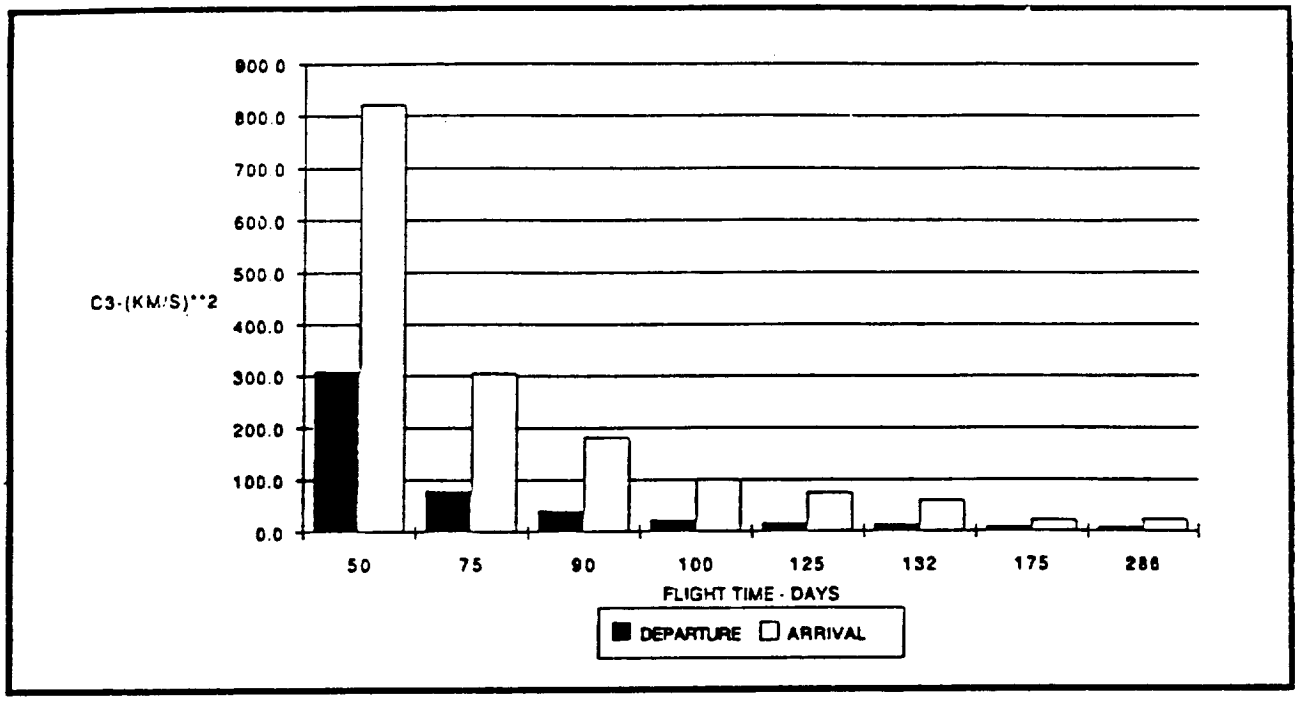

Figure 3.1.1 C3 Sensitivity to Flight Time, Earth to Mars

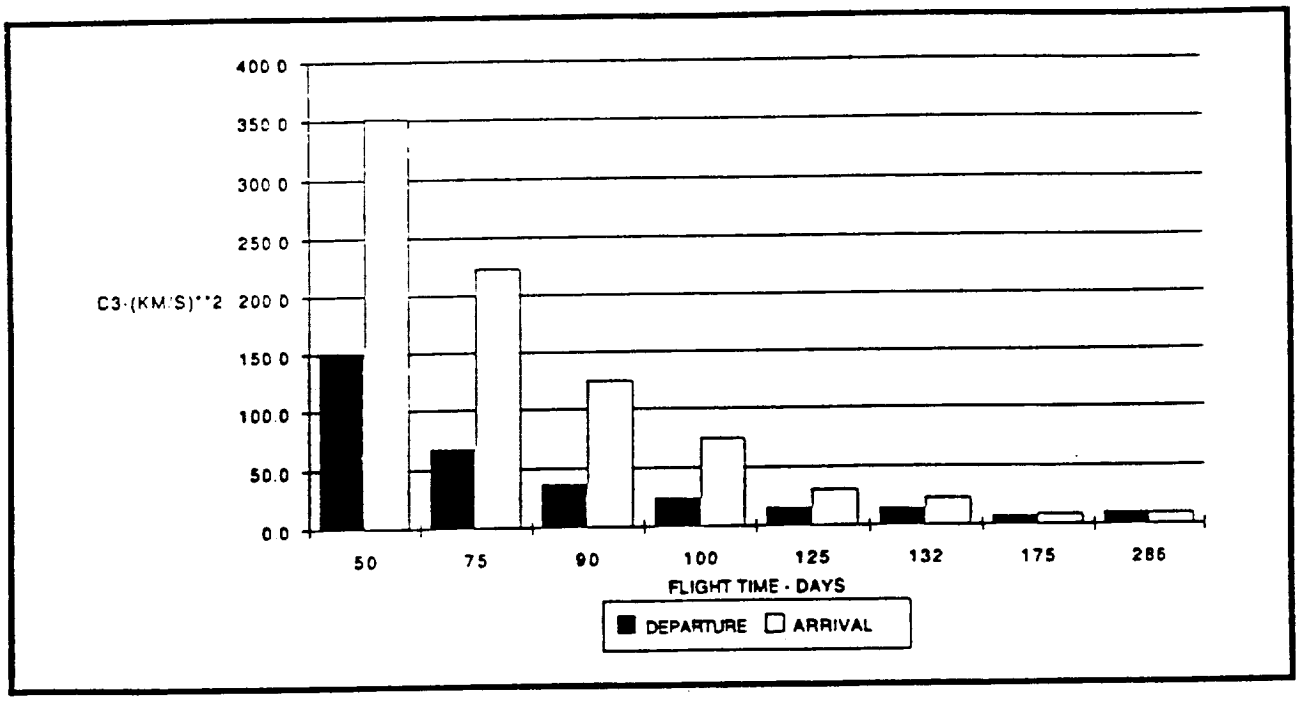

Figure 3.1.2 C3 Sensitivity to Flight Time, Mars to Earth

Tables 3.1.2 through 3.1.7 summarize these trades. These tables contain the orbital parameters, Delta-V's, propulsion systems descriptions, and the various spacecraft elements mass requirements. The Mars Excursion Module (MEM) includes the crew capsule, the aerobrake, the lander structure, and the descent and ascent propulsion system. The crew capsule lands and returns to Mars orbit for rendezvous with the Earth return spacecraft. Mars Delivery/Earth Return total includes all spacecraft elements at Mars encounter required on the mission prior to the Mars Orbit Insertion (MOI). The Mars Departure spacecraft element is that required prior to Mars departure, and includes the interplanetary crew capsule and the required Mars departure propulsion system. The Delta-V's only considered coplanar orbit transfers. The selection of the orbit inclination was considered to be secondary and primarily a mission planning issue which is influenced by the lander site latitude, rendezvous orbit recurrence and the departure asymptote required geometry.

These tables demonstrate, that when the ratio of the MEM return crew capsule mass to the Interplanetary habitat (crew capsule on return to Earth) becomes greater than the ratio (0.36 in this case) of the Isp's of the storable propulsion system to the NTP system, the parking orbit sensitivities begin a reversal. At the lower ratios, the best parking orbit in terms of initial mass required is the highest possible elliptic orbit. This corresponds to MEM mass less than 8.2 Tonnes for an interplanetary habitat (IH) of 23.0 Tonnes. At ratios of 0.38 to 0.50, the parking orbit selection becomes less sensitive. At the larger ratios, the lowest possible orbit is the best. This can be analytically derived. Also at the larger ratios, the initial mass requirements become extreme when compared to the lower ratios.

The above sensitivities would also point to mission scenarios where small ascent to rendezvous spacecraft would provide operational advantages in addition to significant mass advantages. These spacecraft would be individually piloted and add redundancy to the mission spacecraft. In the case of the 5.0 Tonnes crew capsule, these would be about 5 ascent vehicles of 1.0 Tonne each. The surface habitats would have been delivered at an earlier date by separate means. This would limit the MEM aerobrake diameter size to the range of 18 to 48 m. This as opposed to returning the surface habitat to orbit which would require aerobrake diameters on the order of 100 m (Landing the crew habitat on direct hyperbolic entry requires aerobrake diameters on the order of 25 m.). More importantly, the mass required at Mars approach would be about 168 Tonnes as opposed to 506 Tonnes for these respective cases. An additional observation is the lone man mission which would require about 80 Tonnes. This would be only half the mass of the four to five man crew mission with split ascent vehicles as discussed above.

The aerobrake sizing is based on the previous MRSR and TRW IR&D studies. These studies concluded that the preferred ultra-low ballistic coefficient aerobrakes should have ballistic coefficients on the order of 5 to 25 kg/m^2 and nominally 20 kg/m^2. This is also consistent with other recent planetary entry probe studies (Reference 3.6.4) Assuming a hypersonic drag coefficient to be about 1.5, the required circular diameter of the aerobrake can then be computed.

Tables 3.1.2 through 3.1.6 also summarize the requirements for performance of the mission at Mars for the systems other than the aerobrake. These include the Delta-

Vs for Mars orbit insertion, Mars de-orbit, Mars surface landing, Mars orbit ascent and Mars-Earth interplanetary transfer. The related propulsion systems, aerobrakes and lander structural masses are also included in these tables for both the MEM and the Mars Delivery/Earth Return spacecraft at Mars approach. The MEM propulsion system volume represents the fuel (F) volume requirement exclusive of the oxidizer (O). The number of 3m spherical tanks (arbitrary diameter) is inclusive of the oxidizer assuming a O/F ratio of 1. 65. Half the tanks would be fuel, and the other half would be oxidizer. Since fractions of 3m is not reasonable, other sizes need to be sized in the design analysis.

Table 3.1.2 Parking Orbit Trade for a MEM Crew Capsule Mass of 1.0 Tonne

PARAMETER/CASE NO.	1	2	3	4	5	6	7
•PARKING ORBIT							
-PERIAPSIS ALTITUDE - KM	500	500	500	500	500	500	500
-ORBIT PERIOD - HRS	2.1	2.5	5.0	10.0	24.0	48.0	72.0
-SEMI-MAJOR AXIS - KM	3959.3	4447.3	7059.7	11206.6	20088.4	31888.4	41785.6
-APOAPSIS ALTIUDE -KM	631.8	1607.8	6832.6	15126.3	32890.1	56490.0	76284.5
•INTERPLANETARY ENERGY RQMTS							
-ARRIVAL C3 - (KM/S)**2	100.0	100.0	100.0	100.0	100.0	100.0	100.0
-DEPARTURE C3 - (KM/S)**2	20.0	20.0	20.0	20.0	20.0	20.0	20.0
•PROPULSIVE DELTA-V RQMTS - KM/S							
-MARS ORBIT INSERTION	7.0	6.8	6.2	5.9	5.7	5.6	5.5
-MARS SOFT LANDING	0.6	0.6	0.6	0.6	0.6	0.6	0.6
-ENTRY PERIAPSIS LOWERING	0.418	0.384	0.259	0.169	0.096	0.061	0.047
-ASCENT TO RENDEZVOUS	4.12	4.33	4.90	5.22	5.46	5.56	5.60
-MARS DEPARTURE	2.45	2.24	1.67	1.35	1.11	1.01	0.97
•PROPULSION SYSTEM PARAMETERS							
-MARS EXCURSION MODULE							
• ISP - SEC	340.00	340.00	340.00	340.00	340.00	340.00	340.00
•TANKAGE FACTOR	0.15	0.15	0.15	0.15	0.15	0.15	0.15
-MARS PARKING MODULE							
•ISP - SEC	950.00	950.00	950.00	950.00	950.00	950.00	950.00
•TANKAGE FACTOR	0.15	0.15	0.15	0.15	0.15	0.15	0.15
•••MASS PROPERTIES - TONNES							
••MARS EXCURSION MODULE TOTAL	7.54	7.94	9.05	9.70	10.16	10.38	10.46
•CREW CAPSULE	1.00	1.00	1.00	1.00	1.00	1.00	1.00
•AEROBRAKE	0.75	0.79	0.90	0.97	1.02	1.04	1.05
-Aerobrake Dia.(m) at B=20kg/m**2	17.90	18.36	19.60	20.29	20.77	20.99	21.07
•LANDER STRUCTURE	0.58	0.61	0.69	0.74	0.78	0.80	0.80
•PROPULSION SYSTEM	5.22	5.54	6.46	7.00	7.38	7.56	7.62
-Volume -cubic meters	5.18	5.50	6.41	6.94	7.32	7.49	7.56
-Number of 3m sphere tanks O/F	0.28	0.29	0.34	0.37	0.39	0.40	0.40
••MARS DELIVERY/EARTH RETURN TOTA	97.28	94.46	87.36	83.65	81.15	80.06	79.63
•CREW CAPSULE	21.00	21.00	21.00	21.00	21.00	21.00	21.00
•PROPULSION SYSTEM	68.74	65.53	57.31	52.95	49.99	48.69	48.17
••MARS DEPARTURE	31.97	31.28	29.46	28.47	27.78	27.47	27.35

Table 3.1.3 Parking Orbit Trade for a MEM Crew Capsule Mass of 5.0 Tonne

PARAMETER/CASE NO.	1	2	3	4	5	6	7
•PARKING ORBIT							
-PERIAPSIS ALTITUDE - KM	500	500	500	500	500	500	500
-ORBIT PERIOD - HRS	2.1	2.5	5.0	10.0	24.0	48.0	72.0
-SEMI-MAJOR AXIS - KM	3959.3	4447.3	7059.7	11206.6	20088.4	31888.4	41785.6
-APOAPSIS ALTIUDE -KM	631.8	1607.8	6832.6	15126.3	32890.1	56490.0	76284.5
•INTERPLANETARY ENERGY RQMTS							
-ARRIVAL C3 - (KM/S)**2	100.0	100.0	100.0	100.0	100.0	100.0	100.0
-DEPARTURE C3 - (KM/S)**2	20.0	20.0	20.0	20.0	20.0	20.0	20.0
•PROPULSIVE DELTA-V RQMTS - KM/S							
-MARS ORBIT INSERTION	7.0	6.8	6.2	5.9	5.7	5.6	5.5
-MARS SOFT LANDING	0.6	0.6	0.6	0.6	0.6	0.6	0.6
-ENTRY PERIAPSIS LOWERING	0.418	0.384	0.259	0.169	0.096	0.061	0.047
-ASCENT TO RENDEZVOUS	4.12	4.33	4.90	5.22	5.46	5.56	5.60
-MARS DEPARTURE	2.45	2.24	1.67	1.35	1.11	1.01	0.97
•PROPULSION SYSTEM PARAMETERS							
-MARS EXCURSION MODULE							
• ISP - SEC	340.00	340.00	340.00	340.00	340.00	340.00	340.00
•TANKAGE FACTOR	0.15	0.15	0.15	0.15	0.15	0.15	0.15
-MARS PARKING MODULE							
•ISP - SEC	950.00	950.00	950.00	950.00	950.00	950.00	950.00
•TANKAGE FACTOR	0.15	0.15	0.15	0.15	0.15	0.15	0.15
•••MASS PROPERTIES - TONNES							
••MARS EXCURSION MODULE TOTAL	37.71	39.68	45.24	48.48	50.82	51.88	52.30
•CREW CAPSULE	5.00	5.00	5.00	5.00	5.00	5.00	5.00
•AEROBRAKE	3.77	3.97	4.52	4.85	5.08	5.19	5.23
-Aerobrake Dia.(m) at B=20kg/m**2	40.02	41.05	43.83	45.37	46.45	46.93	47.12
•LANDER STRUCTURE	2.89	3.04	3.47	3.72	3.90	3.98	4.01
•PROPULSION SYSTEM	26.09	27.72	32.30	34.98	36.90	37.78	38.12
-Volume -cubic meters	25.88	27.50	32.04	34.70	36.61	37.47	37.82
-Number of 3m sphere tanks O/F	1.38	1.47	1.71	1.85	1.96	2.00	2.02
••MARS DELIVERY/EARTH RETURN TOTA	171.54	170.93	169.45	168.66	168.10	167.85	167.74
•CREW CAPSULE	21.00	21.00	21.00	21.00	21.00	21.00	21.00
•PROPULSION SYSTEM	112.83	110.24	103.21	99.18	96.29	94.97	94.45
••MARS DEPARTURE	31.97	31.28	29.46	28.47	27.78	27.47	27.35

Table 3.1.4 Parking Orbit Trade for a MEM Crew Capsule Mass of 8.2 Tonne

PARAMETER/CASE NO.	1	2	3	4	5	6	7
•PARKING ORBIT							
-PERIAPSIS ALTITUDE - KM	500	500	500	500	500	500	500
-ORBIT PERIOD - HRS	2.1	2.5	5.0	10.0	24.0	48.0	72.0
-SEMI-MAJOR AXIS - KM	3959.3	4447.3	7059.7	11206.6	20088.4	31888.4	41785.6
-APOAPSIS ALTIUDE -KM	631.8	1607.8	6832.6	15126.3	32890.1	56490.0	76284.5
•INTERPLANETARY ENERGY RQMTS							
-ARRIVAL C3 - (KM/S)**2	100.0	100.0	100.0	100.0	100.0	100.0	100.0
-DEPARTURE C3 - (KM/S)**2	20.0	20.0	20.0	20.0	20.0	20.0	20.0
•PROPULSIVE DELTA-V RQMTS - KM/S							
-MARS ORBIT INSERTION	7.0	6.8	6.2	5.9	5.7	5.6	5.5
-MARS SOFT LANDING	0.6	0.6	0.6	0.6	0.6	0.6	0.6
-ENTRY PERIAPSIS LOWERING	0.418	0.384	0.259	0.169	0.096	0.061	0.047
-ASCENT TO RENDEZVOUS	4.12	4.33	4.90	5.22	5.46	5.56	5.60
-MARS DEPARTURE	2.45	2.24	1.67	1.35	1.11	1.01	0.97
•PROPULSION SYSTEM PARAMETERS							
-MARS EXCURSION MODULE							
• ISP - SEC	340.00	340.00	340.00	340.00	340.00	340.00	340.00
•TANKAGE FACTOR	0.15	0.15	0.15	0.15	0.15	0.15	0.15
-MARS PARKING MODULE							
•ISP - SEC	950.00	950.00	950.00	950.00	950.00	950.00	950.00
•TANKAGE FACTOR	0.15	0.15	0.15	0.15	0.15	0.15	0.15
•••MASS PROPERTIES - TONNES							
••MARS EXCURSION MODULE TOTAL	61.84	65.08	74.19	79.51	83.34	85.08	85.77
•CREW CAPSULE	8.20	8.20	8.20	8.20	8.20	8.20	8.20
•AEROBRAKE	6.18	6.51	7.42	7.95	8.33	8.51	8.58
-Aerobrake Dia.(m) at B=20kg/m**2	51.25	52.57	56.13	58.11	59.49	60.11	60.35
•LANDER STRUCTURE	4.74	4.99	5.69	6.10	6.39	6.53	6.58
•PROPULSION SYSTEM	42.80	45.46	52.97	57.37	60.52	61.95	62.52
-Volume -cubic meters	42.45	45.10	52.55	56.90	60.03	61.45	62.02
-Number of 3m sphere tanks O/F	2.27	2.41	2.81	3.04	3.21	3.28	3.31
••MARS DELIVERY/EARTH RETURN TOTA	230.96	232.10	235.12	236.68	237.67	238.08	238.23
•CREW CAPSULE	21.00	21.00	21.00	21.00	21.00	21.00	21.00
•PROPULSION SYSTEM	148.11	146.02	139.93	136.16	133.33	132.00	131.46
••MARS DEPARTURE	31.97	31.28	29.46	28.47	27.78	27.47	27.35

Table 3.1.5 Parking Orbit Trade for a MEM Crew Capsule Mass of 11.5 Tonne

PARAMETER/CASE NO.	1	2	3	4	5	6	7
•PARKING ORBIT							
-PERIAPSIS ALTITUDE - KM	500	500	500	500	500	500	500
-ORBIT PERIOD - HRS	2.1	2.5	5.0	10.0	24.0	48.0	72.0
-SEMI-MAJOR AXIS - KM	3959.3	4447.3	7059.7	11206.6	20088.4	31888.4	41785.6
-APOAPSIS ALTIUDE -KM	631.8	1607.8	6832.6	15126.3	32890.1	56490.0	76284.5
•INTERPLANETARY ENERGY RQMTS							
-ARRIVAL C3 - (KM/S)**2	100.0	100.0	100.0	100.0	100.0	100.0	100.0
-DEPARTURE C3 - (KM/S)**2	20.0	20.0	20.0	20.0	20.0	20.0	20.0
•PROPULSIVE DELTA-V RQMTS - KM/S							
-MARS ORBIT INSERTION	7.0	6.8	6.2	5.9	5.7	5.6	5.5
-MARS SOFT LANDING	0.6	0.6	0.6	0.6	0.6	0.6	0.6
-ENTRY PERIAPSIS LOWERING	0.418	0.384	0.259	0.169	0.096	0.061	0.047
-ASCENT TO RENDEZVOUS	4.12	4.33	4.90	5.22	5.46	5.56	5.60
-MARS DEPARTURE	2.45	2.24	1.67	1.35	1.11	1.01	0.97
•PROPULSION SYSTEM PARAMETERS							
-MARS EXCURSION MODULE							
• ISP - SEC	340.00	340.00	340.00	340.00	340.00	340.00	340.00
•TANKAGE FACTOR	0.15	0.15	0.15	0.15	0.15	0.15	0.15
-MARS PARKING MODULE							
•ISP - SEC	950.00	950.00	950.00	950.00	950.00	950.00	950.00
•TANKAGE FACTOR	0.15	0.15	0.15	0.15	0.15	0.15	0.15
•••MASS PROPERTIES - TONNES							
••MARS EXCURSION MODULE TOTAL	86.73	91.27	104.04	111.51	116.88	119.32	120.29
•CREW CAPSULE	11.50	11.50	11.50	11.50	11.50	11.50	11.50
•AEROBRAKE	8.67	9.13	10.40	11.15	11.69	11.93	12.03
-Aerobrake Dia.(m) at B=20kg/m**2	60.69	62.26	66.47	68.81	70.45	71.18	71.47
•LANDER STRUCTURE	6.65	7.00	7.98	8.55	8.97	9.15	9.23
•PROPULSION SYSTEM	60.02	63.76	74.29	80.45	84.88	86.88	87.68
-Volume -cubic meters	59.54	63.25	73.69	79.80	84.19	86.19	86.98
-Number of 3m sphere tanks O/F	3.18	3.38	3.94	4.26	4.50	4.60	4.65
••MARS DELIVERY/EARTH RETURN TOTA	292.23	295.18	302.85	306.81	309.40	310.50	310.92
•CREW CAPSULE	21.00	21.00	21.00	21.00	21.00	21.00	21.00
•PROPULSION SYSTEM	184.49	182.91	177.80	174.30	171.52	170.18	169.64
••MARS DEPARTURE	31.97	31.28	29.46	28.47	27.78	27.47	27.35

Table 3.1.6 Parking Orbit Trade for a MEM Crew Capsule Mass of 21.0 Tonne

PARAMETER/CASE NO.	1	2	3	4	5	6	7
•PARKING ORBIT							
-PERIAPSIS ALTITUDE - KM	500	500	500	500	500	500	500
-ORBIT PERIOD - HRS	2.1	2.5	5.0	10.0	24.0	48.0	72.0
-SEMI-MAJOR AXIS - KM	3959.3	4447.3	7059.7	11206.6	20088.4	31888.4	41785.6
-APOAPSIS ALTIUDE -KM	631.8	1607.8	6832.6	15126.3	32890.1	56490.0	76284.5
•INTERPLANETARY ENERGY RQMTS							
-ARRIVAL C3 - (KM/S)**2	100.0	100.0	100.0	100.0	100.0	100.0	100.0
-DEPARTURE C3 - (KM/S)**2	20.0	20.0	20.0	20.0	20.0	20.0	20.0
•PROPULSIVE DELTA-V RQMTS - KM/S							
-MARS ORBIT INSERTION	7.0	6.8	6.2	5.9	5.7	5.6	5.5
-MARS SOFT LANDING	0.6	0.6	0.6	0.6	0.6	0.6	0.6
-ENTRY PERIAPSIS LOWERING	0.418	0.384	0.259	0.169	0.096	0.061	0.047
-ASCENT TO RENDEZVOUS	4.12	4.33	4.90	5.22	5.46	5.56	5.60
-MARS DEPARTURE	2.45	2.24	1.67	1.35	1.11	1.01	0.97
•PROPULSION SYSTEM PARAMETERS							
-MARS EXCURSION MODULE							
• ISP - SEC	340.00	340.00	340.00	340.00	340.00	340.00	340.00
•TANKAGE FACTOR	0.15	0.15	0.15	0.15	0.15	0.15	0.15
-MARS PARKING MODULE							
•ISP - SEC	950.00	950.00	950.00	950.00	950.00	950.00	950.00
•TANKAGE FACTOR	0.15	0.15	0.15	0.15	0.15	0.15	0.15
•••MASS PROPERTIES - TONNES							
••MARS EXCURSION MODULE TOTAL	158.38	166.67	189.99	203.63	213.43	217.88	219.65
•CREW CAPSULE	21.00	21.00	21.00	21.00	21.00	21.00	21.00
•AEROBRAKE	15.84	16.67	19.00	20.36	21.34	21.79	21.97
-Aerobrake Dia.(m) at B=20kg/m**2	82.01	84.13	89.82	92.99	95.20	96.19	96.58
•LANDER STRUCTURE	12.15	12.78	14.57	15.62	16.37	16.71	16.85
•PROPULSION SYSTEM	109.60	116.43	135.66	146.91	154.99	158.66	160.12
-Volume -cubic meters	108.72	115.50	134.57	145.73	153.75	157.38	158.83
-Number of 3m sphere tanks O/F	5.81	6.17	7.19	7.78	8.21	8.41	8.48
••MARS DELIVERY/EARTH RETURN TOTA	468.61	476.78	497.82	508.73	515.91	518.99	520.19
•CREW CAPSULE	21.00	21.00	21.00	21.00	21.00	21.00	21.00
•PROPULSION SYSTEM	289.23	289.11	286.82	284.09	281.48	280.11	279.54
••MARS DEPARTURE	31.97	31.28	29.46	28.47	27.78	27.47	27.35

Table 3.1.7 Parking Orbit Trade for a MEM Crew Capsule Mass of 23.0 Tonne

PARAMETER/CASE NO.	1	2	3	4	5	6	7
•PARKING ORBIT							
-PERIAPSIS ALTITUDE - KM	500	500	500	500	500	500	500
-ORBIT PERIOD - HRS	2.1	2.5	5.0	10.0	24.0	48.0	72.0
-SEMI-MAJOR AXIS - KM	3959.3	4447.3	7059.7	11206.6	20088.4	31888.4	41785.6
-APOAPSIS ALTIUDE -KM	631.8	1607.8	6832.6	15126.3	32890.1	56490.0	76284.5
•INTERPLANETARY ENERGY RQMTS							
-ARRIVAL C3 - (KM/S)**2	100.0	100.0	100.0	100.0	100.0	100.0	100.0
-DEPARTURE C3 - (KM/S)**2	20.0	20.0	20.0	20.0	20.0	20.0	20.0
•PROPULSIVE DELTA-V RQMTS - KM/S							
-MARS ORBIT INSERTION	7.0	6.8	6.2	5.9	5.7	5.6	5.5
-MARS SOFT LANDING	0.6	0.6	0.6	0.6	0.6	0.6	0.6
-ENTRY PERIAPSIS LOWERING	0.418	0.384	0.259	0.169	0.096	0.061	0.047
-ASCENT TO RENDEZVOUS	4.12	4.33	4.90	5.22	5.46	5.56	5.60
-MARS DEPARTURE	2.45	2.24	1.67	1.35	1.11	1.01	0.97
•PROPULSION SYSTEM PARAMETERS							
-MARS EXCURSION MODULE							
• ISP - SEC	340.00	340.00	340.00	340.00	340.00	340.00	340.00
•TANKAGE FACTOR	0.15	0.15	0.15	0.15	0.15	0.15	0.15
-MARS PARKING MODULE							
•ISP - SEC	950.00	950.00	950.00	950.00	950.00	950.00	950.00
•TANKAGE FACTOR	0.15	0.15	0.15	0.15	0.15	0.15	0.15
•••MASS PROPERTIES - TONNES							
••MARS EXCURSION MODULE TOTAL	173.47	182.55	208.09	223.03	233.76	238.63	240.57
•CREW CAPSULE	23.00	23.00	23.00	23.00	23.00	23.00	23.00
•AEROBRAKE	17.35	18.25	20.81	22.30	23.38	23.86	24.06
-Aerobrake Dia.(m) at B=20kg/m**2	85.82	88.04	94.00	97.32	99.63	100.66	101.07
•LANDER STRUCTURE	13.31	14.00	15.96	17.11	17.93	18.30	18.45
•PROPULSION SYSTEM	120.04	127.52	148.58	160.90	169.75	173.77	175.37
-Volume -cubic meters	119.07	126.50	147.39	159.61	168.39	172.37	173.96
-Number of 3m sphere tanks O/F	6.36	6.76	7.87	8.53	8.99	9.21	9.29
••MARS DELIVERY/EARTH RETURN TOTA	505.74	515.02	538.86	551.23	559.39	562.89	564.24
•CREW CAPSULE	21.00	21.00	21.00	21.00	21.00	21.00	21.00
•PROPULSION SYSTEM	311.28	311.47	309.77	307.20	304.63	303.25	302.67
••MARS DEPARTURE	31.97	31.28	29.46	28.47	27.78	27.47	27.35

3.2 MARS ENTRY INTERFACE DELIVERY

Selection of the entry interface flight path angle is driven by the g load constraints and the minimization of the target error dispersion at terminal descent. The latter would suggest the steepest entry and the former constrains the steepness. Also, a factor is the delivery accuracy, since the steepness must be biased by this amount. Out of orbit entry does not pose a problem in meeting the 5 to 6 g load constraint for a either a ballistic or lifting entry. On hyperbolic entry, though, the ballistic concept can not meet this constraint at all. A lifting entry is very much required. The amount of lift required is dictated by the hyperbolic excess velocity at planetary encounter.

The constraint of 5 to 6 g's does not apply to either equipment, freight, habitats and other logistical supplies. This would then allow ballistic concepts to be considered for delivery of these items on direct hyperbolic entry.

The delivery accuracy considered was of the same order of magnitude as that projected in the unmanned missions using Earth ground based navigation. It is perceived that an improvement might be possible as manned missions are staged. Order of magnitude improvements are expected during terminal descent as the lander approaches the Mars surface expeditionary staging area. The entry accuracies noted in the literature (References 3.6.5, 3.6.6, 3.6.7, etc.) suggest that on hyperbolic approach entry flight path angle dispersions (Table 3.3.1) of about 0.6 degrees (12 km B-plane) are expected. Out of Mars orbit, the orbit determination suggest 0.03 degrees (1 km). These are 3 sigma estimates.

3.2.1 Analysis

Entry trajectories were simulated with the above constraint and delivery dispersions to arrive at the entry interface delivery requirements. Table 3.2.1 summarizes the results. As a comparison, aeromaneuvering results are also included. The hyperbolic entry results for the ballistic aerobrake assumed a 40 g constraint. The basis for this constraint was arbitrary. The important things to note are the short flight times, low pressure loading and low skin surface temperatures associated with the ballistic aerobrakes. This is due to the high altitude deceleration.

The entry configuration for the aerobrake is in all cases a ballistic zero angle of attack approach with a ballistic coefficient of about 20 kg/m^2. The aeromaneuvering configuration is flown at an angle of attack for flight at maximum lift coefficient (C_{Lmax}) which also results in the minimum achievable ballistic coefficient for a non-sphere-cone lifting vehicle. Flight at minimum ballistic coefficient is highly desirable at Mars for entry to landing due to the very tenuous atmosphere. The aeromaneuvering vehicle considered in this analysis had a ballistic coefficient of 183 kg/m^2 at a Lift to Drag (L/D) ratio of 0.55 and C_{Lmax} of 0.5.

3.2.2 Requirements Summary

There are no specific requirements that can be identified.

Table 3.2.1 Entry Trajectory Summary for Aerobrakes and Aeromaneuvering Systems at Orbital and Hyperbolic Entry

ENTRY TRAJECTORY	Ve - km/sec	γ - deg	$\Delta\gamma$ -deg	Peak g's	Peak Q-mbar	Peak Surface Temp - K deg	Flight Time -sec
Aerobrake Orbital entry - LMO	3.5	-15.0	0.03	6	9.5	1100	242
Aerobrake Orbital entry - 1Sol	4.6	-10.0	0.03	5	6.0	1358	341
Aerobrake Hyperbolic entry - Low C3	5.8	-21.0	0.60	24	27.0	1800	300
Aerobrake Hyperbolic entry - Hi C3	7.2	-21.0	0.60	36	40.0	2600	300
Aeromaneuver Orbital entry - LMO	3.5	-4.0	0.03	1	14.2	1089	920
Aeromaneuver Hyperbolic entry	8	-13.5	0.60	7	224.0	2644	2000

3.3 MARS AEROBRAKE ENTRY

The aerobrake entry phase is primarily dominated by the trajectory between 125 to 10 km altitude. This is inclusive of the peak deceleration to near terminal conditions. Ballistic aerobrakes generally exhibit a relatively short deceleration to near terminal conditions (falling vertically at a flight path angle of about 90 degrees), as opposed to lifting aeromanueuvering entry which tends to glide at near horizontal flight path. The aerobrakes will exhibit much lower (order of magnitude) speeds at 10 km altitudes than aeromaneuvering entry.

3.3.1 Analysis

Conserving the dispersions at the altitude where terminal descent over a target area would be initiated is an important aspect of the aerobrake phase. These dispersions will normally be reduced using propulsive maneuvering. Estimates of these dispersions for the tall error poles are shown in Table 3.3.1. This includes estimates for aerobrakes and aeromaneuvering systems, and orbital and hyperbolic entry as points of comparison. The important thing to note is that for equivalent error source the aerobrake delivery performance is equivalent to an aeromaneuvering system (This only applies to entry-to-landing, not aerocapture!). This has also been seen at Earth for both military and civilian applications where the prime objective is delivery accuracy and not ranging to a target. It can also be noted, that due to the quick deceleration, atmospheric perturbations do not inhibit performance. In ICBM applications, the atmosphere is nothing more than a bias rather than an error source. Also, it should be noted that the initial entry is a rolling entry which results in no significant trajectory deviation from nominal due to lift that could result from small center of mass variations.

Figure 3.3.1 shows a time history of the ballistic aerobrake for entry at 3.5 km/sec. The characteristics are generally the same for entry from orbit or hyperbolic approach. The state at about 10 km will be a near terminal descent at 120 m/sec for a ballistic coefficient of about 20 kg/m^2. This terminal speed will only vary with the ballistic coefficient for a given atmosphere. The equivalent aeromaneuvering trajectory is shown in Figure 3.3.2. The thing to note is the long gliding trajectory and the much higher speed at 10 km altitude (700 m/sec).

Table 3.3.1 Target Site Error Analyses for Aerobrakes and Aeromaneuvering Systems for Orbital and Hyperbolic Entry

AEROBRAKE ORBITAL ENTRY		
ERROR SOURCE		TARGET MISS
DESCRIPTION	REFERENCE VALUE	3 SIGMA CEP - KM
NAVIGATION KNOWLEDGE	1 KM IN POSITION	1
ENTRY FLIGHT PATH ANGLE DELIVERY	.03 DEGREE	1
ATMOSPHERIC DENSITY UNCERTAINTY	COSPAR HIGH, LOW	1
DRAG UNCERTAINTY	5 PERCENT	2
WINDS	10 M/SEC	1
	RSS	3
AEROMANEUVER ORBITAL ENTRY		
ERROR SOURCE		TARGET MISS
DESCRIPTION	REFERENCE VALUE	3 SIGMA CEP - KM
NAVIGATION KNOWLEDGE	1 KM IN POSITION	3
ENTRY FLIGHT PATH ANGLE DELIVERY	.03 DEGREE	1
ATMOSPHERIC DENSITY UNCERTAINTY	COSPAR HIGH, LOW	1
DRAG UNCERTAINTY	5 PERCENT	1
WINDS	10 M/SEC	1
	RSS	4
AEROBRAKE HYPERBOLIC ENTRY		
ERROR SOURCE		TARGET MISS
DESCRIPTION	REFERENCE VALUE	3 SIGMA CEP - KM
NAVIGATION KNOWLEDGE	22 KM IN POSITION	22
ENTRY FLIGHT PATH ANGLE DELIVERY	.6 DEGREE	14
ATMOSPHERIC DENSITY UNCERTAINTY	COSPAR HIGH, LOW	6
DRAG UNCERTAINTY	5 PERCENT	0
WINDS	10 M/SEC	0
	RSS	27
AEROMANEUVER HYPERBOLIC ENTRY		
ERROR SOURCE		TARGET MISS
DESCRIPTION	REFERENCE VALUE	3 SIGMA CEP - KM
NAVIGATION KNOWLEDGE	22 KM IN POSITION	22
ENTRY FLIGHT PATH ANGLE DELIVERY	.6 DEGREE	5
ATMOSPHERIC DENSITY UNCERTAINTY	COSPAR HIGH, LOW	10
DRAG UNCERTAINTY	5 PERCENT	1
WINDS	10 M/SEC	1
	RSS	25

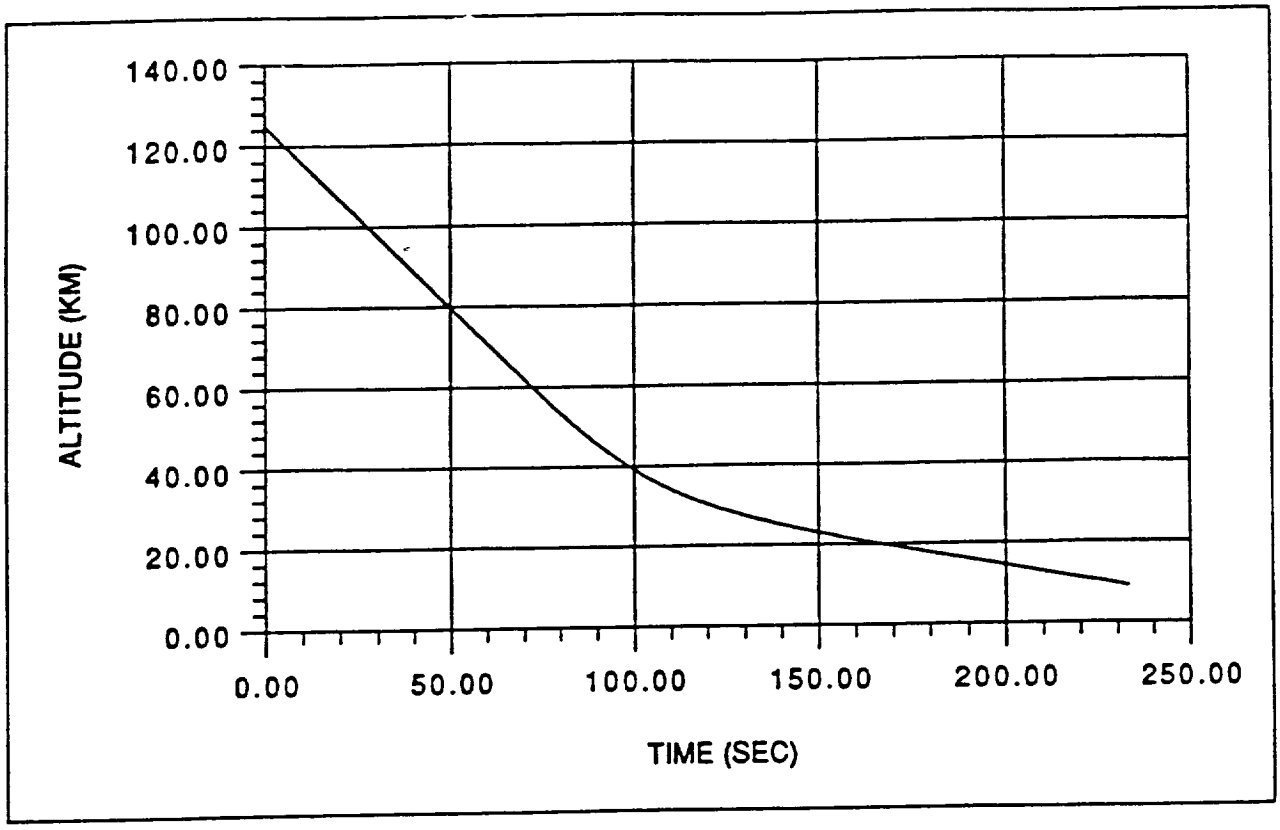

Figure 3.3.1.a Mars Aerobrake Nominal Trajectory Altitude History

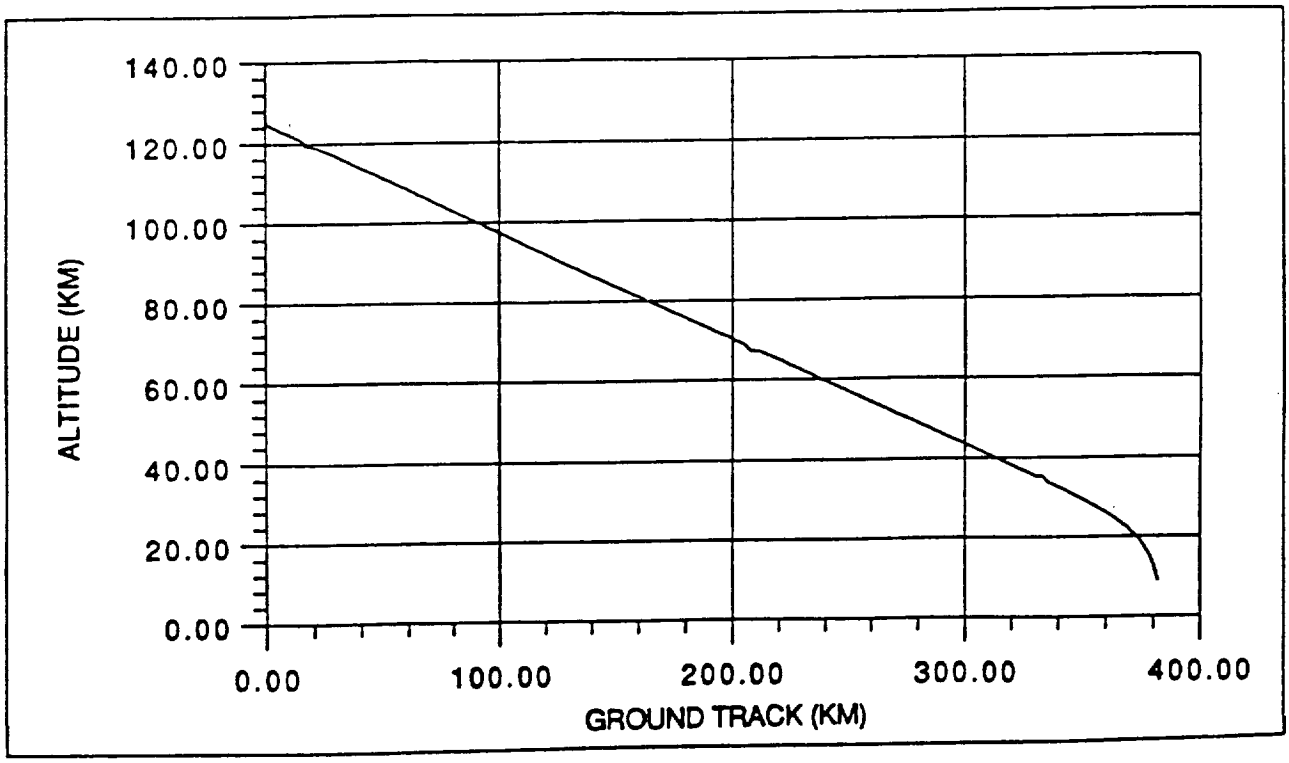

Figure 3.3.1.b Mars Aerobrake Nominal Trajectory Ground Track History

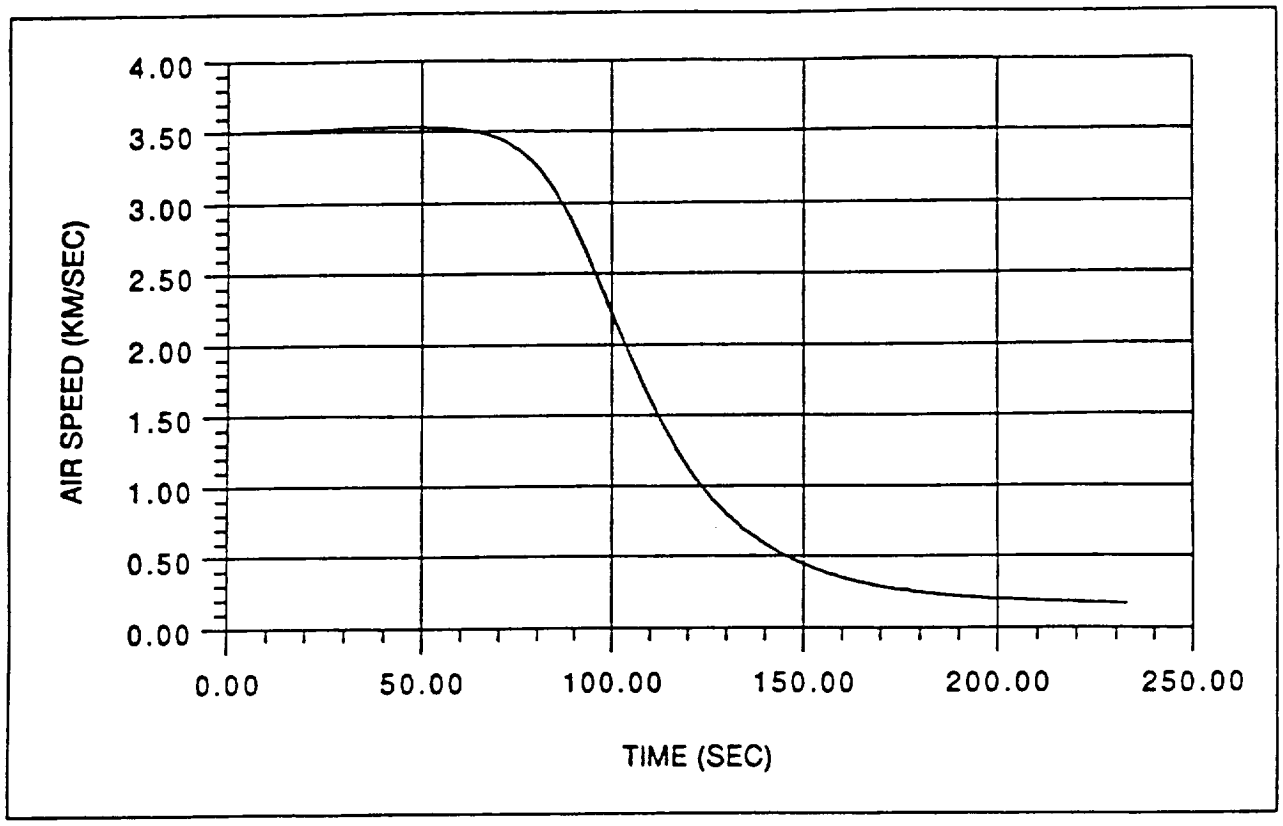

Figure 3.3.1.c Mars Aerobrake Nominal Trajectory Velocity History

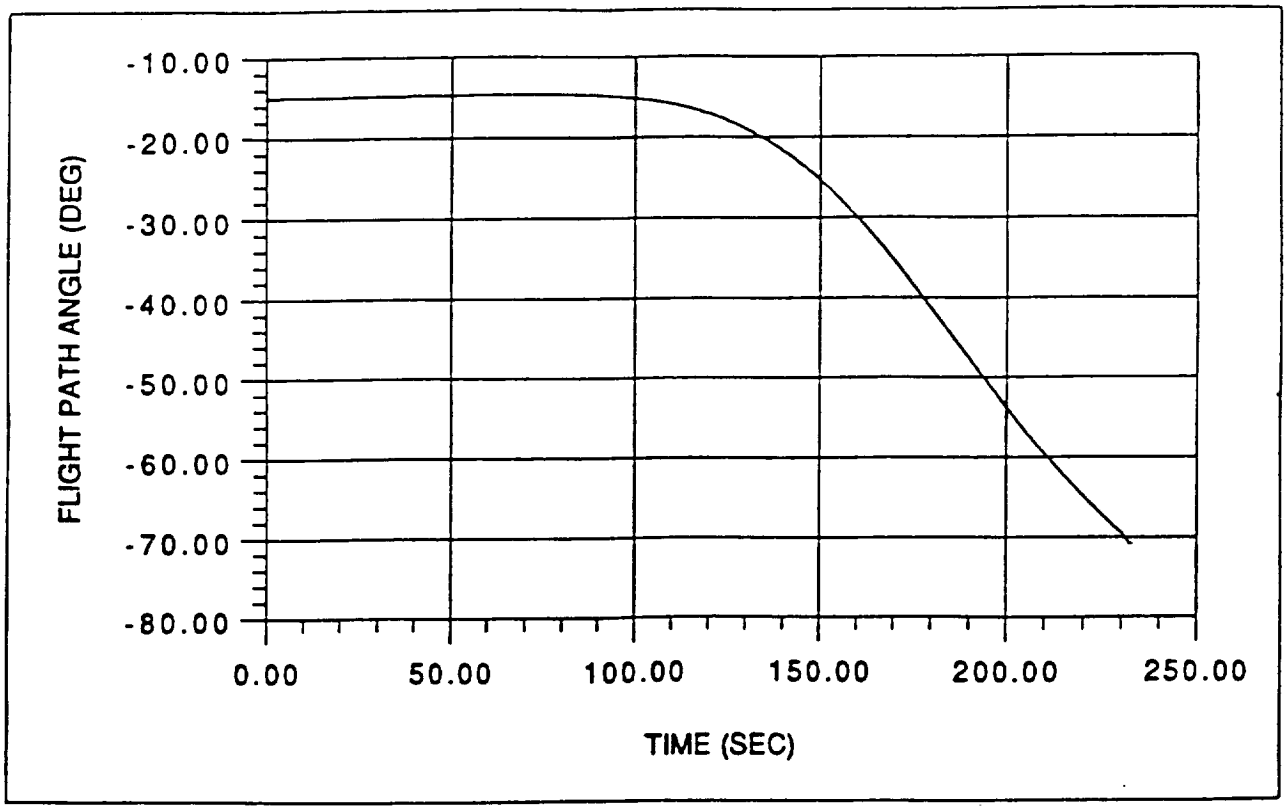

Figure 3.3.1.d Mars Aerobrake Nominal Trajectory Flight Path History

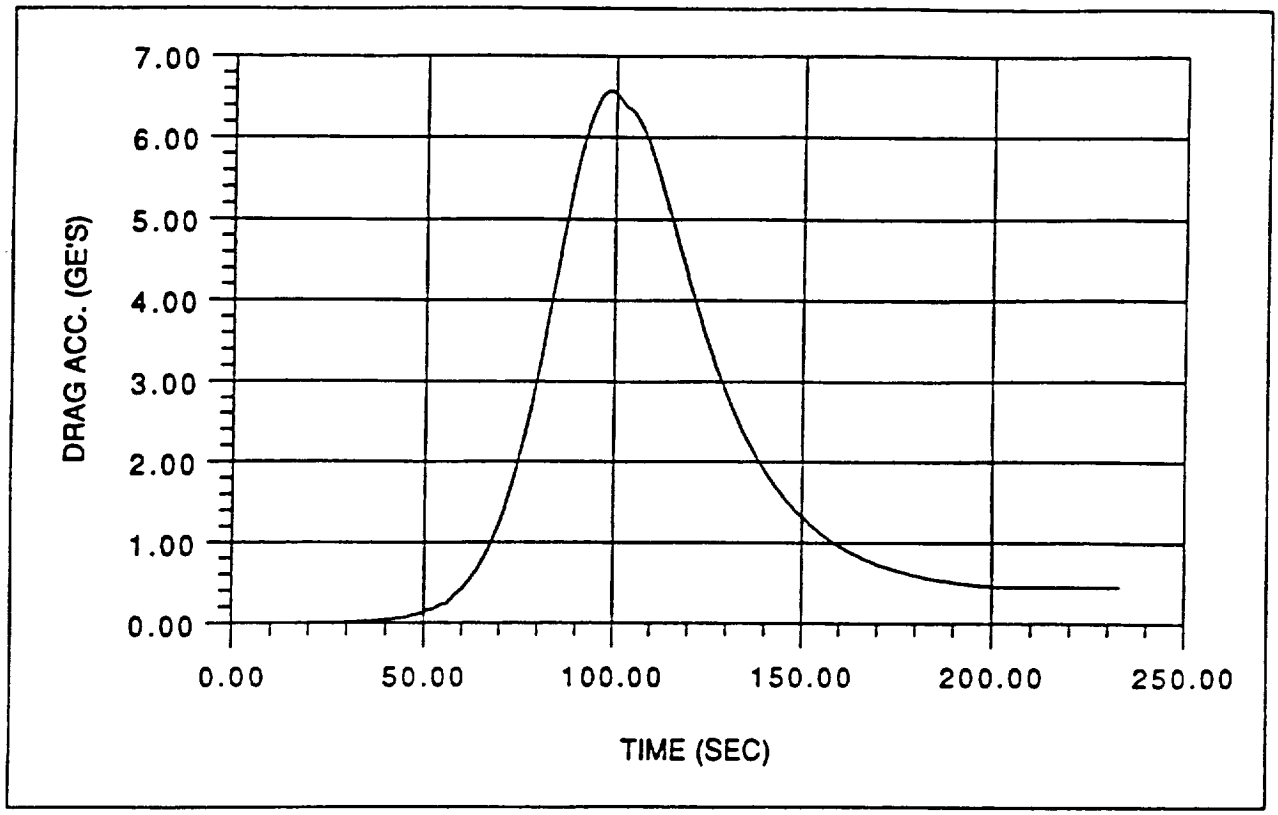

Figure 3.3.1.e Mars Aerobrake Nominal Trajectory Drag History

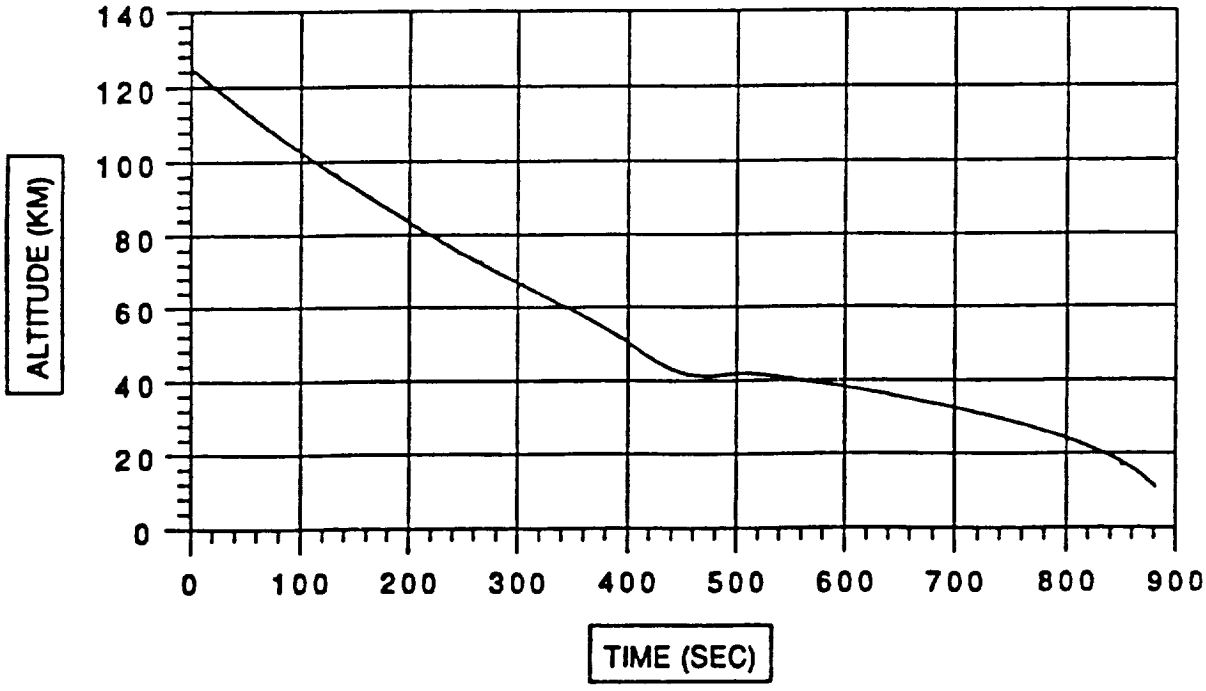

Figure 3.3.2.a Mars Aeromaneuvering Nominal Trajectory Altitude History

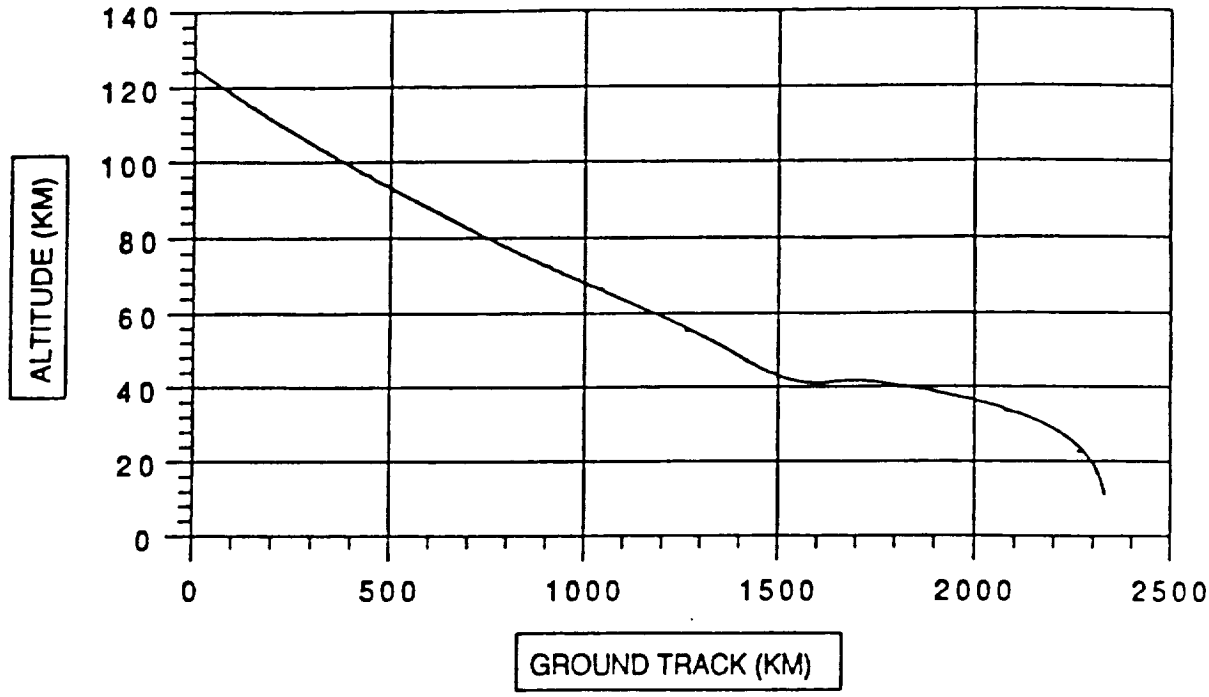

Figure 3.3.2.b Mars Aeromaneuvering Nominal Trajectory Ground Track History

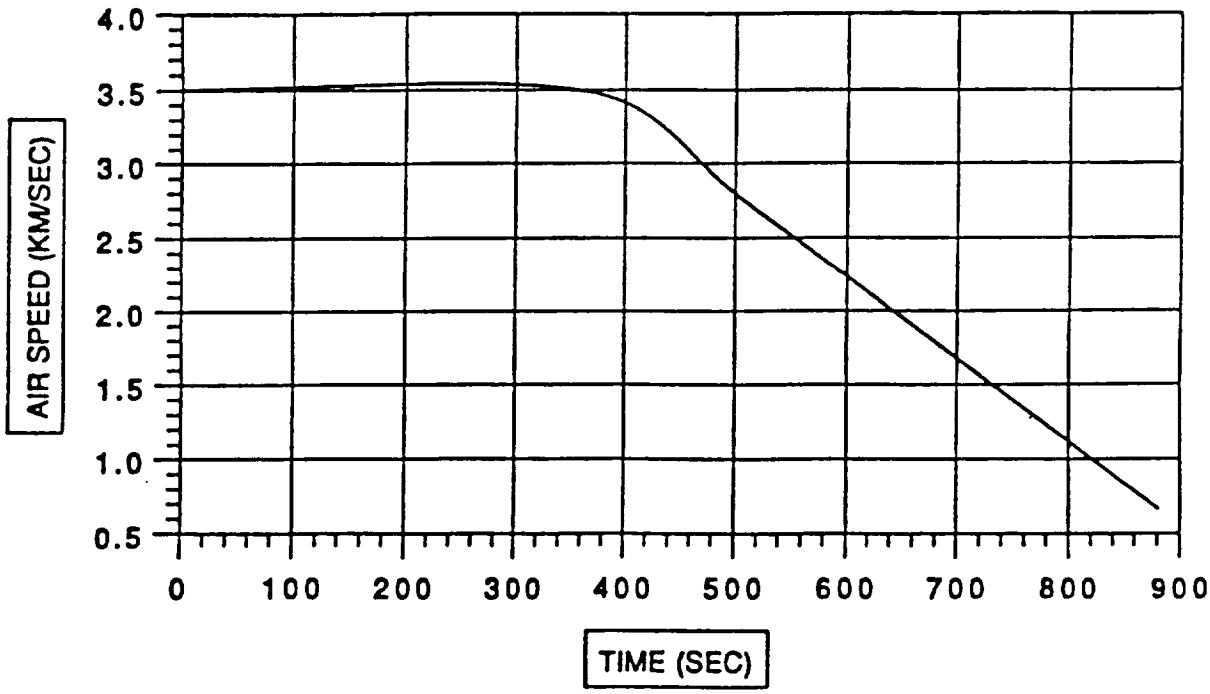

Figure 3.3.2.c Mars Aeromaneuvering Nominal Trajectory Velocity History

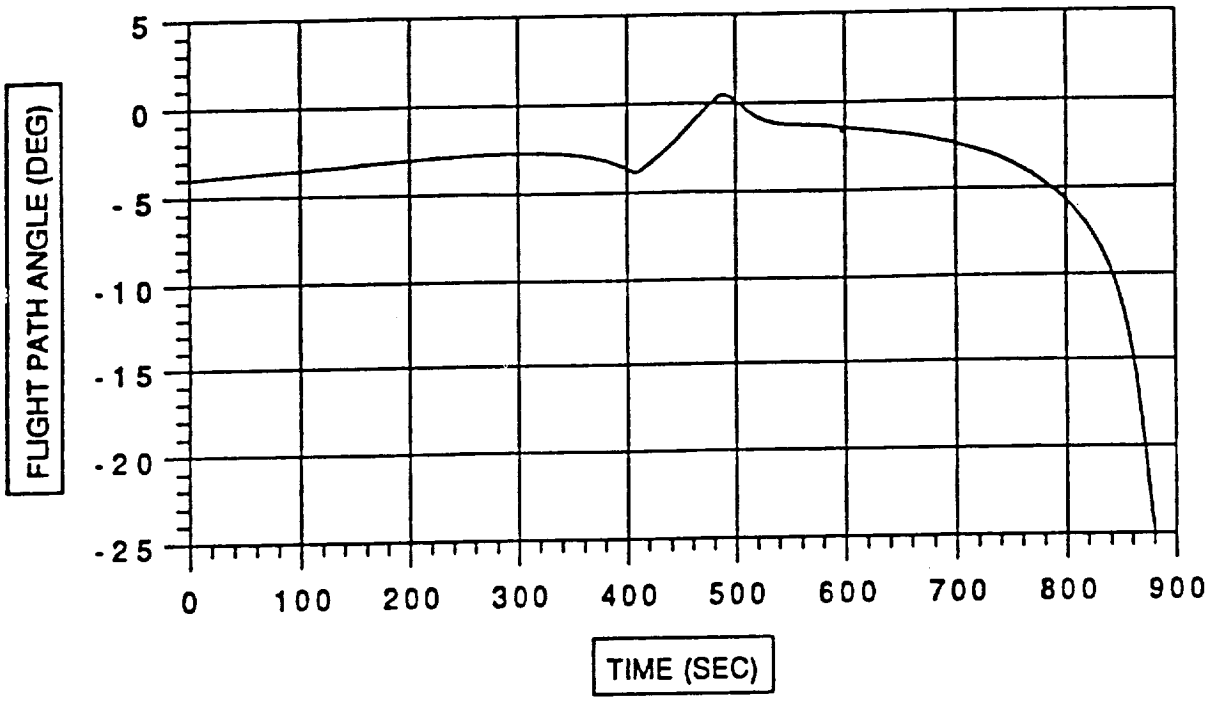

Figure 3.3.2.d Mars Aeromaneuvering Nominal Trajectory Flight Path History

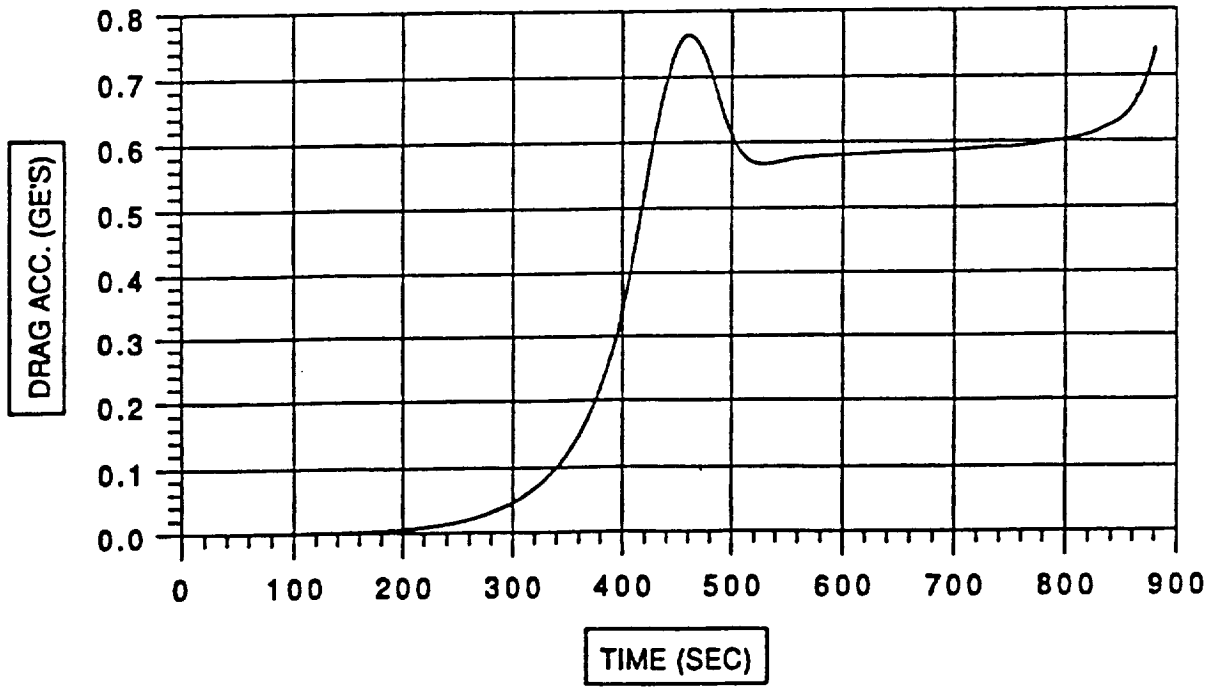

Figure 3.3.2.e Mars Aeromaneuvering Nominal Trajectory Drag History

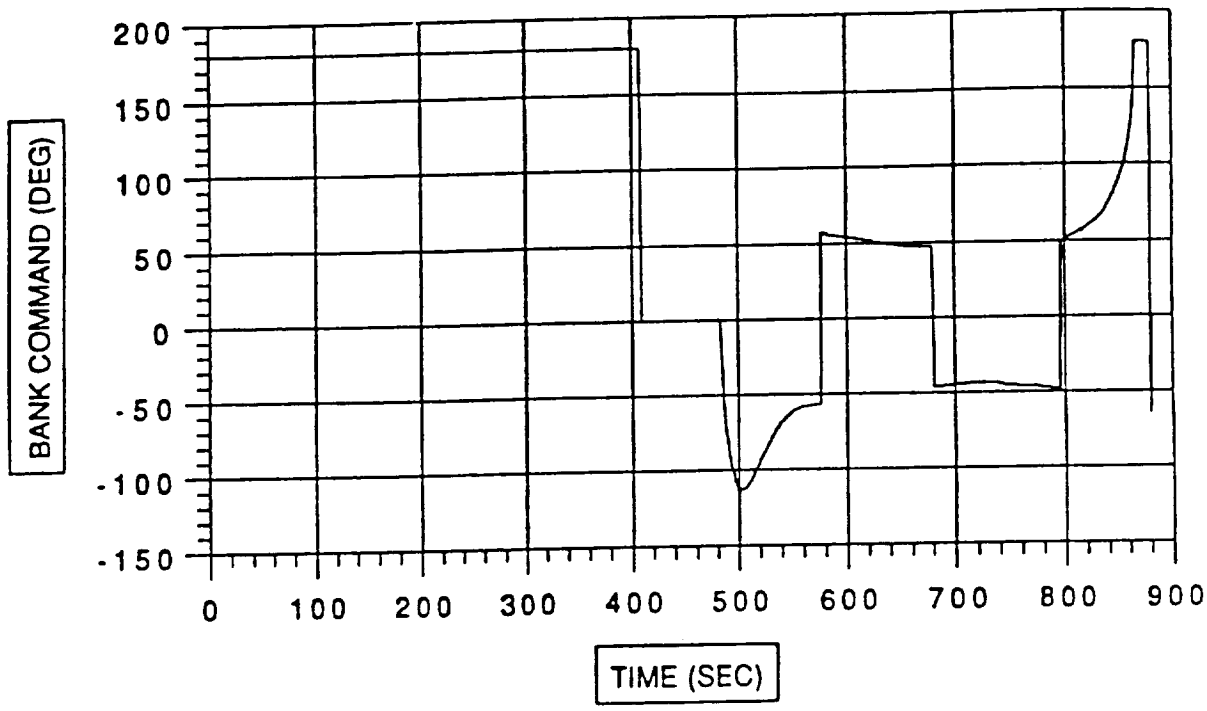

Figure 3.3.2.f Mars Aeromaneuvering Nominal Trajectory Bank Command History

3.3.2 Requirements Summary

Aerobrakes provide significant advantages over an aeromaneuvering system for entry to landing. The ballistic coefficient shall be 5 to 25 kg/m^2 and nominally 20 kg/m^2 . The entry trajectory shall be as steep as possible consistent with any entry aerodynamic load constraints.

3.4 MARS TERMINAL DESCENT

On the ballistic aerobrake, this phase would normally be indistinguishable since it is a subsonic terminal descent which moves quickly into the lander mission. This is as opposed to an aeromaneuvering system which requires the deployment of high drag decelerators (i.e., ballutes, parachutes, etc.) to slow it from supersonic speeds down to subsonic speeds. The aerobrake can conceivably slow down further than 120 m/sec by deploying additional area to further lower its ballistic coefficient, since it is a stable terminal subsonic descent at very low (1 mbar/0.014 psi) ambient pressures.

3.4.1 Analysis

Increasing the area by factor of 9 or the diameter by a factor of 3 would lower the aerobrake terminal descent near surface impact to about 30 m/sec (65 mph). Assuming the use of an airbag of about 3 times the base dimension of the payload, the impact would about 30 g's over msec (a bump). At 120 m/sec (260 mph), this impact would be 1 to 2 orders of magnitude higher. The idea of deploying additional area during terminal descent for the aerobrake by maybe deploying a primary airbag at high (i.e., between 5 to 10 km) altitudes has a significant advantage, as a backup or safety assurance system.

3.4.2 Requirements Summary

The aerobrake shall act as the terminal descent system.

3.5 MARS TERMINAL TOUCHDOWN

The terminal touchdown is primarily a propulsive phase where the terminal descent velocity is reduced to an acceptable residual along with the target dispersions at altitude. On the aerobrake, this can commence at relatively high altitudes of about 10 km (32,000 feet). Aeromaneuvering ordinarily requires a significant terminal descent phase with the terminal propulsive phase being delayed to altitudes as low as 1 km. The advantages of considering a high altitude terminal touchdown phase are time allowed for the sensors to acquire the target and the ability to translate laterally over relatively large distances (km's or 10's % of the range to go).

3.5.1 Analysis

Reference 3.6.11 summarizes work that was conducted to develop concepts and algorithms to partly deal with reducing the landing dispersions at Mars. Apollo Lunar landing E-Guidance algorithms were exercised to determine Delta-v requirements and impact velocities for various terminal descent altitudes and projected navigation dispersions. Alternate gain switching was considered to reduce the impact velocities as well.

Table 3.5.1 compares the performance of E-Guidance and a more Robust approach (RE-Guidance). This table assumes that the terminal touchdown phase is initiated at a 10 km altitude at 120 m/sec with various magnitudes of navigation errors shown as a percentage of the initial range to go (i.e., 10 km). The E-Guidance approach performs well for small navigation errors to null the impact velocity. As the navigation errors grow to the expected magnitudes, the impact velocities become significant (13 m/sec / 30 mph). Modifying the E-Guidance with the more robust approach reduces the impact velocities to manageable levels (less than 1/msec) at the expense of propulsive Delta-V.

Table 3.5.2 compares the performance of the RE-Guidance for various lateral translation distances for target dispersion reduction. This is for the 10 km and 120 m/sec terminal touchdown case. It demonstrates that for this touchdown scenario normally a terminal descent propulsive Delta-V requirement would be about 531 m/sec. This is consistent with the 3 km errors shown in Table 3.3.1.

3.5.2 Requirements Summary

The terminal touchdown propulsion system shall have a Delta-V budget of 600 m/sec when using the aerobrake. The residual Delta-V upon landing shall be less than 1 m/sec.

Table 3.5.1 E- & RE-Guidance Performance Comparison In the Presence of Navigation Error

NAVIGATION ERROR MAGNITUDE	E-GUIDANCE		RE-GUIDANCE	
PERCENT OF CURRENT RELATIVE POSITION	DV - M/S	VFINAL	DV - M/S	VFINAL
0.0	489.4	0.2	508.7	0.2
1.0	486.9	0.6	505.9	0.4
2.5	479.7	1.5	503.4	0.2
5.0	468.2	5.4	497.7	0.5
10.0	447.9	13.0	488.7	0.3

Table 3.5.2 RE-Guidance Delta-V Requirements with Lateral Translation

LATERAL RANGE - KM	DV - M/SEC
0.0	505.6
0.5	506.1
1.0	508.7
2.0	516.7
3.0	530.7
4.0	547.2
5.0	567.0
7.5	620.5
10.0	675.5

4. DELIVERY DESIGN CONCEPT

4.1 AEROBRAKE ENTRY SYSTEM

The aerobrake entry system consists primarily of the blanket, rib support structure and any special aerodynamic stabilization required (i.e., vanes, fins, c.g. offsets, etc.). The concept is based on a simple ballistic entry approach relying on passive control at near zero angle of attack. The very low pressure loading (mbars) at either minimum energy hyperbolic entry or orbital entry speeds allows the use of a flexible blanket on the ultra-low ballistic coefficient entry system. The integrated pressure, though, does result in a number g's being sustained which can be managed by the structure and payload.

4.1.1 Configuration

Two configurations have been investigated which are derived from requirements for entry at hyperbolic entry and orbital entry speeds. The open aerobrake is intended for orbital entry with its aft payload open to the wake. The closed aerobrake on the other hand is intended for hyperbolic entry with the payload enclosed entirely by the aerobrake to preclude wake closure thermal problems.

The open aerobrake configuration was a result of recent Mars Rover Sample Return (MRSR) studies at TRW. It was a result of the payload integration design problems associated with the use of aerocapture (References 4.7.1, 4.7.2 and 4.7.3). The requirements for moderate Lift-to-Drag (L/D) for aerocapture and low ballistic coefficient for entry-to-landing were conflicting. The very benign entry environment (References 4.7.4 and 4.7.5) from Mars orbit allowed for a simple open aerobrake design as shown in Figure 4.1.1. This environment also allowed design considerations for small appendages (soft landing retro-propulsion engines) to be exposed to the on coming gas flow. This is a result of the thick subsonic (1 to 2 m) shock layer which results from the bluntness of the aerobrake.

On MRSR, the entry mass is about 3 Tonne which results in an aerobrake diameter of about 11 m. Considering the results of section 3.1 of the MEM entry mass the manned aerobrake would be between 1.5 to 9 times larger depending on the ascent crew capsule requirements. Potentially, it could also be the same size as the MRSR aerobrake, if single manned ascent vehicles were considered.

The driving mass design parameter is the blanket area. For MRSR, this was about 5% of the entry mass inclusive of the rib support structure. Since the ballistic coefficient is being preserved, the mass fraction for other aerobrakes should remain about the same. The analysis, though, in section 3.1 assumed 10%.

The driving design parameter, though, was maintaining the stiffness in the structure and support of the outer edge. This was controlled by the pre-tension in the outer aerobrake edge or pre-tension hoop. This was coupled to the folding pattern in the bi-conic aeroshell. As the aerobrake becomes larger to maintain the same stiffness will require an increase in pre-tension by the square of the ratio of the larger aerobrake diameter to the MRSR aerobrake diameter. Increase pre-tension levels of 9

since it is usually dominated by turbulent diffusion effects. When it is taken into account, it is usually treated simply in its gradient diffusion form and is written as

$$\overline{\sigma'_{ik}u'_j + \sigma'_{jk}u'_i} \simeq \overline{\mu}(\tau_{ij,k} + \tau_{jk,i} + \tau_{ik,j}). \tag{2.10}$$

The contraction of Eq. (2.10) leads to the appropriate model for the viscous diffusion term in the total energy equation.

The energy flux term, Eq. (2.5c), requires models for both the heat flux and triple velocity correlation terms. At present there has not been any consistent effort to develop alternatives to the gradient diffusion hypothesis for the heat flux term. For simplicity, the heat flux term is then modeled as

$$\overline{\rho}\widetilde{u''_j T''} \simeq -\bar{\kappa}_t \tilde{T}_{,j} \tag{2.11}$$

where $\bar{\kappa}_t$ is the thermal eddy diffusivity which is given here as (cf. Eq. (2.6a)),

$$\bar{\kappa}_t = C_\mu \frac{\overline{\rho}k^2}{\mathrm{Pr}_t\, \epsilon_s} = \frac{\bar{\mu}_t}{\mathrm{Pr}_t}. \tag{2.12}$$

As is seen by the form of Eq. (2.12), the thermal eddy diffusivity used here is simply the usual eddy viscosity divided by the turbulent Prandtl number $\mathrm{Pr}_t(= 0.9)$.

The remaining contribution in the energy flux term is the triple correlation or the turbulent diffusion term. This term is also present in the Reynolds stress equation in its uncontracted form (cf. Eq. (2.7f). This term has also been traditionally modeled with a gradient diffusion hypothesis by using a turbulent eddy viscosity. The form adopted here is given by

$$\overline{\rho}\widetilde{u''_i u''_j u''_k} \simeq -\frac{2}{3} C_s \frac{\overline{\rho}k^2}{\epsilon_s}(\tau_{ij,k} + \tau_{jk,i} + \tau_{ik,j}) \tag{2.13}$$

where C_s is a numerical constant which is assigned the value of 0.18. This is an isotropized version of the model used by Launder, Reece, and Rodi [11]. In their model, the coefficient C_s was chosen to be 0.11, but in its present form the higher value used here is more appropriate. This model incorporates the functional form of the eddy viscosity relationship defined previously but with a different proportionality coefficient, $\bar{\mu}_t/\sigma_k$, with $\sigma_k = 0.75$. Contraction of Eq. (2.13) will lead to the required functional form used in the energy flux model.

The models required for closure of the total energy equation have now been identified and it is necessary to examine the remaining unknown correlations in the Reynolds stress transport equations. The mass flux variation appearing in the Reynolds stress transport equation is represented by Eq. (2.7d). Consistent with the other correlations which are unique to the compressible formulation, the mass flux term is also modeled by invoking the gradient diffusion hypothesis;

$$\overline{u''_i} \simeq \frac{C_\mu}{\overline{\rho}\sigma_\rho}\frac{k^2}{\epsilon_s}\overline{\rho}_{,i} = \frac{\bar{\mu}_t}{\overline{\rho}^2\sigma_\rho}\overline{\rho}_{,i} \tag{2.14}$$

where σ_ρ is a constant whose value is 0.5.

The modeling of the pressure dilatation term has been the subject of analysis following the partitioning ideas invoked earlier for the dissipation rate term [12, 13]. The form proposed in [12] is used here and is given by

$$\overline{p'u'}_{k,k} \simeq \overline{\rho} M_t^2 (\alpha_2 \tau_{ij} \tilde{u}_{i,j} + \alpha_3 \epsilon_s) \tag{2.15}$$

where $\alpha_2 (= 0.6)$ and $\alpha_3 (= 0.2)$ are numerical constants calibrated by comparison with direct numerical simulations [12].

The only remaining model that needs to be determined is for the deviatoric part of the pressure-strain rate correlation, Eq. (2.7b). At present there has been no work directed toward the development of a compressible pressure-strain rate correlation model. The approach taken has been to use variable density extensions of the incompressible form of the model. The compressibility effects have then been isolated into the pressure dilatation term which has been solely derived for compressible flows. In light of this approach and the fact that there are a significant number of pressure-strain rate models presented in the literature, it is sufficient in the present context to present the functional form of a commonly used model and show its incorporation into the numerical algorithm. One of the most commonly used pressure-strain rate correlation models is the model of Launder, Reece and Rodi [11]. While it is only linear in the anisotropies of the Reynolds stress, it has been used extensively on a variety of flows. The high Reynolds number form of the equation is given by

$$\Pi_{ij}^d \simeq \phi_{ij1} + \phi_{ij2} \tag{2.16}$$

$$\phi_{ij1} = -C_1 \overline{\rho} \epsilon b_{ij} \tag{2.16a}$$

$$\phi_{ij2} = -\frac{C_2 + 8}{11}(P_{ij} - \frac{1}{3} P_{kk} \delta_{ij}) - \frac{8C_2 - 2}{11}(D_{ij} - \frac{1}{3} P_{kk} \delta_{ij}) - \frac{30C_2 - 2}{55} \overline{\rho} k (\tilde{u}_{i,j} + \tilde{u}_{j,i} - \frac{2}{3} \tilde{u}_{k,k} \delta_{ij}) \tag{2.16b}$$

where C_1 and C_2 are numerical constants given by 3.0 and 0.4, respectively, and

$$b_{ij} = \frac{1}{2k}(\tau_{ij} - \frac{2}{3} k \delta_{ij}) \tag{2.17a}$$

$$D_{ij} = -\overline{\rho} \tau_{ik} \tilde{u}_{k,j} - \overline{\rho} \tau_{jk} \tilde{u}_{k,i} \tag{2.17b}$$

It should be emphasized that the pressure-strain rate correlation is the subject of extensive research and that other models have been proposed which should perform better than the above model (e.g. [14]). However, comparing a variety of closure models is not the intent of the present report, but is a course of study being actively pursued and will be reported on later.

The remaining equation that needs to be modeled is the solenoidal dissipation rate equation, Eq. (2.9). This equation has been examined recently [15, 10] for application to compressible flows. The models for the terms in Eq. (2.9) are given by

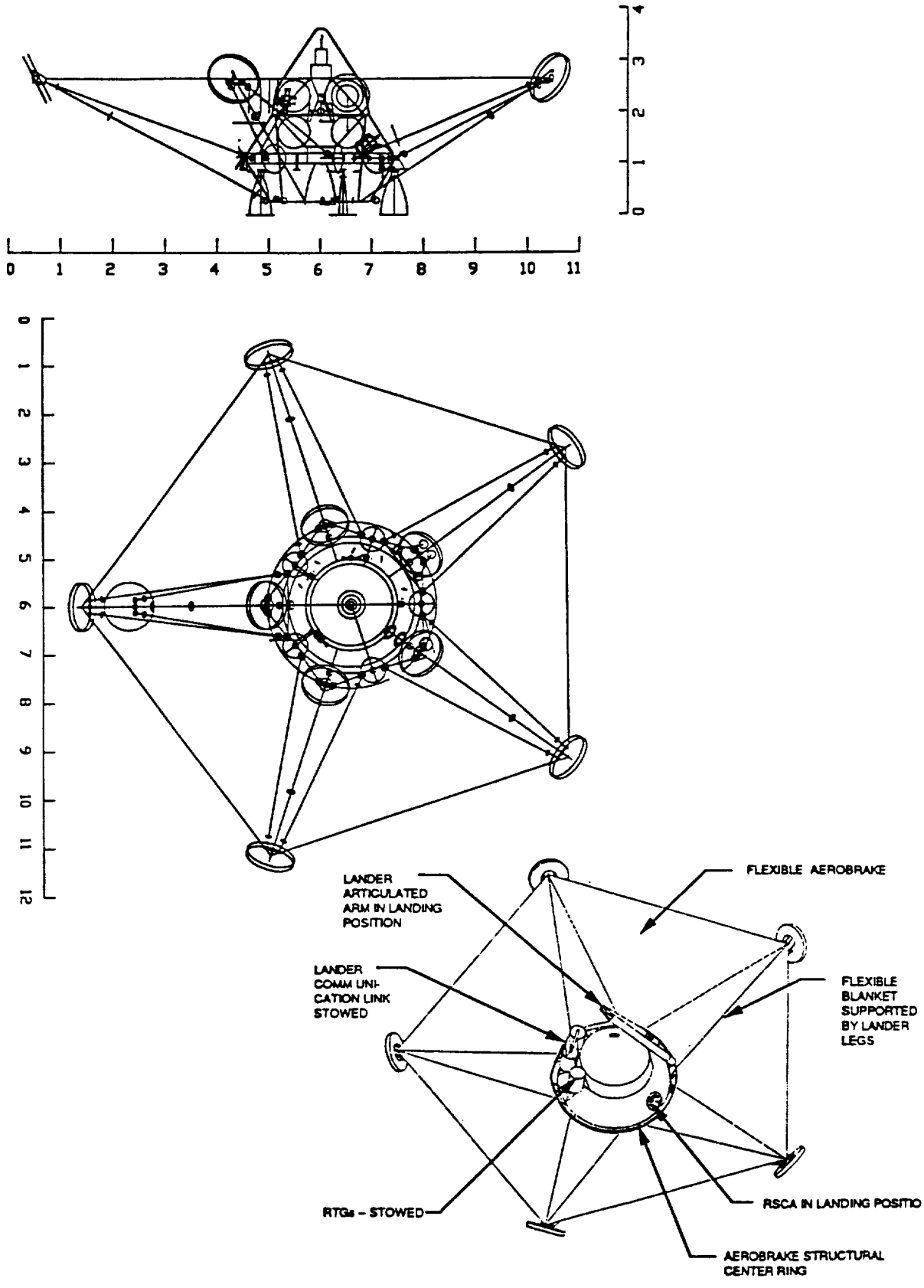

Figure 4.1.1 MRSR Open Aerobrake Design

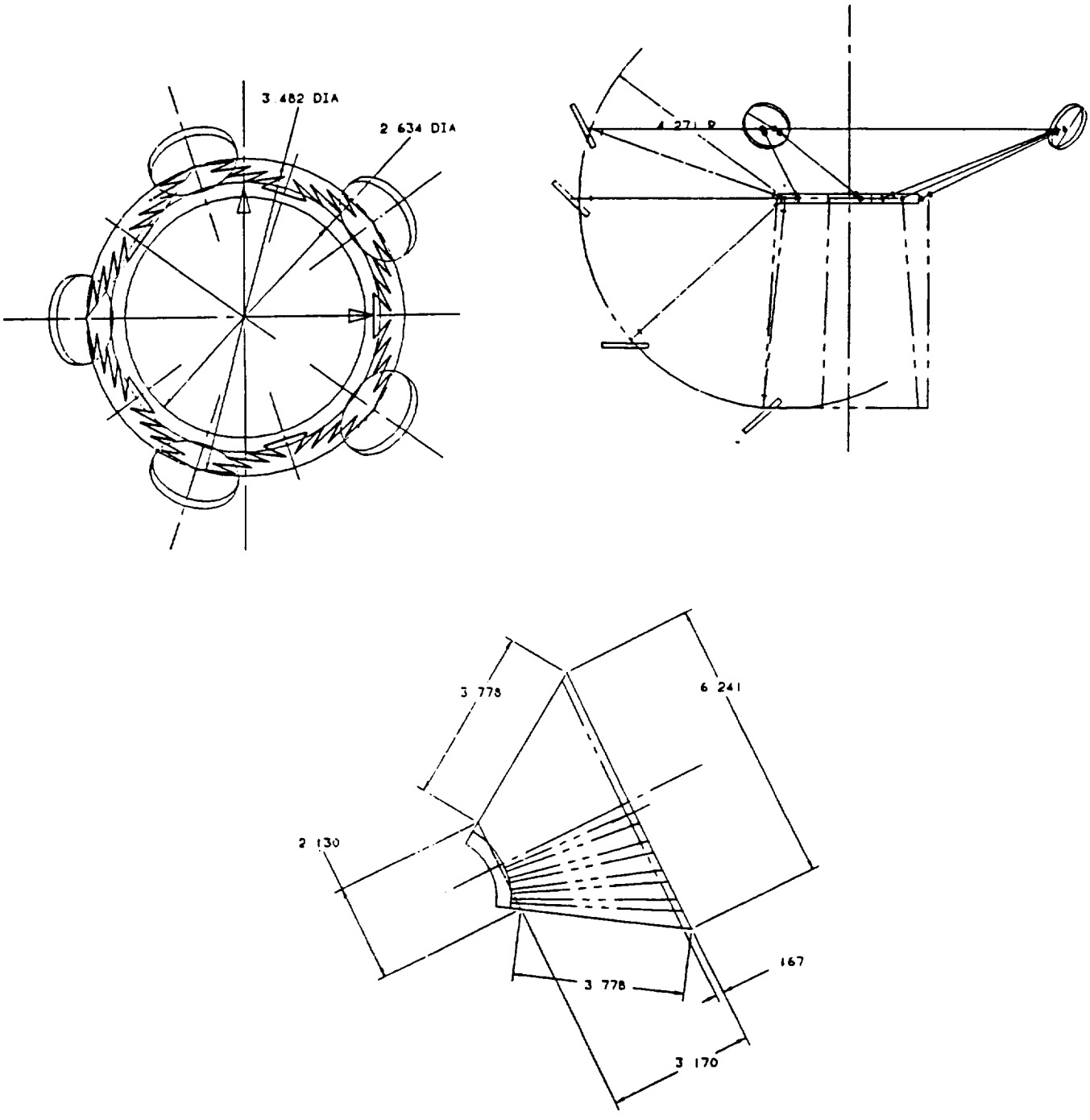

Figure 4.1.2 MRSR Aerobrake Folding Patterns

$$\mathcal{D}_{\epsilon_s} = C_{\epsilon 2} f_2 \overline{\rho} \frac{\epsilon_s^2}{k}, \tag{3.5}$$

where [6]

$$f_2 = \left[1 - \exp\left(\frac{y^+}{4.9}\right)\right]^2 \left[1 - \frac{2}{9}\exp\left(-\frac{Re_t^2}{36}\right)\right] \tag{3.6}$$

Note that in the absence of f_2 the destruction term increases without bound as the wall is approached.

For the Reynolds stress closure, a near-wall correction needs to be used for the pressure-strain rate correlation. This has been the topic of research in wall-bounded incompressible flows for some time [18], but with mixed success. Nevertheless, since the intent here is not to validate or compare models, it suffices to implement a near-wall correction which typifies the form and structure of a near-wall closure that can be implemented in the present numerical formulation. The near-wall modification that is adopted here is a variable density extension of the Shima model [20]. Even though this model has deficiencies which will be pointed out shortly, it is readily amenable to implementation in complex flows because it lacks any dependency on the wall normals [21] which cause ambiguities in complex flow situations. The Shima model introduces a near-wall correction to the pressure-strain correlation given by

$$\Pi_{ij} \simeq \phi^*_{ij1} + \phi_{ij2} + \phi_{ijw} \tag{3.7}$$

where

$$\phi^*_{ij1} \simeq -C_1^* \overline{\rho} \epsilon b_{ij} \tag{3.8}$$

with

$$C_1^* = C_1 + (1 - C_1) f_w \tag{3.8a}$$

$$f_w = \exp\left[-(0.015\sqrt{k}y/\bar{\nu})^4\right], \tag{3.8b}$$

ϕ_{ij2} given by Eq. (2.16b), and $C_1 = 3.0$. The coordinate y is measured normal to the surface. The near-wall correction ϕ_{ijw} is given by

$$\phi_{ij2} = [\alpha(P_{ij} - \frac{1}{3}P_{kk}\delta_{ij}) + \beta\overline{\rho}k(\tilde{u}_{i,j} + \tilde{u}_{j,i} - \frac{2}{3}\tilde{u}_{k,k}\delta_{ij})]f_w, \tag{3.9}$$

where $\alpha = 0.45$ and $\beta = 0.08$.

A near-wall correction to the solenoidal dissipation rate needs to be implemented. For consisitency, the model proposed by Shima [20] is again used in the present study. The solenoidal dissipation rate equation is easily modified to include the near-wall Shima correction by replacing $C_{\epsilon 1}$ with a $C^*_{\epsilon 1}$ defined as

$$C^*_{\epsilon 1} = C_{\epsilon 1}(1 + f_w), \tag{3.10}$$

The inverse of the symmetry matrix, T^{-1}, is given as:

$$\mathbf{T^{-1}} = \begin{bmatrix}
1-\Upsilon q^2/2 & \Upsilon u & \Upsilon v & \Upsilon w & -\Upsilon & \Upsilon/2 & \Upsilon/2 & \Upsilon/2 & 0 & 0 & 0 & 0 \\
-\overline{V} & \hat{l}_x & \hat{l}_y & \hat{l}_z & 0 & 0 & 0 & 0 & 0 & 0 & 0 & 0 \\
-\overline{W} & \hat{m}_x & \hat{m}_y & \hat{m}_z & 0 & 0 & 0 & 0 & 0 & 0 & 0 & 0 \\
\Upsilon q^2/4-\overline{U}/2a & \hat{n}_x/2a-\Upsilon u/2 & \hat{n}_y/2a-\Upsilon v/2 & \hat{n}_z/2a-\Upsilon w/2 & \Upsilon/2 & -\Upsilon/4 & -\Upsilon/4 & -\Upsilon/4 & 0 & 0 & 0 & 0 \\
\Upsilon q^2/4+\overline{U}/2a & -\hat{n}_x/2a-\Upsilon u/2 & -\hat{n}_y/2a-\Upsilon v/2 & -\hat{n}_z/2a-\Upsilon w/2 & \Upsilon/2 & -\Upsilon/4 & -\Upsilon/4 & -\Upsilon/4 & 0 & 0 & 0 & 0 \\
-\tau_{xx} & 0 & 0 & 0 & 0 & 1 & 0 & 0 & 0 & 0 & 0 & 0 \\
-\tau_{yy} & 0 & 0 & 0 & 0 & 0 & 1 & 0 & 0 & 0 & 0 & 0 \\
-\tau_{zz} & 0 & 0 & 0 & 0 & 0 & 0 & 1 & 0 & 0 & 0 & 0 \\
-\tau_{xy} & 0 & 0 & 0 & 0 & 0 & 0 & 0 & 1 & 0 & 0 & 0 \\
-\tau_{xz} & 0 & 0 & 0 & 0 & 0 & 0 & 0 & 0 & 1 & 0 & 0 \\
-\tau_{yz} & 0 & 0 & 0 & 0 & 0 & 0 & 0 & 0 & 0 & 1 & 0 \\
-\epsilon & 0 & 0 & 0 & 0 & 0 & 0 & 0 & 0 & 0 & 0 & 1
\end{bmatrix}$$

where

$$\Upsilon = (\gamma-1)/a^2$$

The vectors $\hat{l}$ and $\hat{m}$ are non-unique, mutually orthogonal to n, and tangent vectors in the plane of the cell interface. The flux differences given in Section 4 use metric identities to provide a form which is independent of these tangency vectors for computational efficiency.

Entry Mass = 87 Tonnes

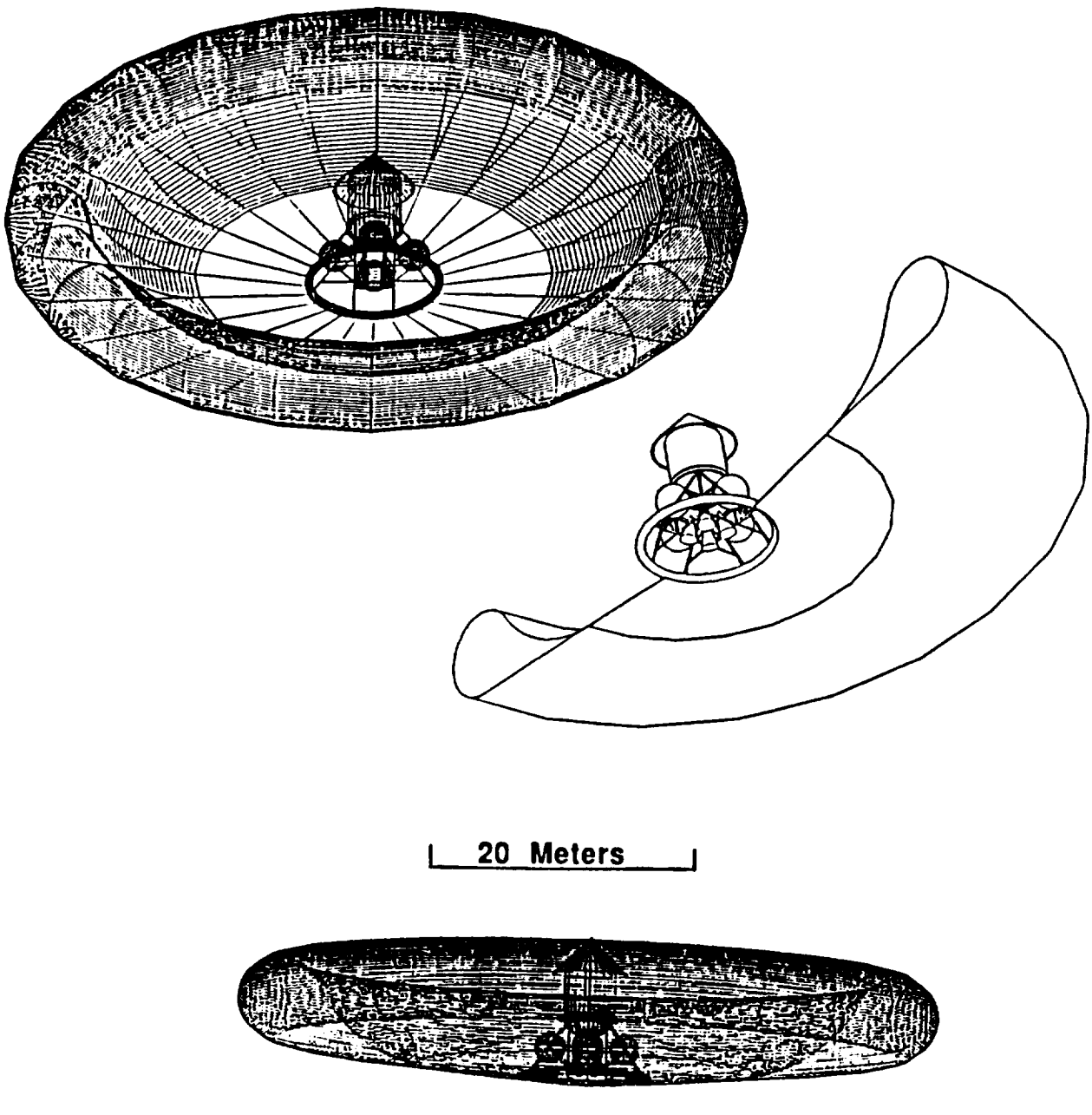

Figure 4.1.5 Manned Aerobrake Entry Design Concept

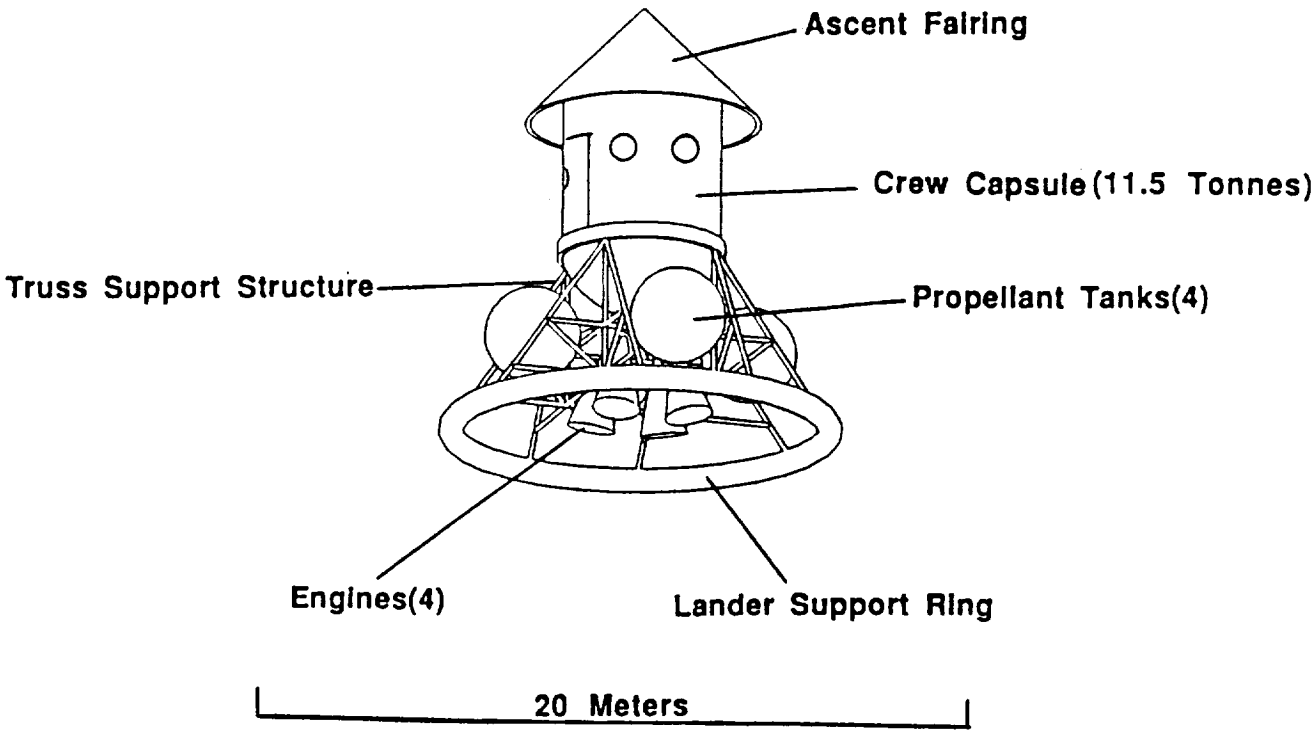

Figure 4.1.6 Mars Excursion Module Strawman Payload

[25] van Leer, B., "Towards the Ultimate Conservative Difference Schemes V. A Second Order Sequel to Godunov's Method", *J. Comp. Physics*, Vol. 32, pp. 101-136,1979.

[26] Chakravarthy, S. R., Szema, K-Y., Goldberg, U. C. and Gorski, J. J., "Application of a New Class of High Accuracy TVD Schemes to the Navier-Stokes Equations," *AIAA 23th Aerospace Sciences Meeting*, Paper No. 85-0165, January 14-17, Reno, Nevada, 1985.

[27] Swanson, R. C., and Turkel, E., "A Multistage Time-Stepping Scheme for the Navier-Stokes Equations," *AIAA 24th Aerospace Sciences Meeting*, Paper No. 85-0035, January 14-17, Reno, Nevada, 1985.

[28] Shih, T. I.-P. and Chyu, W. J., "Approximate Factorization with Source Terms", AIAA Journal, Vol. 29, No. 10, October 1991, pp. 1759-1760.

[29] Pulliam, T.H., and Steger, J.L.: "Recent Improvements in Efficiency, Accuracy, and Convergence for Implicit Approximate Factorization Algorithms," *AIAA 23th Aerospace Sciences Meeting*, Paper No. 85-0360, January 14-17, Reno, Nevada, 1985.

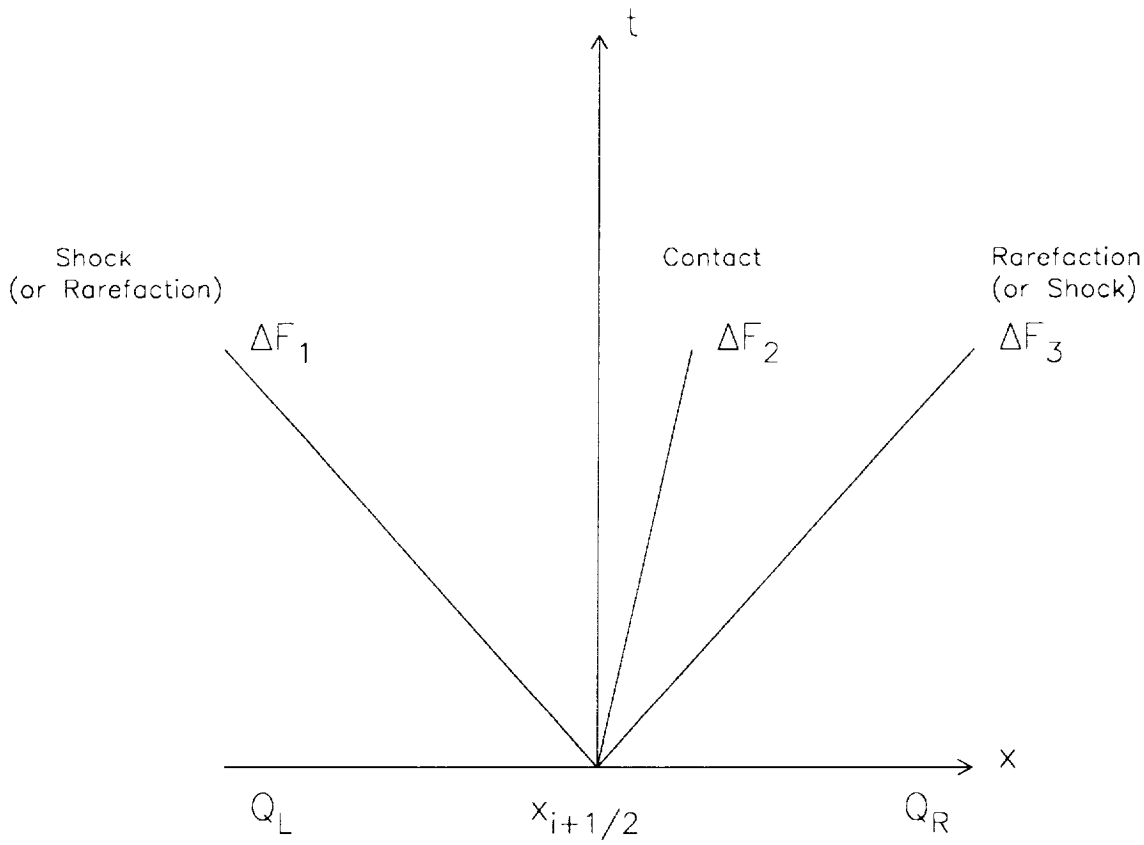

Figure 1: Diagram of shock and rarefaction wave solution to Riemann problem.

4-11

4.3 TERMINAL TOUCHDOWN SYSTEM

The terminal touchdown system will consist of a propulsion and shock attenuation system for soft and safe landing of the exploration elements. The key to a soft landing will be the chemical propulsion system which will most likely be a storable bi-propellant system. The shock attenuation system which will take out the residual Delta-V and act as a back-up for a cushioned landing in case of a propulsion system failure will be a mechanism which acts a spring shock attenuation system. The propulsion system for descent and ascent will be the major part of the landed mass in most cases. For the manned elements, this will be about 69% of the mass.

4.3.1 Configuration

The propulsion configuration will depend on the size of the landed mass. This could be anywhere between 4 to 100 Tonnes as shown in Section 3.1. With a potential requirement of a 4:1 thrust to mass ratio, this would mean a propulsion motor thrust of 16 to 400 kilo-newtons (knt). The Lunar Module Descent Engine (LMDE) delivered about 2.4 knt with a 10:1 variable thrust capability. This would suggest a cluster of 7 LMDE for the lower landed mass or an entirely new design. As the mass lift off requirement will most likely be larger than the minimum, a new design along the lines of the LMDE will most likely be the direction taken.

The shock attenuation system at Mars may not be as heavy as the propulsion system, but its system requirements will be significant when acting as a back-up. The residual Delta-V's after the propulsive phase will not exceed 1 m/sec. The Delta-V's that the back-up cushioned landing may have to tolerate will about 30 to 100 m/sec depending on the terminal descent ballistic coefficient. At constant deceleration for a 40 g instant impact, the stroke required is between 1 to 12 m for respective impact speeds between 30 to 100 m/sec. The stroke required for less impact loads increases linearly (i.e, 2 to 24 m for 20 g). The mass of the mechanism will be dependent on the landed mass requirements. For an airbag subsystem, this is usually about 10% of the landed mass. The advantages of the airbag are the ability to be readily stored and instantly deploy. An example of an airbag is shown in Figure 4.3.1 as proposed for the MESUR mission. This figure shows two airbag configurations which are utilized to further lower the aerobrake ballistic coefficient in much the same way as a parachute or ballute, and provide crushable shock attenuation at surface impact, respectively. The initial is deployed at about a 10 km altitude and internal pressure is sustained until surface impact. The larger airbag is deployed instantaneously at surface impact and deflates thereafter to attenuate the surface impact shock. A structural and mechanical system would take up a great deal of space, but this is all relative in magnitude to the size of the required landed mass.

As a point of comparison, the airbag size required for a manned crew capsule of 11.5 Tonnes shown earlier in Figure 4.1.5 is shown in Figure 4.3.2. This system would ordinarily be activated in case of a propulsion system failure at altitudes of about 5 to 10 km. This is sized for an 8 g impact load at about 30 m/sec. The over pressure required would be about 68 mbar (1 psia). It is expected that the airbag thickness would on the the order of mm's. The external pressure loading would be on the order of a mbar (0.014 psi) and would result in a stable aerodynamic deployment shape due to the scale of the airbag. The primary airbag used on the aerobrake would assist the propulsion system to cushion the residual 1 m/sec. Assuming the above overpressure,

8 g impact, and 300 deg. K and 10 mbar ambient conditions, the sodium azide gas generator system would weight approximately 4.5 Tonnes to support the 160 m airbag.

4.3.2 Subsystems

The propulsion system will be the largest set of subsystems for the lander, or at least the most massive. The shock attenuation system will most simplistic in terms of subsystems. The airbag consists of a cloth bag, a gas generator and an impact sensor (i.e.,trigger)

4.3.3 Requirements

At a minimum, the propulsion system will require about 600 m/sec propulsive Delta-V capability (Section 3.1and 3.5) for landing. The shock attenuation will require sufficient stroke and force capability to land at impact speeds of 30 to 100 m/sec with masses of 4 to 100 Tonnes.

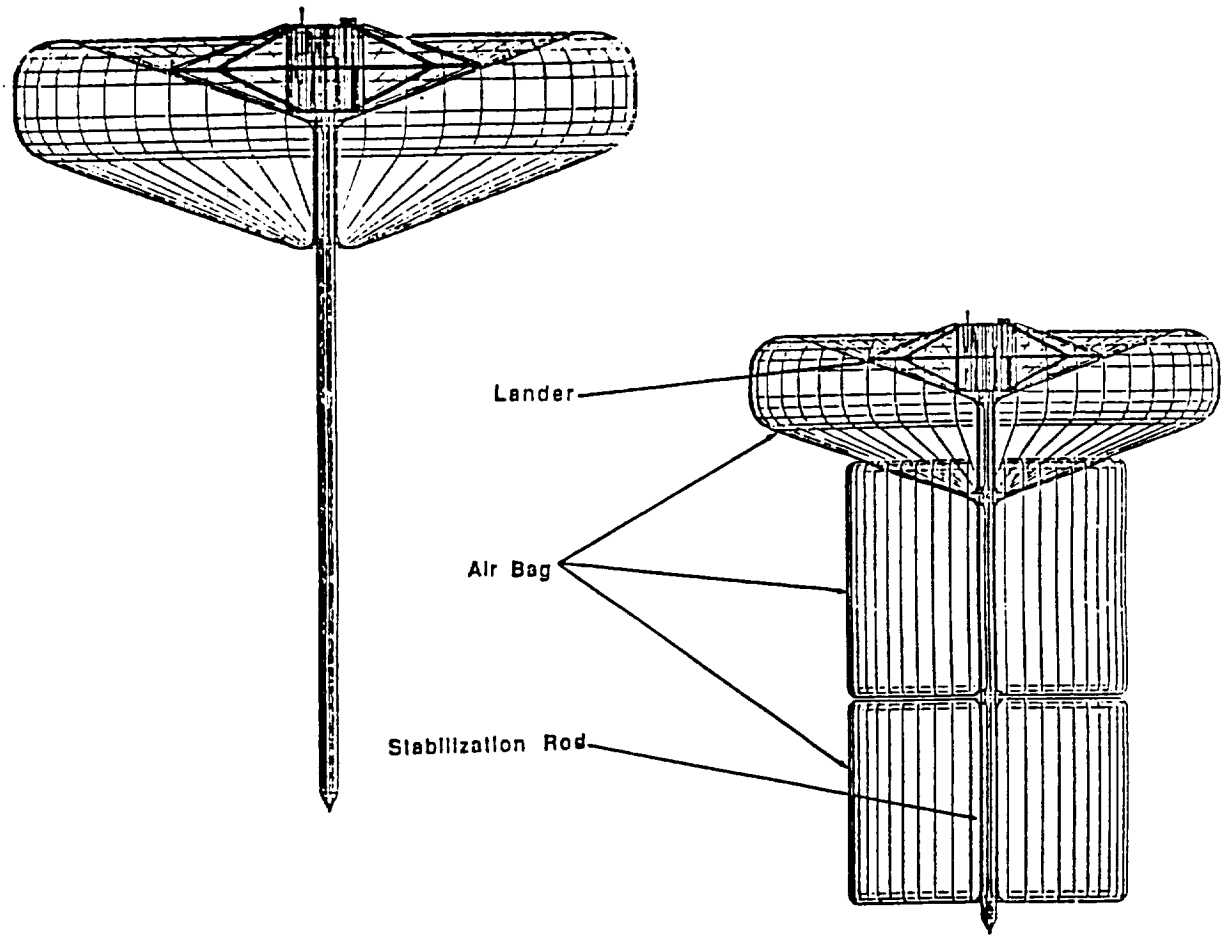

Figure 4.3.1 MESUR Cushioned Landing Airbag Design

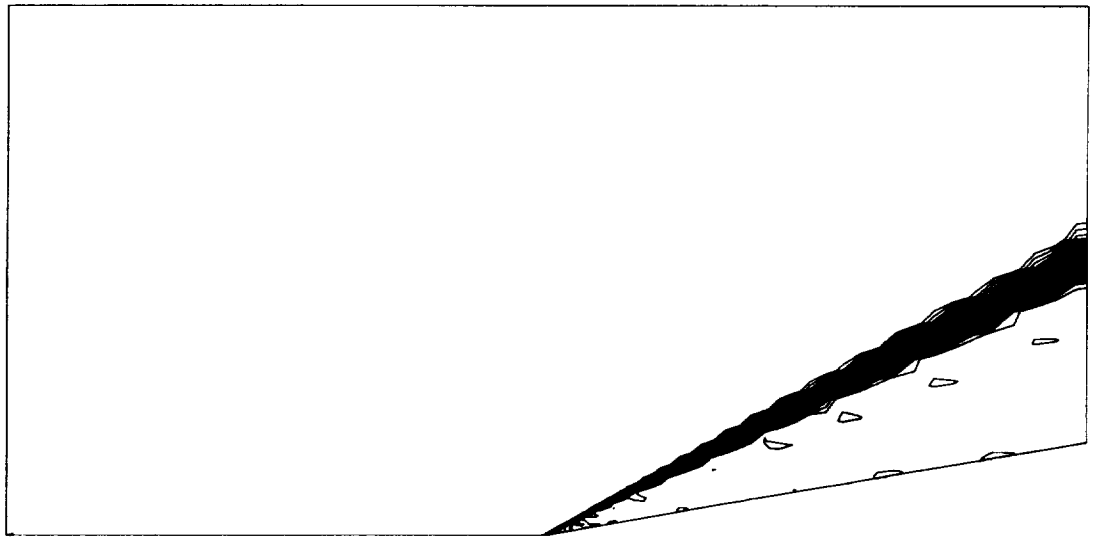

Figure 6: Pressure contours for Mach 3, 10° compression ramp using a Reynolds stress turbulence model.

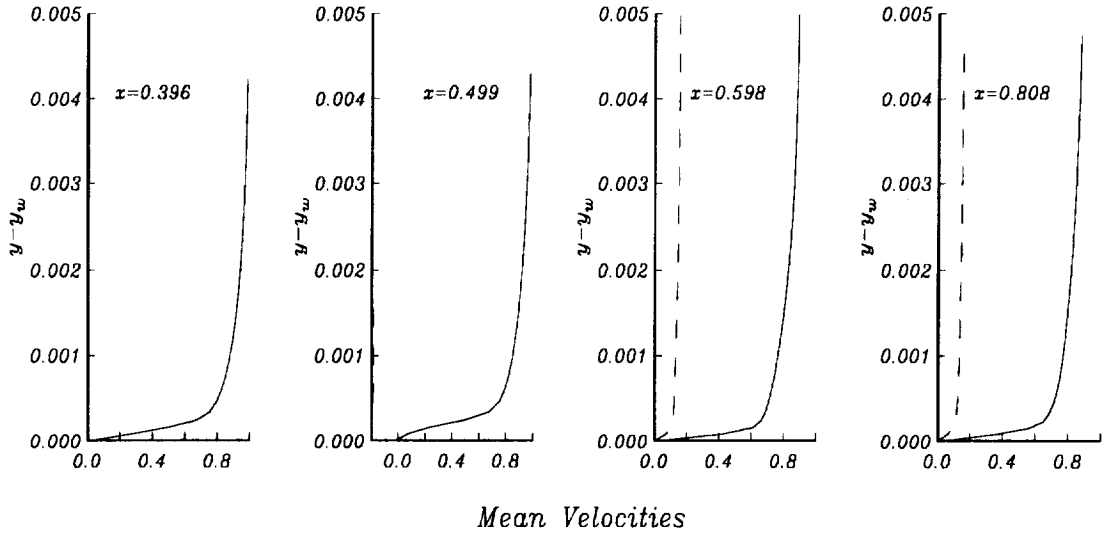

Figure 7: Streamwise variation of mean velocity profiles for 10° compression ramp using a Reynolds stress turbulence model: $\tilde{u}/U_\infty$, ——; $\tilde{v}/U_\infty$, — —.

4.4 PERFORMANCE CHARACTERISTICS

4.4.1 Aerodynamic Design

The major portion of the aerodynamic design presented here is a result of work performed in support of the MRSR and MESUR missions. It is assumed that the manned missions would capitalize on these configuration in terms of the aerobrake ballistic coefficient, bluntness (half cone angles of about 70 deg.) and overall shape. As such, the aerodynamic design analyses discussed here would not vary a great deal from the MRSR, MESUR and SEI manned missions.

As the first step in determining the aerodynamics of the aerobrake, the flight regime was defined. The aerobrake will be deployed shortly before the de-orbit burn at the first apoapsis before atmospheric entry (to limit the state perturbation errors due the large size and solar wind). The entry altitude is defined as 125 km. Initially, the aerobrake will have passed through the viscous free molecular and slip flow regimes, and then descend through the viscous and continuum regimes (Fig 4.4.1). An inviscid, ideal gas flow-filed analysis was initially performed at the point on the trajectory of maximum dynamic pressure, which is in the continuum regime.

As it will be noted in Figure 4.4.1, comparisons were made at a variety of entry speeds which correspond to an entry out of low Mars orbit (500 km circular) and moderate hyperbolic trajectory, respectively. Entry scenarios for freight, habitats, equipment and man could then be evaluated. Due the nature of the steep entry and ultra-low ballistic of the aerobrake, the flight regimes are not expected to differ greatly with most of the braking to occur at altitudes below 62 km.

The SAIC CM3DT code was used to solve for the shock layer ahead of the body. A lambda-differencing scheme was used to march in time to steady state. This non-conservative axisymmetric Euler scheme was chosen for its ability to compute flow past complex shapes and is applicable to high Reynolds number flow without separation. A body oriented computational grid was generated using a conformable transformation within the code. CM3DT is typically used for the subsonic/transonic flow in the nose region of a body to produce a starting solution for a steady supersonic afterbody code. Thus, the axial component of Mach number at the outflow boundary must be supersonic. **However, due to the extreme bluntness of this configuration, the flow in the shock layer is subsonic/transonic.** The cone was extended with a 40 degree expansion fairing to achieve supersonic outflow. This is a credible addition to the geometry since the flow will accelerate around the corner of the entry vehicle.

A full Navier Stokes solution has been formulated which investigates both the fore and aft flowfields. Figure 4.4.2 shows the grid structure for flowfield which is being analyzed on the NAS Crays at NASA/ARC.

The open flexible aerobrake design consists of five panels of flexible insulated fabric. These five panels are swept at a 70 degree angle around the payload/lander modules. A preliminary analysis, using the a finite element program ADINA to model the entire structure was performed where the outer edge of the brake was fixed. Later

results for more realistic outer edge conditions will be shown. This preliminary calculation was intended to define the best possible circumstance. A modulus of elasticity of 2070 MPa and an external load of 24 mbar(low Mars orbit entry) which produced a deformation profile with a maximum deflection of 13.4 cm over the 5.5 m span resulted in the best aerodynamic response of all edge conditions and modulus values investigated. Perfect gas computations with a specific heat ratios of 1.08,1.09 and 1.29 were performed to estimate the shock standoff distance and the aerodynamic load on the aerobrake, respectively at Mach 17, 10 and 5. Results of these axisymmetric computations for the fixed 70 degree edge are depicted in Figures 4.4.3, 4.4.4 and 4.4.5. Surface pressures profiles agree with the Newtonian predictions. The maximum aerodynamic loading on the aerobrake will be experienced near the Mach 10 condition.

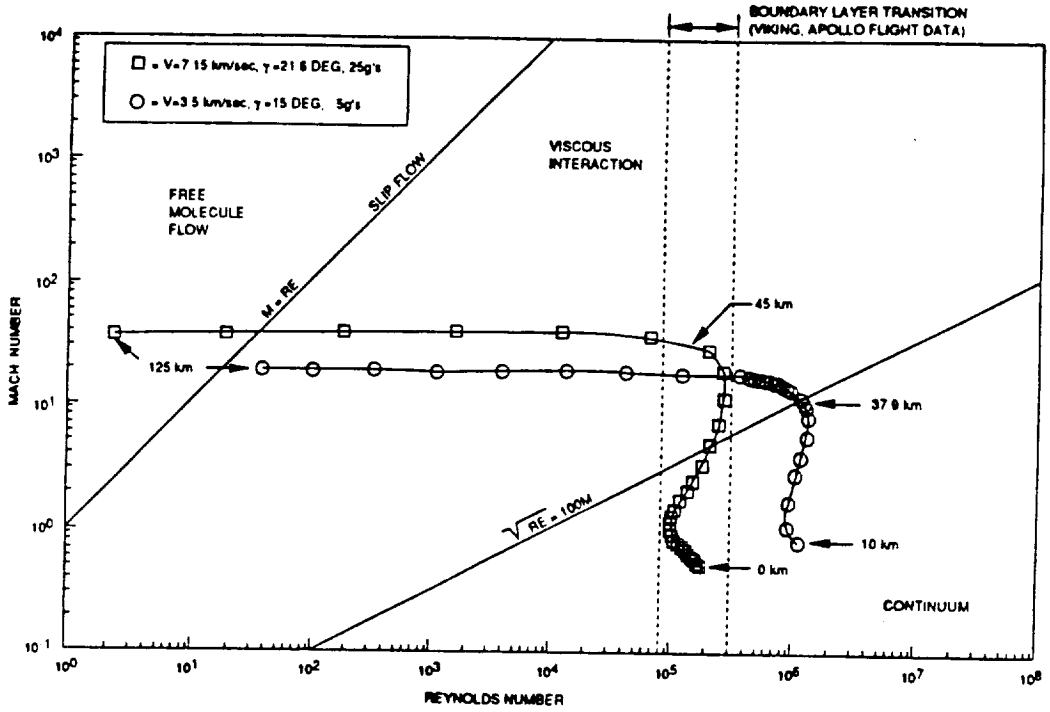

Figure 4.4.1 Aerobrake Flight Regimes

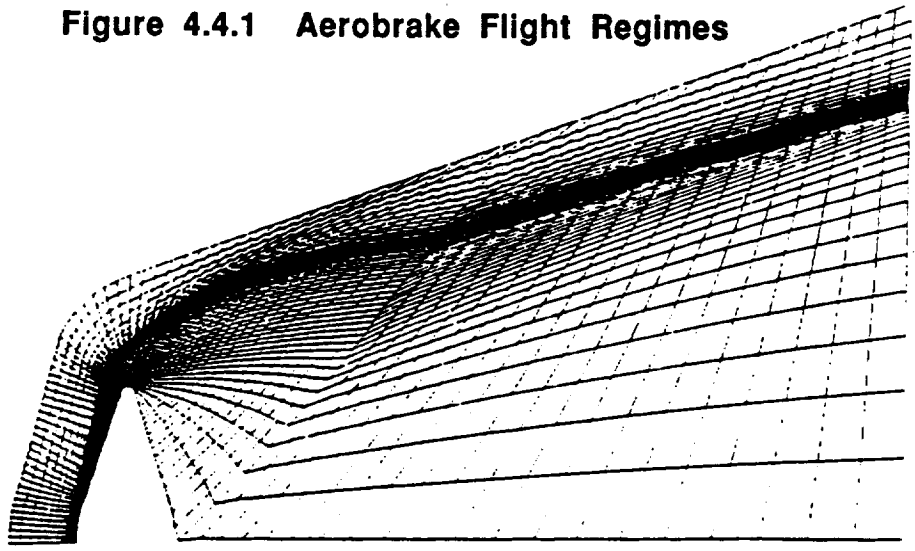

Figure 4.4.2.a Single Block Computational Grid

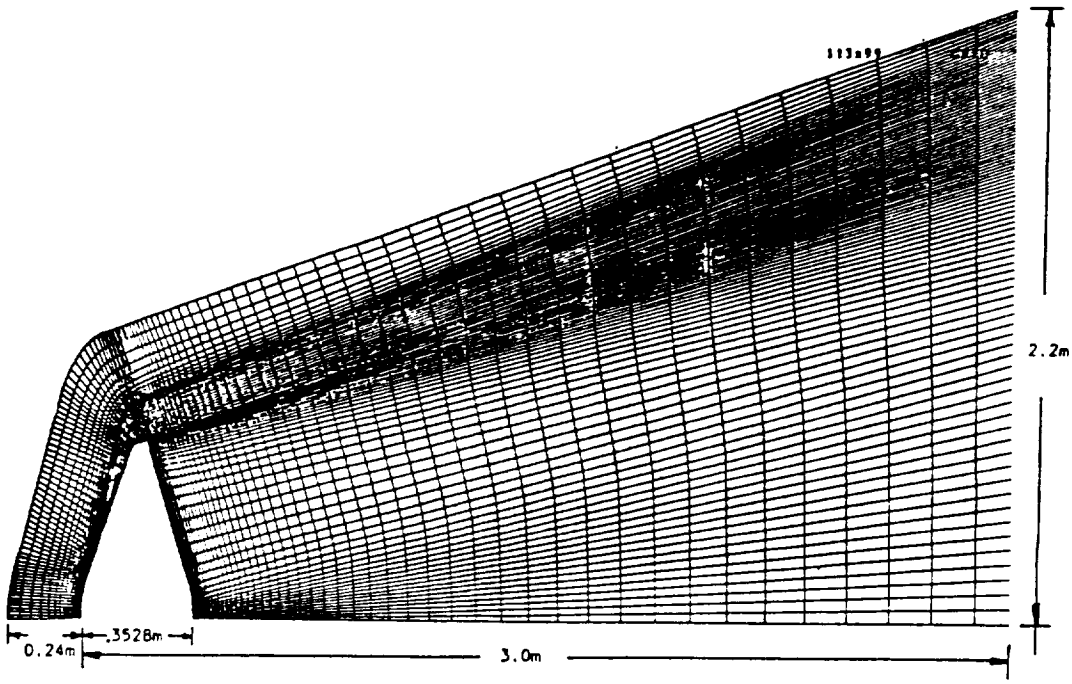

Figure 4.4.2.b Multi-Block Computational Grid

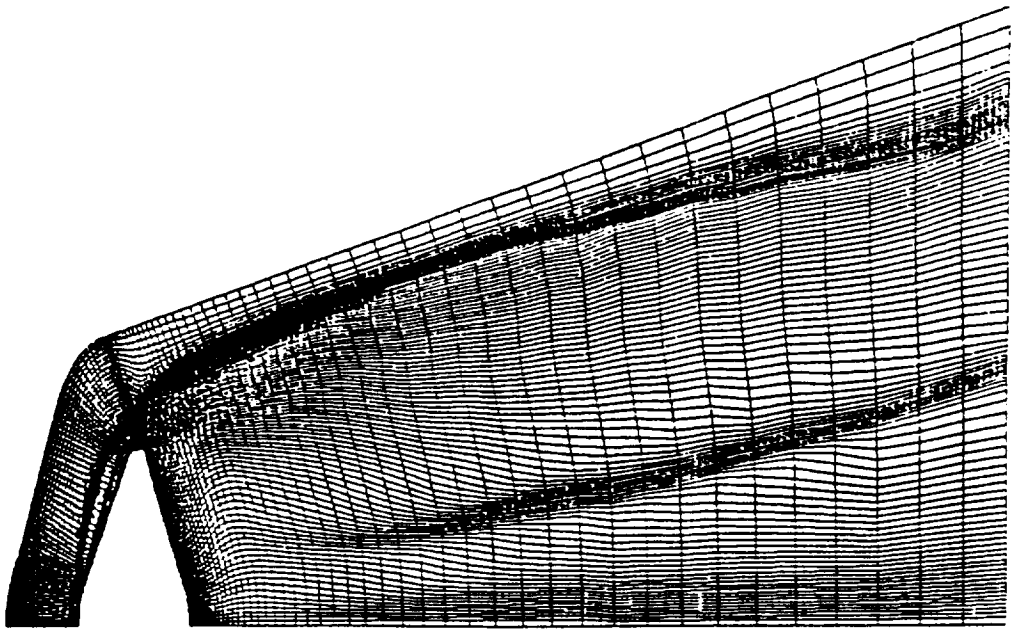

Figure 4.4.2.c Adapted Grid

The deformation produced a concave surface and reduced the equivalent cone angle of the body. It was found that the shock was brought in closer to the body and resulted in what appears to be expansion and compression waves reflected from the body and reinforcing and cancelling the bow shock wave. Interestingly enough, Navier-Stokes computations performed as part of the wing leading edge study for hypersonic vehicles produced similar results (reference 4.7.7). This prompted concern that an aeroelastic instability would make the aerobrake concept infeasible. The literature was reviewed for applicable work done in the area. Past investigations of aeroelasticity in the Mars atmosphere revealed that, due to the low dynamic pressures, there is negligible energy in the airstream for excitation (reference 4.7.8). TRW launched its own precursory study in this area, which produced the same conclusion (Reference 4.7.9). However, a more sophisticated analysis is currently being pursued, exploring the applicability of an aeroelasticity code such as ENSAERO (Reference 4.7.10), typically used for fighter aircraft configurations. This code couples the Navier-Stokes equations with the modal structural equations of motion and uses configuration-adaptive dynamic grids which are accurately time-generated using the aerodynamically deformed shape of the wing.

Computed stagnation point shock standoff distance approaches the limiting value for a sphere at cone angles below 60 degree (Figure 4.4.6). In comparison, experimental data obtained with much higher density ratios across the shock (lower specific heat ratio) exhibit smaller shock standoff distances and the limit for a sphere is approached at the slightly higher cone angle of 67 degree (Figure 4.4.7).

Computed shock standoff distance for a sphere using ideal gas relationships with the constant heat ratio of 1.09 agrees with shock tube data within 20%. The specific heat ratio will vary through the shock layer. Ideal gas computations, though, can be employed with an effective specific heat ratio to estimate the correct shock standoff distance. Figure 4.4.8 presents the variation in shock standoff distance with specific for a Mach number set.

CO_2 dissociation must be considered at Mach numbers greater than 10. As dissociation is initiated and driven towards completion, the density ratio across the shock wave increases, and from mass conservation, the shock standoff distance decreases. Reference 4.7.11 has shown that density ratio across the shock wave is a primary factor controlling shock standoff distance. Real gas effects (vibration, dissociation and ionization) can produce density ratios across the shock as high as 20 to 25 for Mar entry.

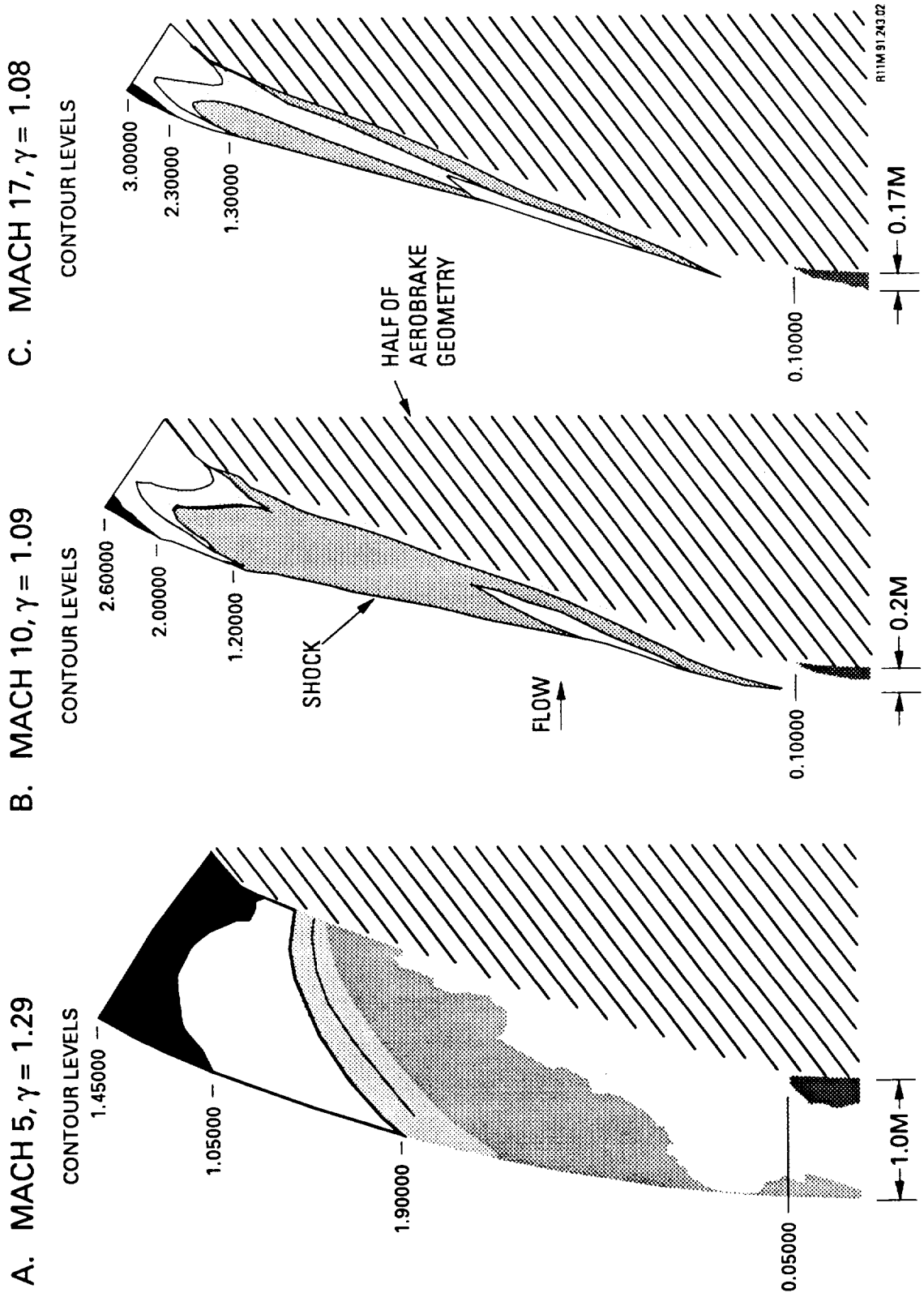

Figure 4.4.3 Axisymmetric Results for 70 deg Undeformed Shape Mach Number Contours

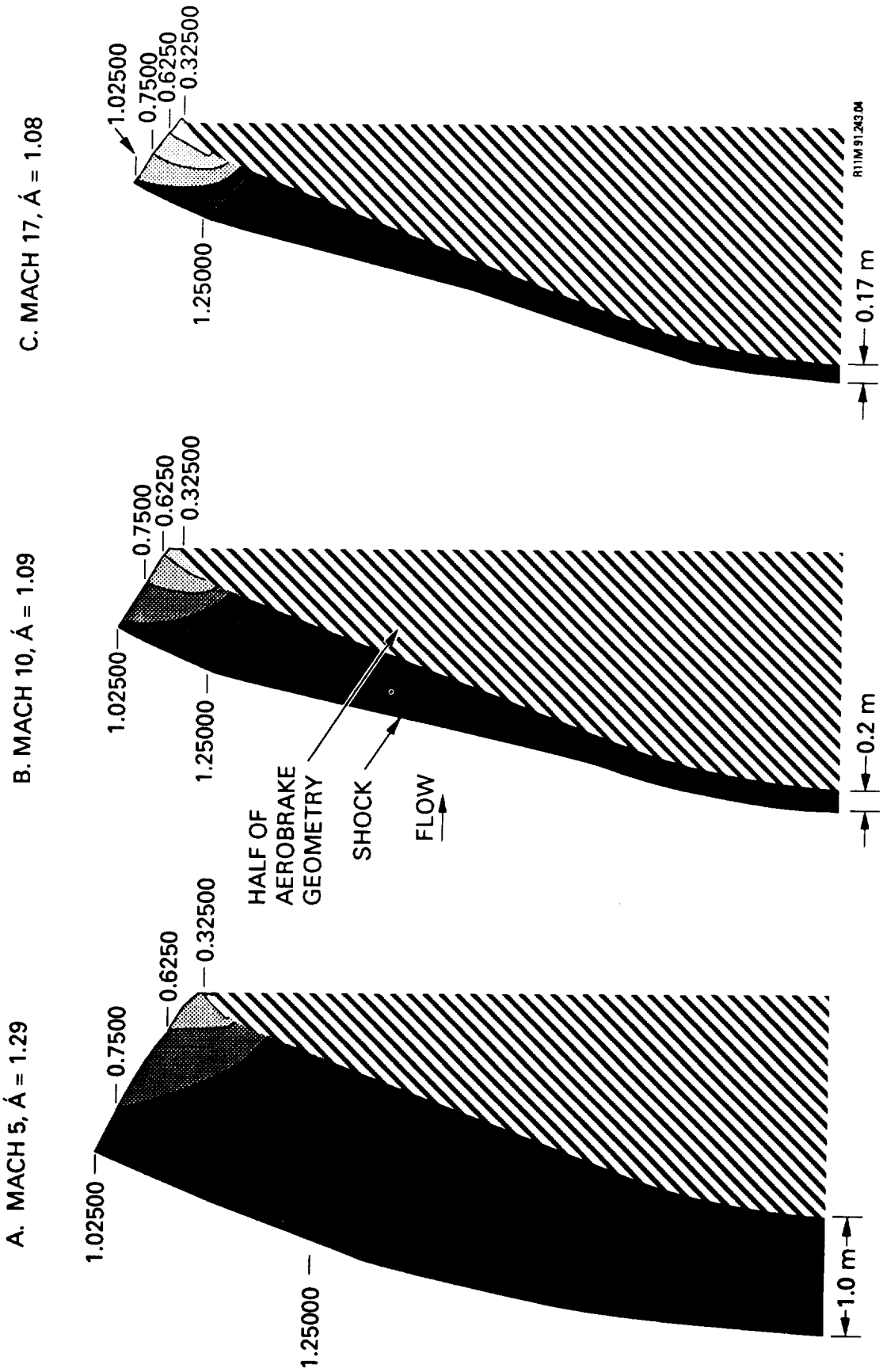

Figure 4.4.4 Axisymmetric Results for 70 deg Undeformed Shape Pressure Contours

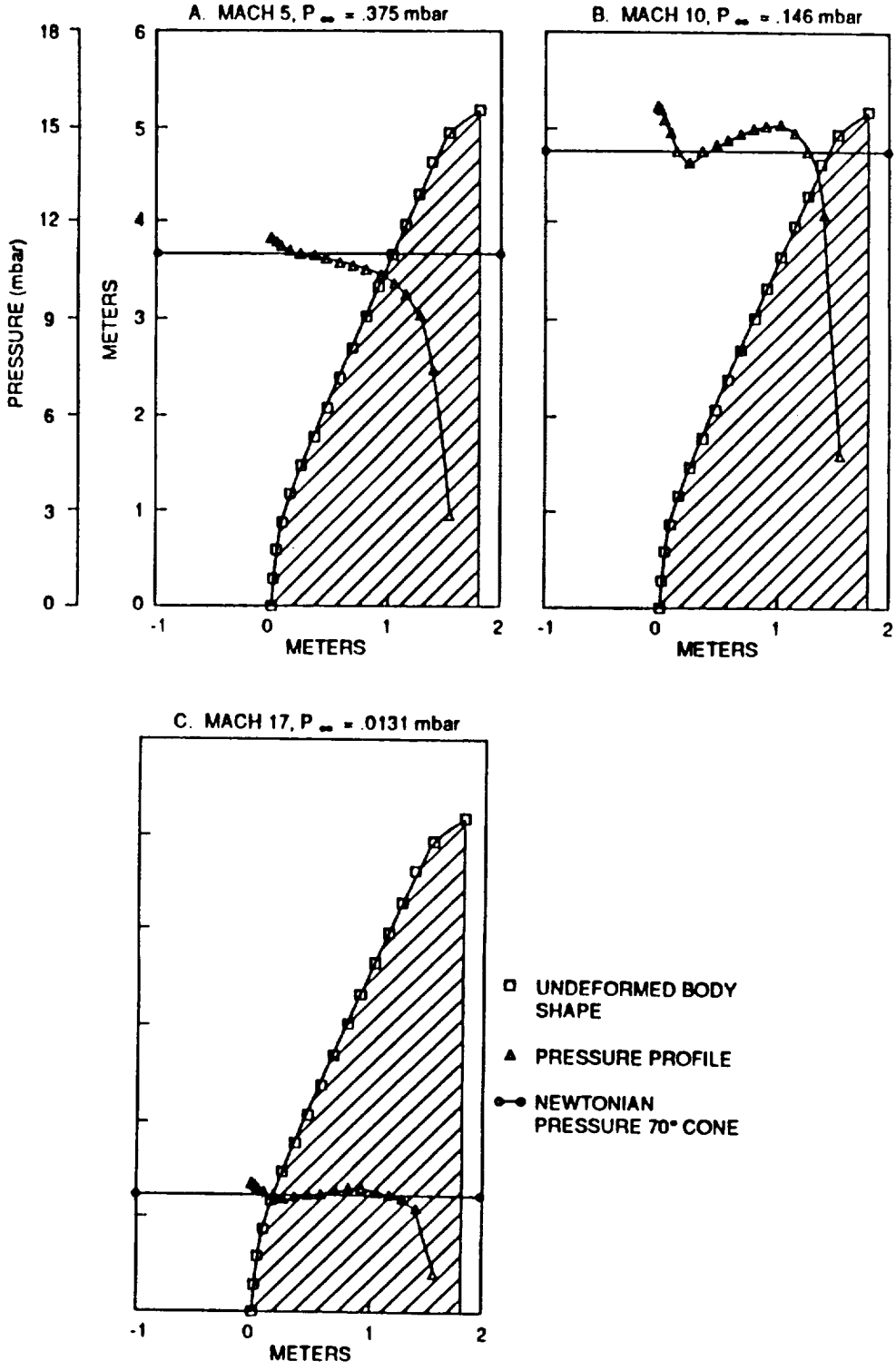

Figure 4.4.5 Pressure Profiles at Mach 5, 10 and 17

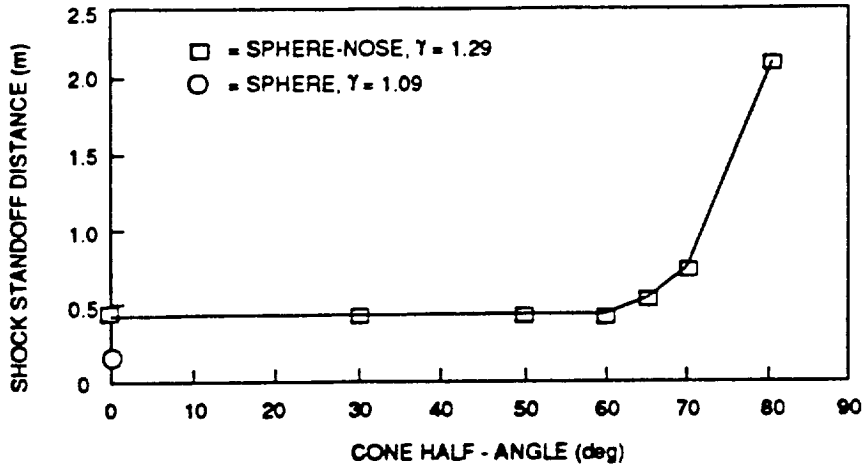

Figure 4.4.6 Variation of Stagnation Point Shock Standoff Distance with Cone Angle, Mach 10 Computations, Ideal Gas

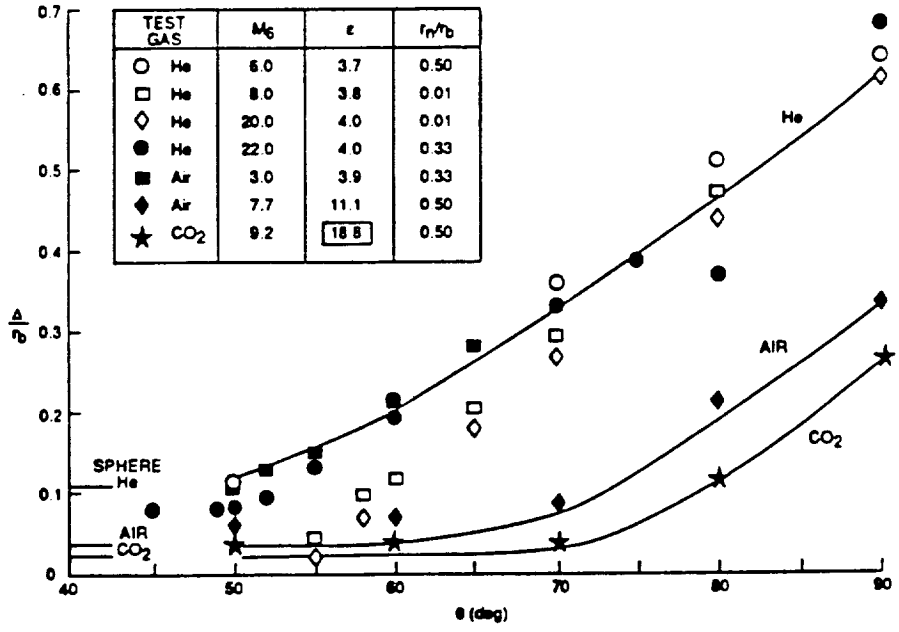

Figure 4.4.7 Variation of Stagnation Point Shock Standoff Distance with Cone Angle, Test Data

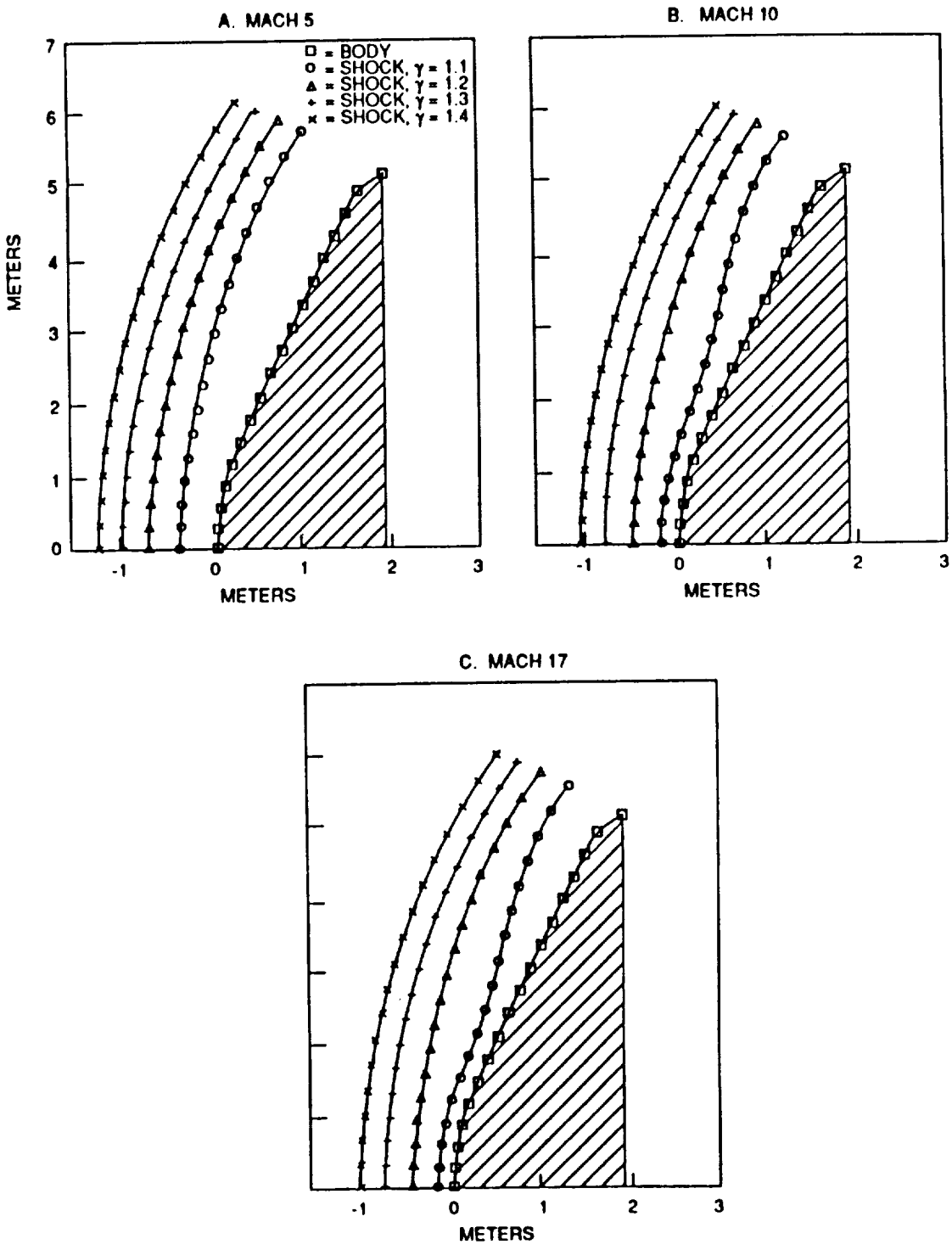

Figure 4.4.8 Sensitivity of Bow Shock Shape to Specific Heat Ratio

4.4.2 Aerothermodynamic Design

The major portion of the aerodynamic design presented here is a result of work performed in support of the MRSR and MESUR missions. It is assumed that the manned missions would capitalize on these configuration in terms of the aerobrake ballistic coefficient, bluntness (half cone angles of about 70 deg.) and overall shape. As such, the aerodynamic design analyses discussed here would not vary a great deal from the MRSR, MESUR and SEI manned missions.

To determine the aerobrake surface temperatures, aerothermodynamic heating analyses were performed. To determine convective heat transfer (the dominant component for low speed, less than 7 km/sec, entry), the analysis relied on models which were verified with hypersonic CO_2 atmospheric entry data. Since these models are a spherical geometry, a three dimensional time dependent ideal gas inviscid flow field solution was used to predict the shock shape and therefore a resulting equivalent nose radius. Using this equivalent nose radius, a maximum cold wall convective heat flux of 2.0 w/cm^2 is predicted for the front face of the aerobrake. At the edge of the aerobrake, heat flux will increase due to the presence of a large pressure gradient. Using Remtech and Apollo flight data, a maximum edge heat flux of 5.0 w/cm^2 is predicted. This would also be the case along the aerobrake scallop and seam lines that could form on the tensioned surface. Although the aerobrake has a large nose radius, gas cap radiation both equilibrium and non-equilibrium is predicted to be negligible at orbital entry and minimum energy heliocentric transfer entry speeds. Heat flux histories for Mars orbital entry are shown in Figure 4.4.9. The heat flux at the hyperbolic entry speeds are an order of magnitude greater.

The viscous results obtained on NAS computer are shown in Figure 4.4.10 for the hyperbolic entry conditions. These were an entry speed of 7.15 km/sec and entry flight path angle of 21.6 deg below the local horizontal. The Heat fluxes correspond to the peak values attained at 25 km altitude and Mach 31.2. The accompanying pressure profile is shown in Figure 4.4.11. A gas flow velocity distribution is shown in Figure 4.4.12. The important things to note are the large recirculation and reflected shock in the wake of the closed aerobrake. The normalized pressure contours in the flow field are shown in Figure 4.4.13 along with the temperature and departure from ideal gas β contours.

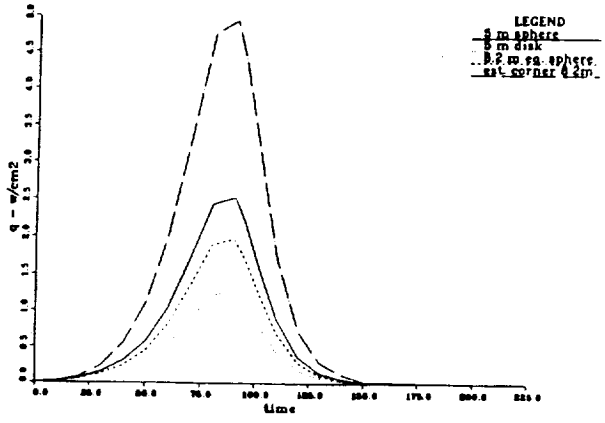

Figure 4.4.9 Heat Flux Histories for Mars Orbital Entry

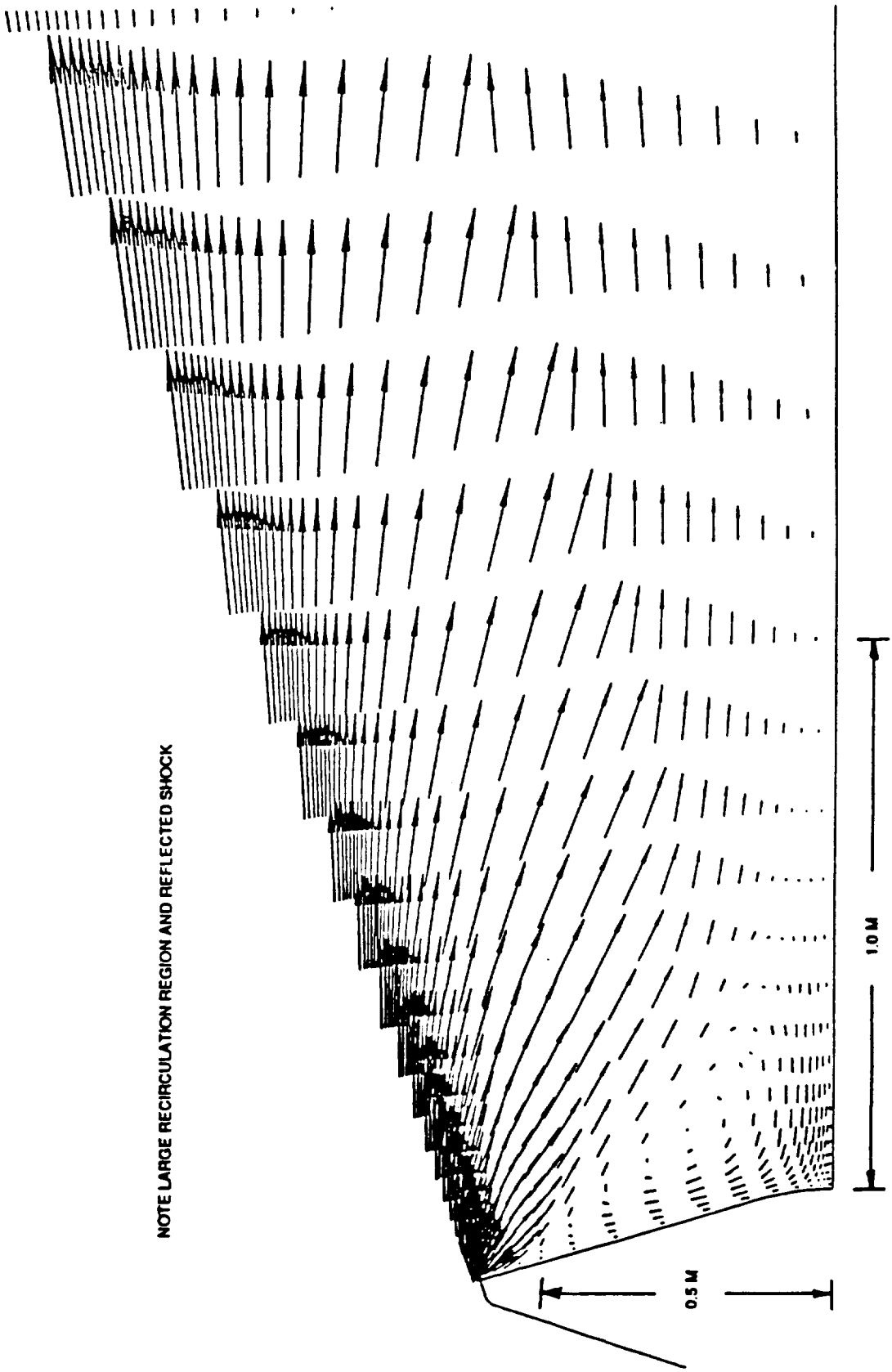

Figure 4.4.12 Gas Flow Distribution on Closed Aerobrake at Hyperbolic

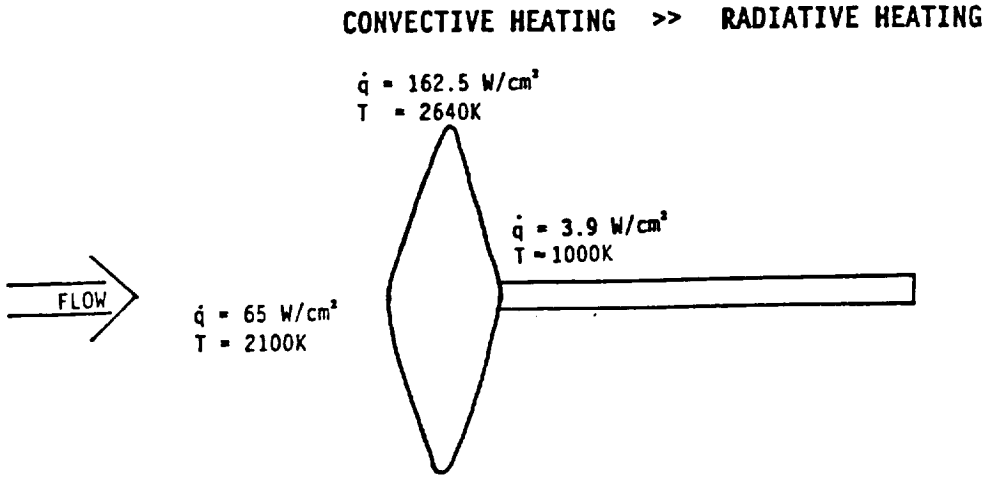

Figure 4.4.10 Aeroheating on Closed Aerobrake at Hyperbolic Entry

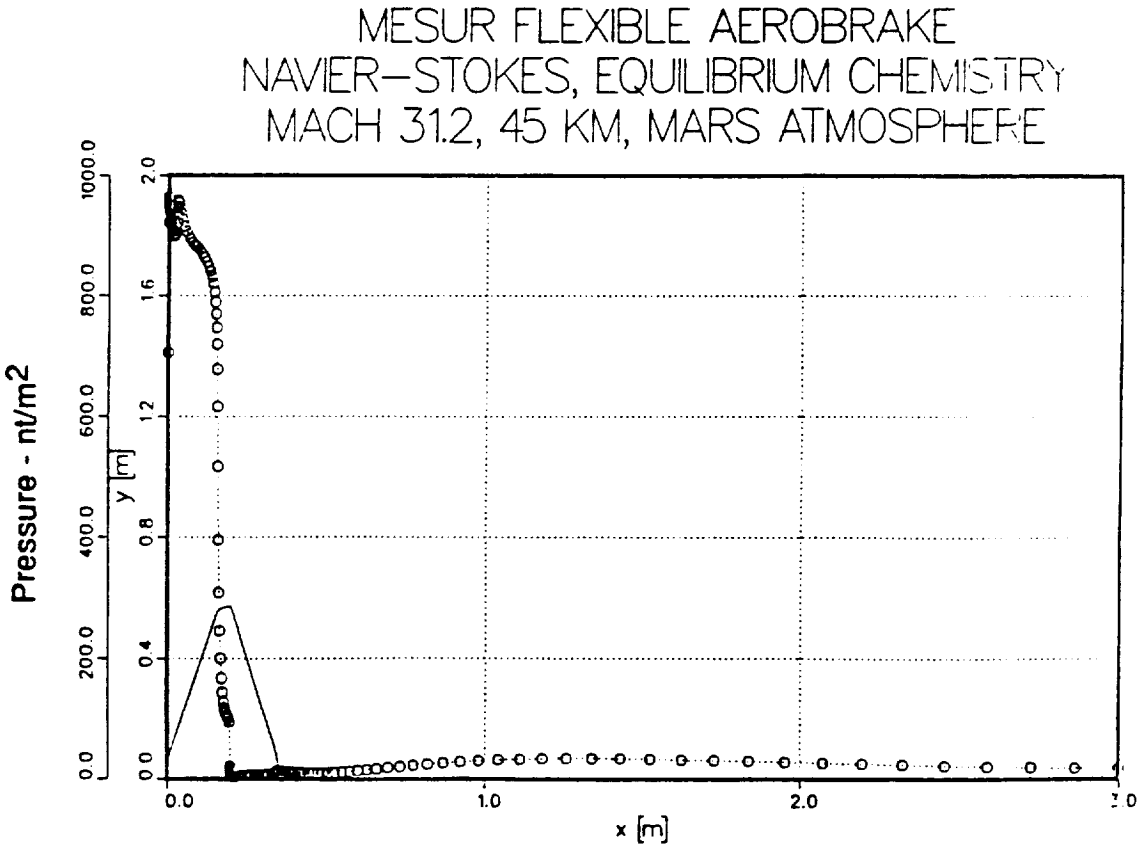

Figure 4.4.11 Pressure Profile on Closed Aerobrake at Hyperbolic Entry

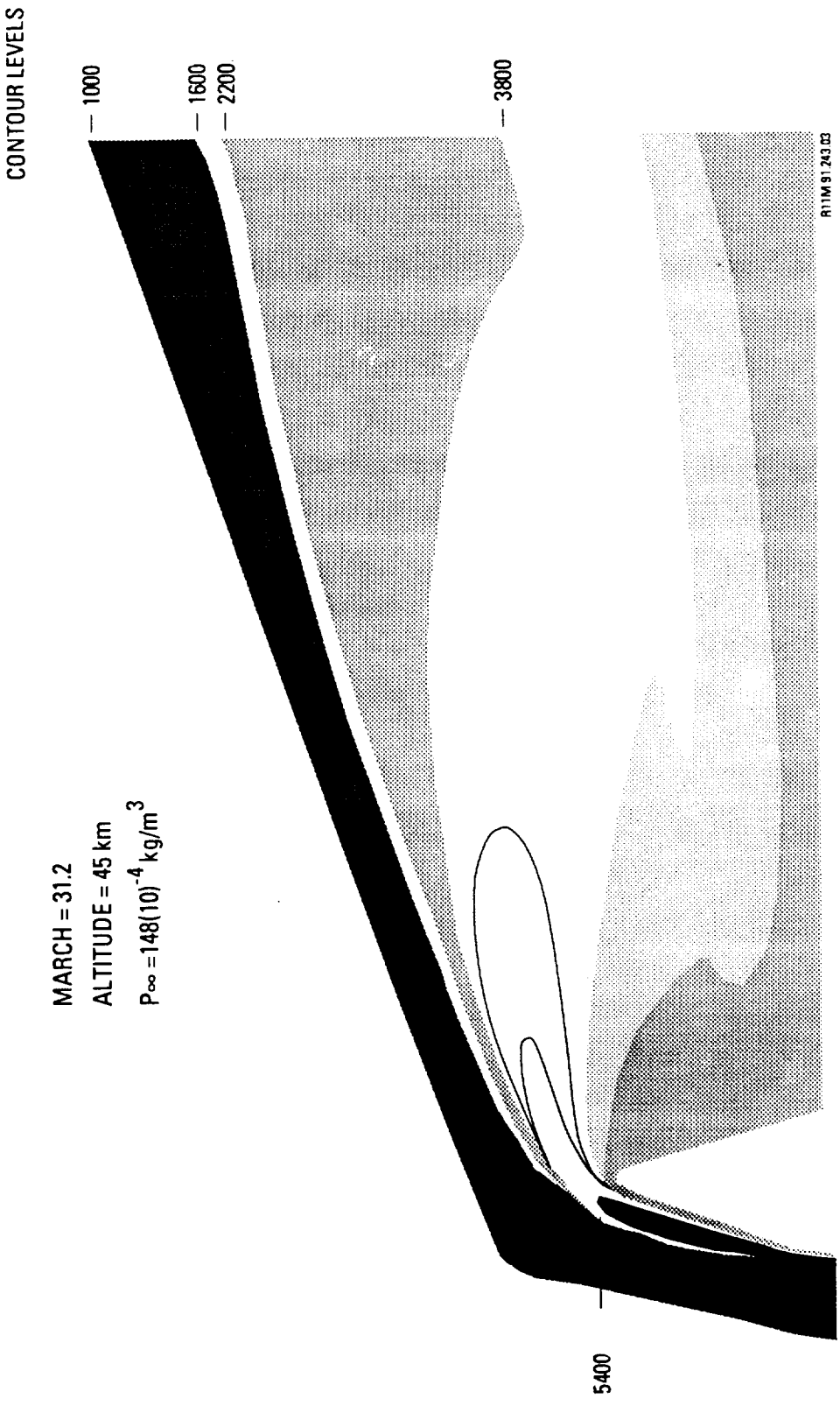

Figure 4.2.13a Flowfield Contours, Temperature

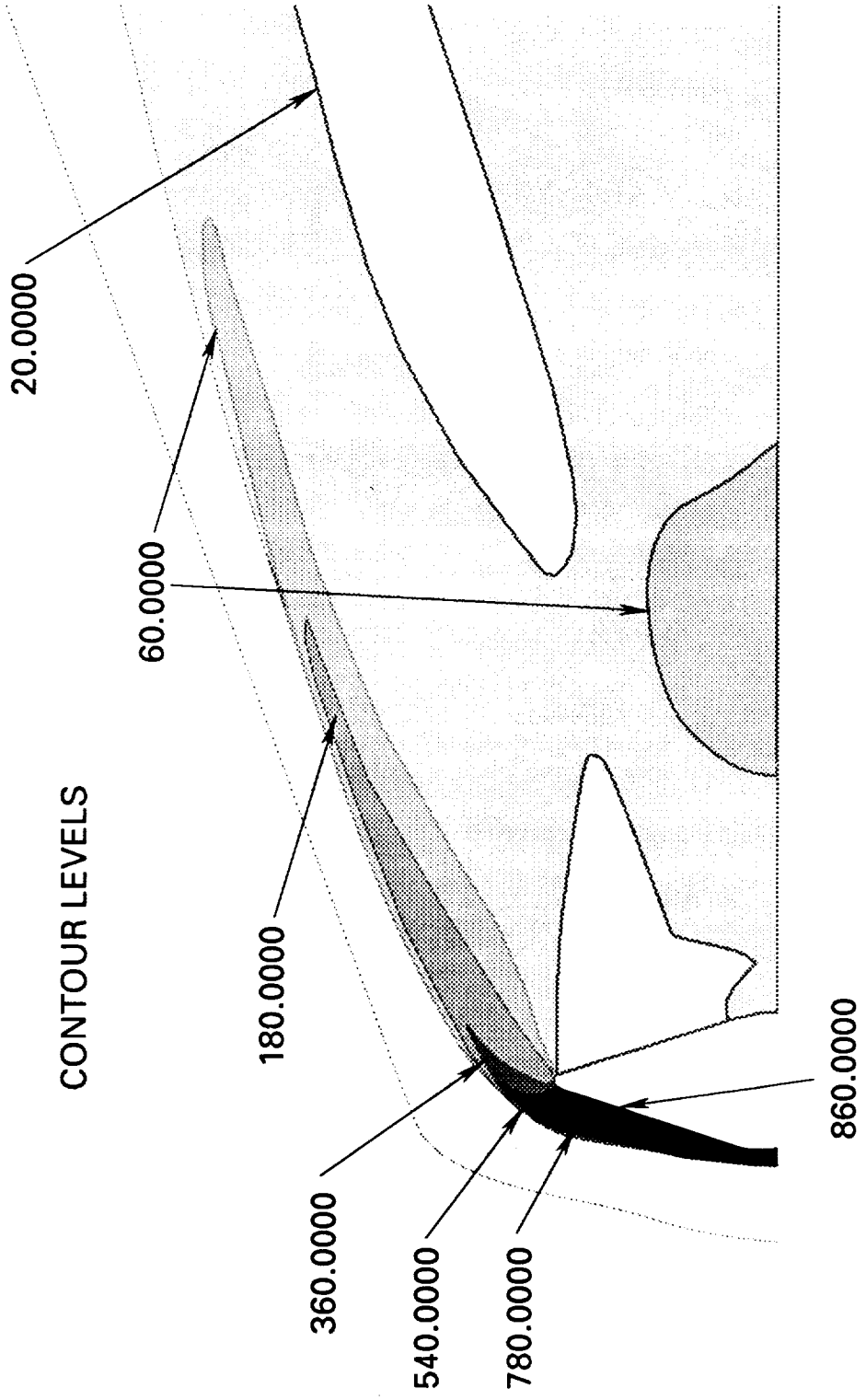

Figure 4.2.13b Flowfield Contours, Normalized Pressure

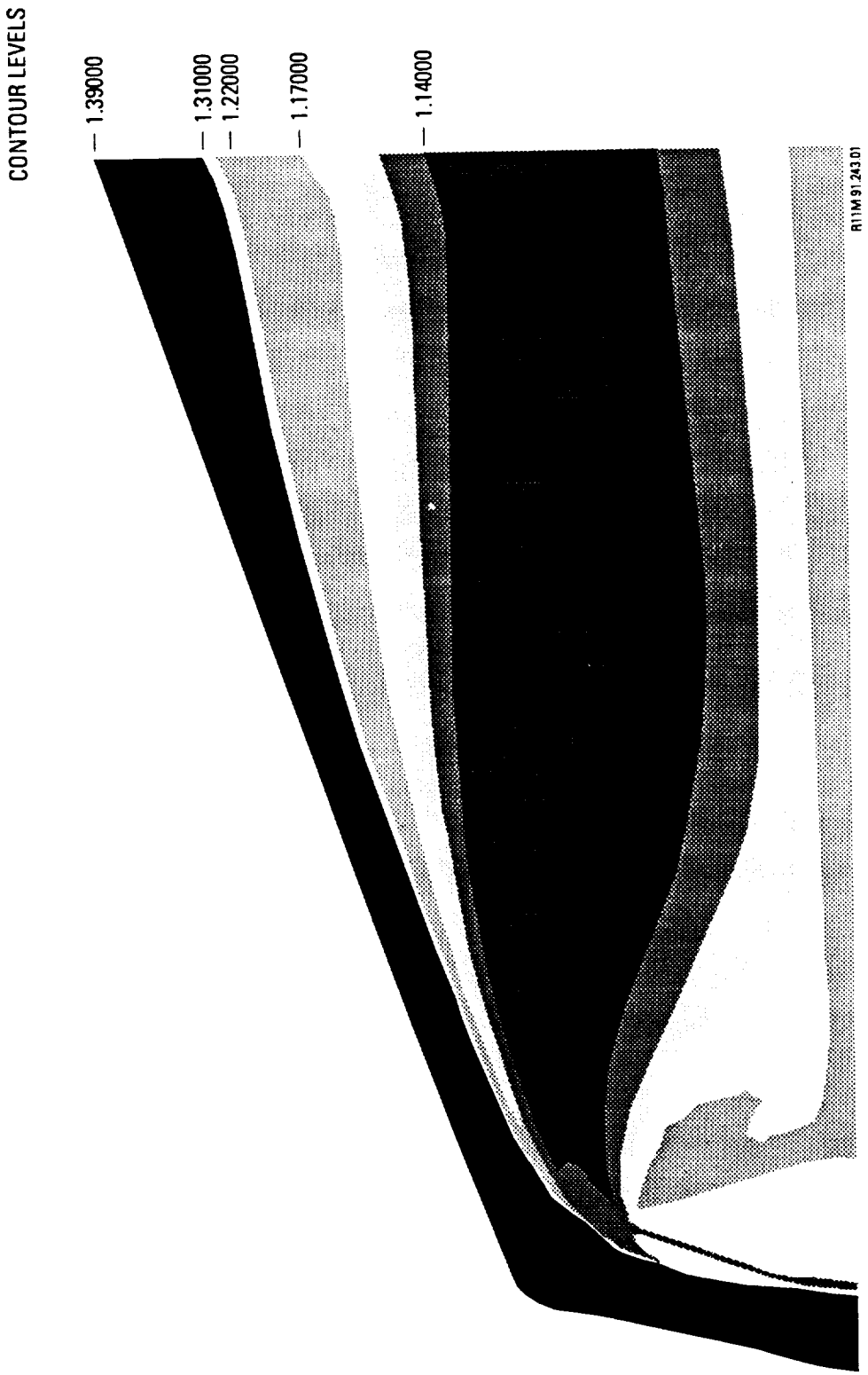

Figure 4.2.13c Departure from Ideal Gas, β Contours

4.4.3 Thermal Protection Design

Assuming the use of the 3M NEXTEL (Reference 4.7.12) blanket for orbital entry, the corresponding aerobrake surface temperature time histories are computed and shown in Figure 4.4.14. The expected backface temperatures are shown in Figure 4.4.15 as a function of the blanket thickness. The aerobrake design will not normally be driven by the backface or insulating properties of the blanket. As a result, the thickness will be driven by the strength and rigidity required to sustain the aerodynamic loads. A summary of the maximum expected aerobrake surface temperatures are shown in Table 3.2.1. At hyperbolic entry, the blanket will most likely require higher temperature a carbon graphite, silicon carbide or ablative cloth material (Reference 4.7.13). The thermal properties associated with the aerobrake blanket materials are shown in Table 4.4.1.

An option to provide structural stiffness to the aerobrake which requires additional study considers the use of waste water produced during the interplanetary transfer. The water be frozen and made part of the aerobrake blanket. This would not only provide structural stiffness, but the required edge support structure. In addition, design margin to the thermal protection system would be gained by the sublimation properties associated with ice during the entry environment. This would particularly be important for the hyperbolic entry. Reference 4.7.14 discusses the concept in greater depth.

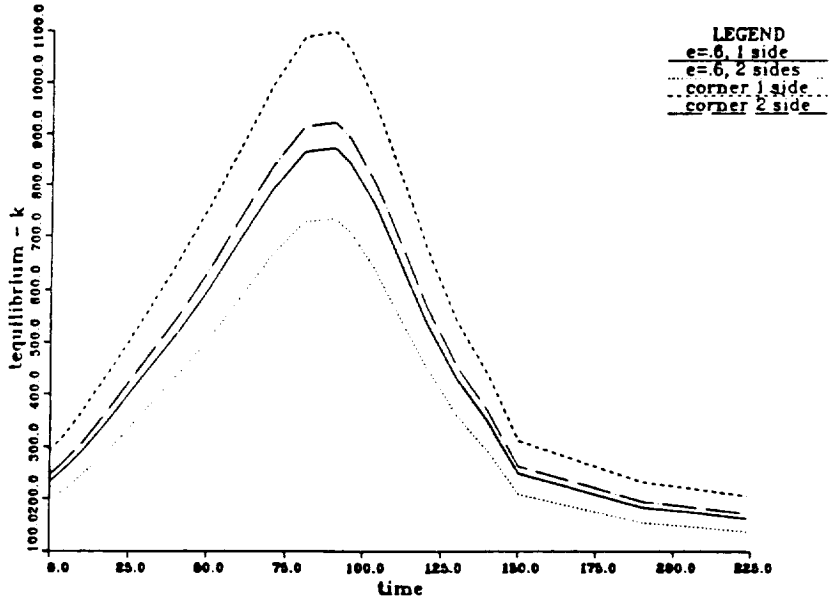

Figure 4.4.14 Open Aerobrake Surface Temperature Histories at Orbital Entry

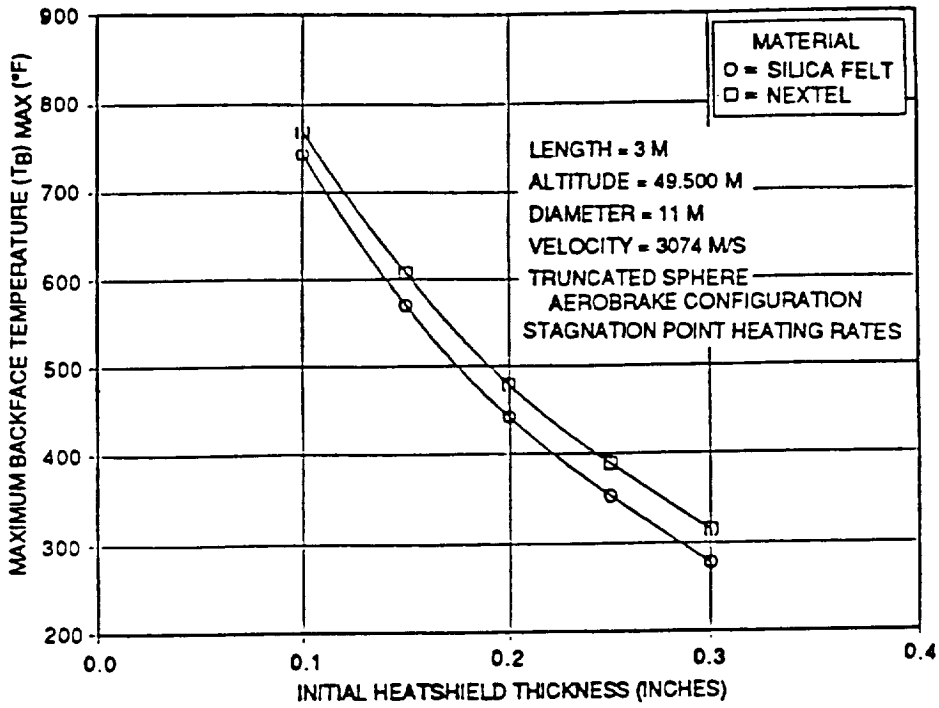

Figure 4.4.15 Open Aerobrake Backface Temperature as Function of Blanket Thickness

Table 4.4.1 Blanket Thermal Properties

Material	Density gm/cm^3	Shape Change Threshold Estimate deg K/deg F	Thermal Conductivity w-m/m^2	Specific Heat J/g-deg C
NOMEX	0.0830	811 / 1000	0.048	2.051
Aluminoboro-Silicate(14%B_2O_3)	0.1280	2073/ 3272	0.150	1.260
NEXTEL 312 Aluminoboro-Silicate(2%B_2O_3)	0.0670	2073/ 3272	0.150	1.260
NEXTEL 440 Silica	0.0960	1973/ 3092	0.069	1.090
Silicon Carbide	0.0864	2033/ 3200	21.00	0.670
TABI/AFRSI	0.0960	1700/ 2600	0.016	1.461

4.4.4 Structural Design

The major portion of the structural design presented here is a result of work performed in support of the MRSR and MESUR missions. It is assumed that the manned missions would capitalize on these configuration in terms of the aerobrake ballistic coefficient, bluntness (half cone angles of about 70 deg.), overall shape, structural support and structural stiffening concepts. As such, the structural design analyses discussed here would not vary a great deal from the MRSR, MESUR and SEI manned missions.

Structural dynamics and stress analyses were conducted on the two aerobrake configurations at both low Mars orbit (3.6 km/sec) and moderate hyperbolic (7.2 km/sec) entry speeds. The open aerobrake was considered for the low Mars orbit entry, and the closed aerobrake was considered for the hyperbolic entry. Linear and non-linear analysis techniques were applied to the problem to understand the effect of loading on the design of these ultra-low ballistic coefficient concepts.

The aerobrake designs normally utilized rib structure to hold the blanket in an umbrella like shape as dictated by the required aerodynamic characteristics. At the low entry speeds, it was deemed that deployment of the lander legs in the thick shock layer was a viable concept with the aft end of the aerobrake opened to the wake. At the higher speeds, closure of the aft end appeared to be more appropriate due to potential higher wake closure pressure and heating on the payload as well as providing additional aerobrake blanket edge support structure.

The aerobrake rib structure considered primarily composite materials having a Young's modulus of about 110,000 Mega(M) Pascal (Pa) or 16,000 ksi. The aerobrake blanket consisted of three quilted layers (two outer load carrying members and a thicker core material on the order of a 1 cm thick acting as thermal insulation). The variations in blanket mechanical properties due to the thermal load during entry were considered. The effective Young's moduli are about 3900 M Pa (563 ksi) and 10,800 M Pa (1,570 ksi) for a NEXTEL heat cleaned and a sized blanket, respectively. The non-linear bi-modal stress-strain relationships for these materials are shown in Figure 4.4.15 (Reference 4.7.15).

Initial trades were conducted to understand the effects of the materials and aerobrake outer edge support conditions. Table 4.4.2 presents these trades results for the low Mars orbit entry case at Mach 10 (the peak aerodynamic pressure condition)

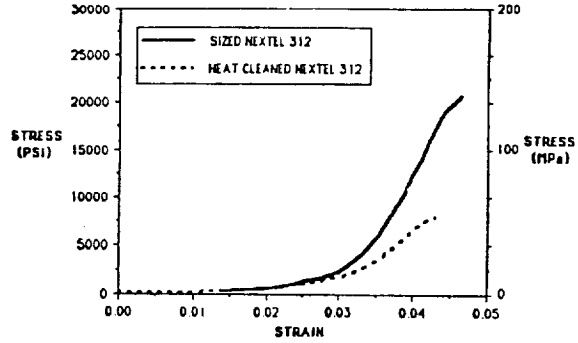

Figure 4.4.15 NEXTEL 312 Blanket Stress-Strain Curves

Table 4.4.2 Trade Studies of Aerobrake Responses

Trade Studies of Aerobrake Responses					
Material Name/ Peak Young's Modulus	Condition of Outer Edge of Blanket	Peak Displacement (Center of Blanket)	Peak Stress	Lowest Two Eigenvalues	
				Before Load	After Load
Nextel	Free	13 Cm (23.6 in)	20 MPa (2901 psi)	.65/1.0 Hz	7.7/9.5 Hz
1.1E4 MPa (1.57 msi)	Fully supported by beam	16 Cm (6.3 in)	41 MPa (5947 psi)	1.2/1.5 Hz	7.3/14.6 Hz
Heat treated Nextel					
3.9 E3 MPa (561 ksi)	Fully supported by beam	4 Cm (8.3 in)	28 MPa (4061 psi)	.35/.44 Hz	7.4/13.4 Hz

assuming a 17 mbar (0.238 psi) pressure distributed uniformly over the aerobrake. The non-linear finite element code ADINA (Reference 4.7.16) was used to generate these results. The non-linear procedure was required due to the nature of the blanket elastic properties which are affected by weave construction and loading. The aerobrake blanket responses primarily as a membrane, having a stiffness which is highly affected by load, as opposed to a linear more conventional structure where loading has little influence on the steady state response. The results indicate that the first mode frequencies may change by as much as an order of magnitude depending on the loading, which makes the usage of such linear analysis tools as the NASTRAN unreliable.

The simply supported aerobrake outer edge design solution did not present a demanding support structure due to the low loading nature of the entry environment of 17 mbar. To understand the effects of the higher entry speeds and the closure of the aerobrake aft end, subsequent analyses were conducted. Table 4.4.3 presents the results of these analyses which also investigated the effects of pre-tension applied to the blanket by the support structure. The pressure distribution in this case corresponded to about 40 mbar (0.56 psi) at Mach 20. The important thing to note is the significant increase in the structural stiffness due to the aerobrake aft end closure and the relative insensitivity of the structural modal response to orders of magnitude

increase of the pre-tensioning loads. Also, the MESUR aerobrake is much smaller (1.0 m in diameter as compared to the MRSR which about 15 m in diameter).

Again, the nature of the low aerodynamic loading environment does not pose significant design structural design issues with the aerobrake. This is a result of the ultra-low ballistic of the entry aerobrake. State of the art blanket materials have sufficient strength and stiffness to meet preliminary performance requirements for the aerobrake in terms of deflection, stress and response frequency.

Table 4.4.3 Modal Frequencies and Steady State Loads at Various Pre-Tension Loads

OUTER EDGE PRE-LOAD	FREQUENCY	OUTER SUPPORT FORCE	FABRIC STRESS	FABRIC MAX DISPLACEMENT
10**5 dyne/cm	1st mode-Hz	10**8 dyne	10**7 dyne/cm**2	cm
1.00	70.50	1.00	9.50	0.84
15.00	71.00	1.05	9.45	0.79
30.00	73.00	1.30	10.10	0.68
100.00	77.00	1.70	10.75	0.58
150.00	79.00	1.75	11.10	0.53

4.4.5 Shock Attenuation Design

The lander will normally descend to the planetary surface with the aid of a chemical propulsion system to effect a soft landing with impact velocities of less than 1.0 m/sec (2.2 mph). This is preceded by a terminal deceleration or descent phase where normally a high drag device such as a parachute would be used to lower the terminal descent speed to be taken out by the chemical propulsion system. An alternate concept is the use of an airbag to increase the area of the aerobrake during terminal descent. This airbag along with others (to augment the load stroke capacity) that would be deployed just prior to impact can provided the shock attenuation due to the residual impact velocities. In addition, this cushion system would provide a low loading (less than 40 g's at impact velocities of 30 m/sec or 66 mph over msec) backup in the event of a chemical propulsion system failure. The initial airbag would reduce the terminal descent velocities from about 120 m/sec to about 30 m/sec.

Figure 4.4.16 shows the inflatable part of the terminal descent aerobrake system considered in this study for the initial airbag. The dashed lines indicate the size of the airbag prior to inflation and the solid lines indicate the inflated shape after a 41,000 Pa (6 psi) internal pressure is applied. Figure 4.4.17 provides the deformed shape after the aerodynamic load of 6,900 Pa (1 psi) is applied. The frequencies of the air bag for a 41,000 Pa internal and 6,900 Pa external pressure are listed in Table 4.4.4. At the velocity at which this airbag is deployed (about 120 m/sec or less), the peak pressure over the aerobrake would not exceed 1 mbar (0.014 psi). The required gage of this initial airbag would be about 0.25 mm (10 mil). For a landed mass of 38 kg (MESUR), the initial airbag added mass would be about 1.0 kg.

The equivalent design for the manned lander with an 8 g peak impact load at impact speeds of 30 m/sec is shown in Figure 4.4.18. This is for a crew capsule of 11.5 Tonnes. The entry mass is about 87 Tonnes. It is assumed that this system would only function in the case of a propulsion system failure. The design shows a large toroidal airbag (about 180 m in diameter) with tension cables holding the aerobrake in place. The aerobrake and lander will crush the airbag upon landing attenuating the impact load to about 8 g's. The airbag is inflated with a gas generator in a matter of micro-seconds. The potential for later use of the airbag as a habitat has not been considered.

The typical deployment scenario for an airbag is as follows: The inflation sensor detects a "fire" cue (i.e., in the automotive application an excessive acceleration at the front of the vehicle) and sends an electric signal to the igniter. The igniter causes the propellant (i.e., sodium azide) to combust creating a high pressure gas. This gas, along with that sucked in through the fixture porous sides (i.e., aspirated gas), fills the bag. There will be 3 molecules of Nitrogen produced for every molecule of Sodium that remains in the gas generator cannister. In this case, the details of the design are proprietary and under patent by the TRW automotive sector. Typically in automotive applications, fill time is within 4msec (where the pressure in the generator is a couple of hundred bars and that in the bag around 0.5 bars); the bags are composed of a woven nylon fabric (see reference 4.7.6 for a more thorough description of larger airbag system concepts).

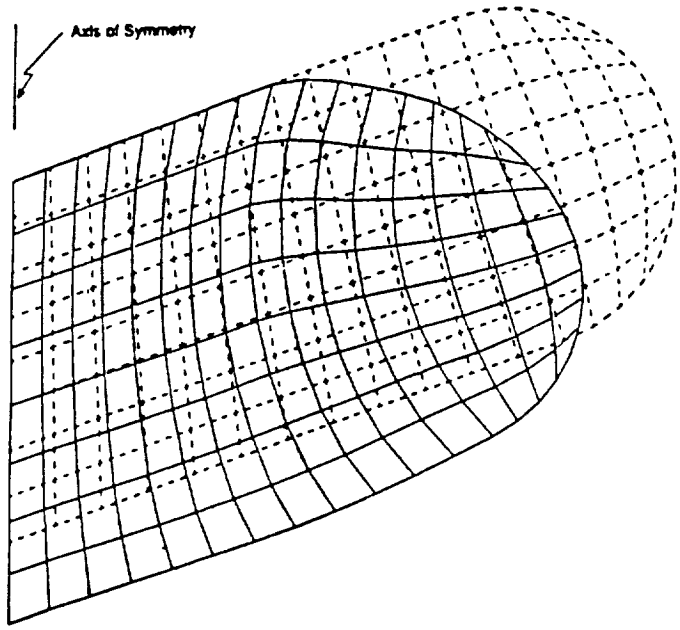

Figure 4.4.16 Initial Configuration of Inflatable Terminal Descent Aerobrake

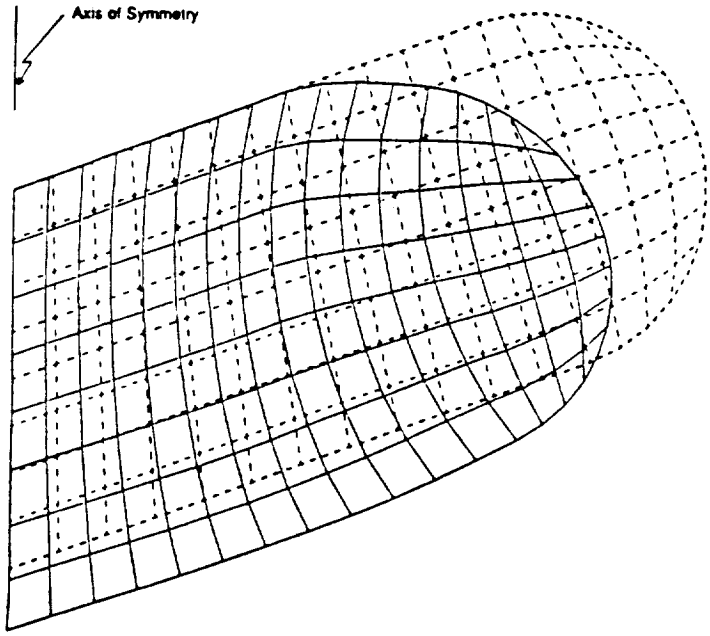

Figure 4.4.17 Deformed Configuration of Inflatable Terminal Descent Aerobrake under 1 psi Pressure in Z-Direction

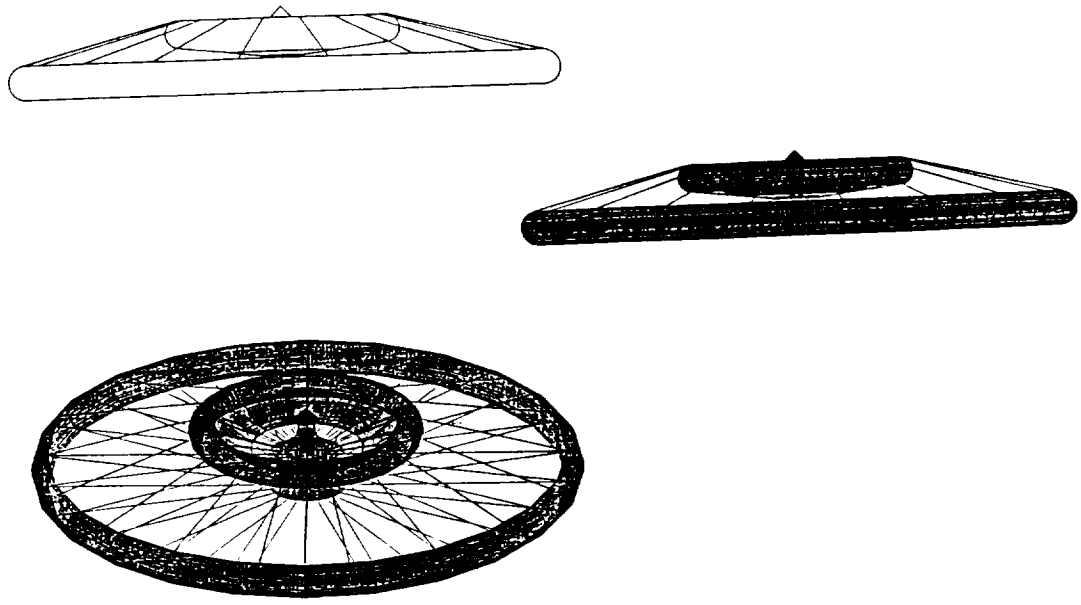

Figure 4.4.18 Equivalent Manned Terminal Descent and Touchdown System for a 11.5 Tonne Crew Capsule

Table 4.4.4 Inflatable Aerobrake Modal Frequencies

Inflatable Aerobrake Frequencies (Inflation Pressure 41,400 Pa (6 psi), loading 6900 Pa (1 psi))		
Model Number Number	Frequency (Cycles/Sec)	Period (Milliseconds)
1	8.5	117.0
2	12.8	77.9
3	13.9	72.0
4	16.8	59.5
5	17.5	57.1
6	17.8	56.1
7	20.0	49.9
8	20.9	47.9
9	22.2	45.0
10	23.4	42.8
11	23.9	41.8
12	24.1	41.5

4.4.6 Chemical Propulsion Design

The chemical propulsion system will most likely be bi-propellant and storable. Section 4.3 presented some requirements which ranged from a 16 to 400 knt thrust on the engines. The propulsion system for the manned module made well consume about 69% of the landed mass.

4.4.7 Attitude Control Design

Attitude control will be passive during the entry to landing phase. Attitude control during the propulsive phase will depend on the propulsion system.

4.4.8 Flight Sensors

There are no stringent requirements on the flight sensors above those that would have been implemented on the rest airborne equipment.

4.4.9 Electrical Power

The entry to landing system will not require power in excess of that already on board the payload for the expeditionary phase.

4.5 DECISION CRITERIA

The decision criteria utilized in the MRSR study was adopted. The elements involved did not require an exhaustive use of the methodology. Table 4.5.1 shows the criteria utilized in this study.

4.5.1 Trade Space

The trade space developed for spacecraft elements is shown in Figure 4.5.1. The oval and hi-lited blocks show the preferences based on the decision criteria

4.5.2 Rating Methodology

For each of the decision criteria, the candidate concepts were assigned scores in the 1 to 10 range. These scores were multiplied by the weighting factors assigned to each criterion. The products of this action were then summed to provide a weighted score for ranking each candidate.

Weighting factors were developed using a "preference matrix" in which each criterion was compared to the other criteria. The relative importance of each comparison ranged from "much less important" to "much more important" and was given a corresponding score from 0 to 4. The scores were added to provide weighting factors. In the standard shown in Table 4.5.2, mass was judged "equal in importance" to reliability and complexity, receiving a value of 2 in each case and was judged "more important" than performance, risk, cost and interaction, receiving a value of 3 in each case. The cumulative total is 16. Each of the other criteria in subsequent rows was similarly treated. The Totals for each row provide the weighting factors applied to the candidate scores.

A constraint value of 5 was placed on the maximum total score attainable for all the options evaluated. The maximum for each option was the product of 5 and the number of options, N. For each criterion, the total could not exceed 5XN and the scores were distributed accordingly, which allowed a clearer decision process.

Table 4.5.1 Decision Criteria

Criteria	Definition	Rationale for Adopting Criterion	Examples of Desirable Attributes	Soundness of Criterion
Mass	Determines weight required to implement a segment, element, or subsystem	Determines the ability to carry out the mission given the available launch vehicles	• Low weight	Mass needs to be identified separately to stress its importance
Reliability	Numerically predicts the probability of equipment operation within specification	Determines the probability of mission success	• High probability number • Large mean-time-between-critical failures	Probability of success is of overriding importance. Reliability is a quantitative measure of success probability
Performance	Measures level of achievement in meeting mission/system, subsystem-specific requirements	A principal indicator of relative merit of system design or mission mode alternatives	• Efficient design • High specific impulse • High accuracy (G&N) • Fuel and time efficiency	A primary criterion for evaluation. Reflects the ability of system/component to accomplish the required function
Risk	Measures the degree of uncertainty and impact on meeting mission/system requirements and constraints (e.g., development, technology, schedule, operational risk)	Compares mission/system design alternatives for relative assurance of mission success and meeting cost and schedule constraints	• Proven design concept and hardware • Proven operational sequence • Interface simplicity • Easy to develop and test	Schedule certainty is critical to mission success due to launch constraints and ultimately costs
Complexity	Measures system design and functional complexity in terms of parts count, interfaces/interactions, process difficulty, etc.	Compares design alternatives for selection of simplest option that meets requirements and constraints	• Low parts count • Simple operation sequence • Interface simplicity • Easy to develop and test	Compatibility will drive cost and probability of success. Complexity is to be avoided where possible
Interactions (requirements on other segments/elements/subsystems)	Indicates the requirements and constraints on or by other mission segments/elements by or on segment/element being evaluated	Determines level of interaction with other segments or elements in selecting a faborable, low-interaction design option	• Minimum number and minimum complexity of interaction s • Minimum requirements and constraints imposed by or on other elements	Interactions and interdependence between subsystems can impact cost and schedule due to propagation of a change in one element through others
Cost	Measures cost items of concern (i.e., engineering, production, test, launch, life-cycle cost of candidate designs)	A principal indicator of relative compliance of design alternatives with cost goals, budget constraints, etc.	• Cost-effective design, operation • Available (off-the-shelf) hardware • Low development, test cost • State-of-the-art design	Overall mission cost is critical to obtaining mission authorization and successful program execution

MARS ENTRY -TO-LANDING TRADES

TRADE	OPTION 1	OPTION 2	OPTION 3	OPTION 4
MANNED SPACECRAFT				
MARS ORBIT INSERTION	AEROCAPTURE	CHEMICAL	**NUCLEAR THERMAL**	LOW THRUST
MARS ENTRY	**BALLISTIC**	MANEUVERING	CHEMICAL	NUCLEAR
AERODYNAMIC CONFIGURATION	**ZERO LIFT**	LOW L/D	MODERATE L/D	HIGH L/D
TERMINAL DESCENT	**AEROBRAKE**	PARACHUTE	CHEMICAL	NUCLEAR
TERMINAL TOUCHDOWN	**CHEMICAL**	NUCLEAR	CUSHIONED	
SHOCK ATTENUATION	MECHANICAL	**AIRBAG**	NONE	
CHEMICAL PROPULSION	**BI-PROPELLANT STORABLE**	BI-PROPELLANT CRYOGENIC		
ENGINES	XLR-132	LMDE	VTE(OMV)	**NEW**
MARS ASCENT	**SINGLE MODULES**	MODERATE SIZE SINGLE MODULE	SELF SUFFICIENT HABITAT	
MARS DEPARTURE	CHEMICAL	**NUCLEAR THERMAL**	LOW THRUST	

Figure 4.5.1 Study Trade Space (Continued)

MARS ENTRY -TO-LANDING TRADES

TRADE	OPTION 1	OPTION 2	OPTION 3	OPTION 4
UNMANNED SPACECRAFT- SUPPLIES, EQUIPMENT, HABITATS, ETC.				
MARS ORBIT INSERTION	**DIRECT ENTRY-TO-LANDING**	CHEMICAL	NUCLEAR THERMAL	LOW THRUST
MARS ENTRY	**BALLISTIC**	MANEUVERING	CHEMICAL	NUCLEAR
AERODYNAMIC CONFIGURATION	**ZERO LIFT**	LOW L/D	MODERATE L/D	HIGH L/D
TERMINAL DESCENT	**AEROBRAKE**	PARACHUTE	CHEMICAL	NUCLEAR
TERMINAL TOUCHDOWN	**CHEMICAL**	NUCLEAR	CUSHIONED	
SHOCK ATTENUATION	MECHANICAL	**AIRBAG**	NONE	
CHEMICAL PROPULSION	**BI-PROPELLANT STORABLE**	BI-PROPELLANT CRYOGENIC		
ENGINES	XLR-132	LMDE	VTE(OMV)	**NEW**

Figure 4.5.1 Study Trade Space (Continued)

Table 4.5.2 Criteria Preference Matrix

CRITERIA	MASS	RELIAB.	PERF.	RISK	COMP.	INTER.	COST	TOTAL
Mass		2	3	3	2	3	3	16
Reliability	2		2	2	2	3	2	13
Performance	1	2		3	3	2	2	13
Risk	1	2	1		3	3	2	12
Complexity	2	2	1	1		2	1	9
Interaction	1	1	2	1	2		1	8
Cost	1	2	2	2	3	3		13

Relative Importance	Much less	Less	Equal	More	Much more
Score	0	1	2	3	4

4.6 TECHNOLOGY ASSESSMENT

4.6.1 Technology Readiness Criteria

The technology readiness criteria utilized in this report is the NASA standard which categorizes 7 levels, as follows:

Level 1: Basic principles observed and reported

Level 2: Conceptual design formulated

Level 3: Conceptual design tested analytically or experimentally

Level 4: Critical functions and characteristics demonstrated

Level 5: Components breadboard tested in relevant environment

Level 6: Prototype engineering model tested in relevant environment

Level 7: Engineering model tested in space

4.6.2 Enabling and Enhancing Technology Needs

The technology needs were categorized for three major spacecraft elements. These included the orbital entry aerobrake design, hyperbolic entry aerobrake design and airbag design.

The orbital entry aerobrake design is as a system design viewed to be at Level 3. The component technologies (i.e., materials, analytical tools, experimental facilities, design elements, etc.) are viewed to be at Levels between 6 and 7.

The hyperbolic entry aerobrake design is also viewed to be at the same Level of technology readiness as the orbital entry aerobrake design. The only exception is a need for flexible materials for a aerobrake blanket design that can tolerate single use temperatures as high as 2640 deg. K (4293 deg. F).

The airbag is a very mature technology which is now commonly used for automotive restraint systems. In the case of the manned applications, it is a matter of scale (i.e., 60 to 180 m diameters as compared to 1 m) which requires deployment tests.

Overall the technology needs are driven by the integrated system Research and Development (R&D) as opposed to Research and Technology (R&T) needs.

4.7 REFERENCES

4.7.1 "Mars Rover Sample Return (MRSR) Delivery and Return Study", TRW Final Report NAS9-18141 to NASA/JSC, June, 1990.

4.7.2 D. M. Cooper and J. O. Arnold, "Technology for Aerobraking", IAF No. 90-037, 41st Congress of the International Astronautical Federation, October, 1990, Dresden, GDR.

4.7.3 "Generic Planetary Aerocapture Research and Technology Development Final Report", JPL Document D-691, May, 1983.

4.7.4 D. L. Post and M. I. Cruz, "CFD Application to Flexible Aerobrake Design for Mars Entry", AAS/AIAA No. 91-424, AAS/AIAA Astrodynamics Specialist Conference, August, 1991, Durango, Colorado.

4.7.5 E. F. Zabrensky, D. L. Post, L. A. Cassel and T. P. Shivananda, "Aerothermodynamics of the Mars Rover and Sample Return Lander", AAS/AIAA No. 91-423, AAS/AIAA Astrodynamics Specialist Conference, August, 1991, Durango, Colorado.

4.7.6 J. E. Crawford, "A Cushioned Landing System for PLS" TRW White Paper H937 submitted to NASA/LaRC Space Systems Division, May, 1991.

4.7.7 A . P. Kothari and K. G. Bowcutt, "Leading Edge Optimization for Hypersonic Vehicles", Proceedings of the 1st International Hypersonic Waverider Symposium, October, 1990.

4.7.8 E. G. Menkes and J. C. Houbolt, "Evaluation of Aerothermoelasticity Problems for Unmanned Mars Entry Vehicles", J. Spacecraft, Vol. 6, No 2, p. 178-184, February, 1969.

4.7.9 R. M. Traci, "Unsteady Hypersonic Bluff Body Flow and Aeroelastic Modal Analysis/Scaling", FPI-R90-11-10, December, 1990.

4.7.10 G. P. Guruswamy, "Navier-Stokes Computations on Swept-Tapered Wings, Including Flexibility", AIAA Paper 90-3066.

4.7.11 M. E. Tauber and J. V. Bowles, "The Use of Atmospheric Braking During Mars Missions", AIAA Paper No. 89-1730.

4.7.12 "Ceramic Fiber Products for High Temperature Applications", 3M Marketing Brochure, St. Paul, Minnesota.

4.7.13 P. M. Sawko and H. K. Tran, "Strength and Flexibility Properties of Advanced Ceramic Fabrics", SAMPE Quarterly, Volume 17, No. 1, October, 1985, pp 7-13.

4.7.14 H. Goldstein, "Thermal Protection and Structure for SEI Aerobrakes" NASA/ARC Draft White Paper 229, May, 1991.

4.7.15 M. I. Cruz, "Planetary Entry Flexible Aerobrake Design", TRW IR&D Project No. 91363857, February 2, 1991.

4.7.16 "ADINA 5 (Automatic Dynamic Incremental Non-Linear Analysis)", ADINA RNDE, Inc., 1990.

REPORT DOCUMENTATION PAGE

Form Approved
OMB No. 0704-0188

1. AGENCY USE ONLY (Leave blank)	2. REPORT DATE	3. REPORT TYPE AND DATES COVERED
	June 1992	Contractor Report

4. TITLE AND SUBTITLE
Aerobrake Concepts for NTP Systems Study

5. FUNDING NUMBERS
C NAS1-19291

WU 593-11-11-02

6. AUTHOR(S)
Manuel I. Cruz

7. PERFORMING ORGANIZATION NAME(S) AND ADDRESS(ES)
TRW
Federal Systems Division
Space & Technology Group
One Space Park
Redondo Beach, CA 90278

8. PERFORMING ORGANIZATION REPORT NUMBER

9. SPONSORING/MONITORING AGENCY NAME(S) AND ADDRESS(ES)
NASA Langley Research Center
Hampton, VA 23665-5225

10. SPONSORING/MONITORING AGENCY REPORT NUMBER
NASA CR-4441

11. SUPPLEMENTARY NOTES
Langley Technical Monitor: Charles H. Eldred

12a. DISTRIBUTION/AVAILABILITY STATEMENT
Unclassified - Unlimited

Subject Category 16

12b. DISTRIBUTION CODE

13. ABSTRACT *(Maximum 200 words)*

This report, the result of work performed for the NASA Langley Research Center by TRW between June 1991 and October 1991 under contract NAS1-19291 "Aerobrake Concepts for NTP Systems Study", describes design concepts for landing large spacecraft masses on the Mars surface in support of manned missions with interplanetary transportation utilizing Nuclear Thermal Propulsion (NTP). Included are the mission and systems analyses, trade studies and sensitivity analyses, design analyses, technology assessment, and derived requirements to support this concept. The mission phases include the Mars de-orbit, entry, terminal descent and terminal touchdown. The study focused primarily on Mars surface delivery from orbit after Mars orbit insertion utilizing an NTP. The requirements associated with delivery of logistical supplies, habitats and other equipment on minimum energy Earth to Mars transfers were also addressed in a preliminary fashion.

14. SUBJECT TERMS	15. NUMBER OF PAGES
Aerobrake, Mars Lander, NTP, SEI	80
	16. PRICE CODE: A05

17. SECURITY CLASSIFICATION OF REPORT	18. SECURITY CLASSIFICATION OF THIS PAGE	19. SECURITY CLASSIFICATION OF ABSTRACT	20. LIMITATION OF ABSTRACT
Unclassified	Unclassified	Unclassified	

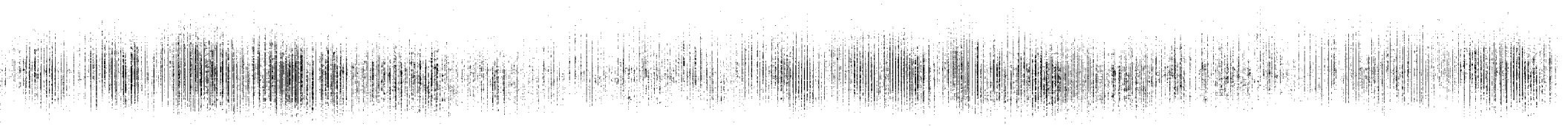

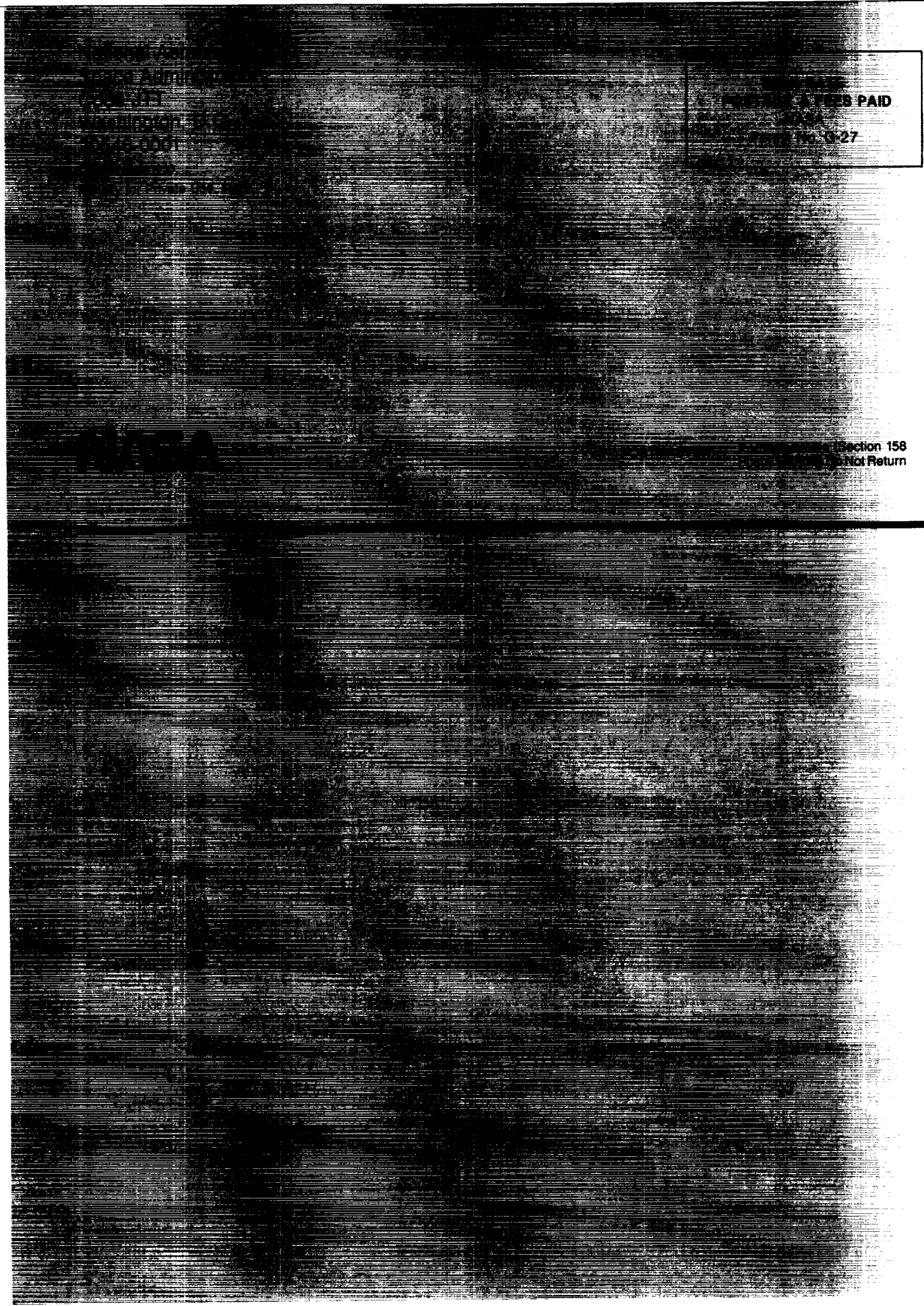
PAID
Section 158
Not Return